



ALFRED-WEGENER-INSTITUT
HELMHOLTZ-ZENTRUM FÜR POLAR-
UND MEERESFORSCHUNG



Release of dissolved organic carbon from coastal erosion into the southern Canadian Beaufort Sea

Master thesis

to attain the academic degree

Master of Science in Geography

Submitted by

George Tanski

born on the 10th of July 1986 in Potsdam, Germany

Freie Universität Berlin

Institute for Geographical Science

Berlin, June 2013

1. Gutachter

Prof. Dr. Karl-Tilman Rost

Freie Universität Berlin

Institut für Geographische Wissenschaften

Malteserstr. 74-100, 14195 Berlin

2. Gutachter

Prof. Dr. Hans-Wolfgang Hubberten

Alfred-Wegener-Institut für Polar- und Meeresforschung

Telegrafenberg A43, 14473 Potsdam

Für meine Familie.

„Was wir wissen ist ein Tropfen, was wir nicht wissen ein Ozean.“

Isaac Newton

Contents

List of figures	I
List of tables	III
Abbreviations and nomenclature	IV
Abstract	1
Kurzfassung	3
1 Introduction	5
1.1 State of the Art	5
1.2 Aims & Objectives	11
1.3 Project framework	11
2 Geographical and geological background	12
2.1 The periglacial environment	12
2.2 Permafrost	12
2.3 Ground ice	14
2.4 Thermokarst and coastal erosion	16
2.5 Dissolved organic carbon and the Arctic organic carbon cycle	19
2.6 Study area and regional setting.....	21
2.6.1 Yukon Coastal Plain	21
2.6.2 Permafrost and geomorphology	22
2.6.3 Climate	24
2.6.4 Vegetation	25
2.6.5 Study sites	26
3 Methods	27
3.1 Field Work.....	28
3.1.1 Preprocessing at the Cold lab	29
3.1.2 Hydrochemical analyses	29
3.1.3 pH measurement	30
3.1.4 Electrical conductivity measurement.....	30
3.1.5 Determination of DOC	30
3.2 Ice content	34
3.3 Mapping and spatial distribution of massive ground ice.....	35
3.3.1 Volume of ice wedges.....	37
3.3.2 Volume of massive ice bodies	38
3.4 Estimation of dissolved organic carbon stocks	39
3.5 Calculation of DOC fluxes	40

4 Results	41
4.1 Permafrost profiles and hydrochemical characteristics	41
4.1.1 Ice wedge TSA12-IW	41
4.1.2 Ice wedge TSC12-IW.....	43
4.1.3 Ice wedge TSD12-IW1.....	45
4.1.4 Ice wedge TSD12-IW2.....	47
4.1.5 Massive ice body TSD12-MI	49
4.1.6 Massive ice body HIWCS12-MI	52
4.1.7 Ice wedge series RB12-IW	54
4.1.8 Massive ice body KP12-MI	57
4.1.9 Ice wedge KP12-IW	60
4.2 Synthesis hydrochemistry	62
4.3 Massive ground ice contents.....	64
4.4 Coastal erosion rates	66
4.5 Coastline height	68
4.6 DOC stocks.....	69
4.7 DOC fluxes	72
5 Discussion	75
5.1 Origin of massive ground ice and sources of DOC	75
5.1.1 Massive ice bodies	75
5.1.2 Ice wedges	80
5.1.3 Comparison between massive ice bodies and ice wedges.....	81
5.2 DOC fluxes from coastal erosion.....	82
5.2.1 DOC fluxes and its control factors.....	82
5.2.2 Possible sources of error	88
5.3 DOC fluxes and the arctic carbon budget.....	89
5.3.1 DOC fluxes from coastal erosion	89
5.3.2 Coastal erosion vs. River discharge.....	92
5.3.3 Incorporation of DOC fluxes into the Arctic carbon budget.....	95
5.4 Fate of DOC in the near shore zone.....	97
6 Conclusions and Outlook.....	100
References.....	102
Appendix.....	122
Danksagung.....	129
Selbständigkeitserklärung.....	130

List of figures

Figure 2.1: Permafrost map of the Northern Hemisphere	13
Figure 2.2: Idealized latitudinal distribution of permafrost	14
Figure 2.3: Classification of massive ground ice	15
Figure 2.4: Idealized scheme of the evolution of an ice wedge	16
Figure 2.5: Scheme of a retrogressive thaw slump	17
Figure 2.6: Coastal processes and responses at arctic permafrost coasts.....	18
Figure 2.7: Continuum of dissolved organic carbon in natural waters	19
Figure 2.8: Dissolved organic carbon as part of the Arctic carbon budget.....	21
Figure 2.9: Map showing the Yukon Coastal Plain and study sites	22
Figure 2.10: Distribution of sediments along the Yukon Coastal Plain	23
Figure 2.11: Temperature and precipitation data of Komakuk Beach.....	25
Figure 2.12: Divisions of the Yukon Coastal Plain and study sites	26
Figure 3.1: Flow chart illustrating the work flow used in the thesis.....	27
Figure 3.2: Flow chart of the dissolved organic carbon measurement	33
Figure 3.3: Dissolved organic carbon measurement procedure	34
Figure 3.4: Terrain units along the Yukon Coastal Plain	35
Figure 4.1: Cryostratigraphic profile of ice wedge TSA12-IW	42
Figure 4.2: Cryostratigraphic profile of ice wedge TSC12-IW.....	44
Figure 4.3: Cryostratigraphic profile of ice wedge TSD12-IW1.....	46
Figure 4.4: Cryostratigraphic profile of ice wedge TSD12-IW2.....	48
Figure 4.5: Cryostratigraphic profile of massive ice body TSD12-MI.....	51
Figure 4.6: Cryostratigraphic profile of massive ice body HIWCS12-MI	53
Figure 4.7: Cryostratigraphic profile of ice wedge series RB12-IW	56
Figure 4.8: Cryostratigraphic profile of massive ice body KP12-MI	59
Figure 4.9: Cryostratigraphic profile of ice wedge KP12-IW	61
Figure 4.10: Results of DOC concentration measurements	63
Figure 4.11: Results of pH measurements.....	63
Figure 4.12: Results of electrical conductivity measurements.....	64
Figure 4.13: Massive ground ice contents along the Yukon Coastal Plain	65
Figure 4.14: Coastal erosion rates along the Yukon Coastal Plain	67
Figure 4.15: Coastline height along the Yukon Coastal Plain.....	69

Figure 4.16: DOC stocks in massive ground on the Yukon Coastal Plain	71
Figure 4.17: DOC fluxes from massive ground on the Yukon Coastal Plain.....	74
Figure 5.1: Genetic classification of massive ground ice.....	77
Figure 5.2: Relationship of ice contents and DOC concentrations	79
Figure 5.3: DOC concentrations in massive ice bodies and ice wedges	81
Figure 5.4: Relationship of DOC fluxes and its control factors	87
Figure 5.5: Comparison of carbon fluxes from rivers and coastal erosion	93
Figure 5.6: Arctic carbon budget and DOC fluxes.....	96
Figure 5.7: Fate of DOC in the nearshore zone	97

List of tables

Table 1.1: Organic carbon fluxes into the Beaufort Sea.....	9
Table 3.1: List of used quality control standards and their features.....	31
Table 3.2: List of the laboratory reagent blanks and processing procedure	32
Table 3.3: Terrain units and location names of the Yukon Coastal Plain	36
Table 4.1: Ice contents and hydrochemistry of ice wedge TSA12-IW	42
Table 4.2: Ice contents and hydrochemistry of ice wedge TSC12-IW	44
Table 4.3: Ice contents and hydrochemistry of ice wedge TSD12-IW1	46
Table 4.4: Ice contents and hydrochemistry of ice wedge TSD12-IW2	48
Table 4.5: Ice contents and hydrochemistry of massive ice body TSD12-MI ...	51
Table 4.6: Ice contents & hydrochemistry of massive ice body HIWCS12-MI ..	53
Table 4.7: Ice contents and hydrochemistry of ice wedge series RB2-IW	56
Table 4.8: Ice contents and hydrochemistry of massive ice body KP12-MI	59
Table 4.9: Ice contents and hydrochemistry of ice wedge KP12-IW.....	61
Table 4.10: Synthesis of ice contents and hydrochemical analyses.....	62
Table 5.1: DOC concentration in laboratory process blanks	89
Table 5.2: Comparison of carbon fluxes by coastal erosion and rivers	91
Table 5.3: DOC fluxes from massive ground ice on a circum-arctic scale.....	95

Abbreviations and nomenclature

Notation	Meaning	SI Unit
°C	degree Celsius	273.15°K
°K	degree Kelvin	K
a	Latin: <i>annus</i> , year	3.1536×10^7 s
BP	before present (1950)	a
CO ₂	carbon dioxide	
conc.	concentration	
d. n.	decimal number	
DOC	Dissolved Organic Carbon	
DOM	Dissolved Organic Matter	
E	East	
e.g.	Latin: <i>exempli gratia</i> , for example	
Electrical cond.	Electrical conductivity in $\mu\text{S}/\text{cm}$	$\text{S} = \Omega^{-1}; \text{m}^{-2} \times \text{kg}^{-1} \times \text{s}^3 \times \text{A}^2$
Eq.	Equation	
g	gram	10^{-3} kg
Gt	gigaton	10^{12} kg
H ₂ O	water	
HI	Herschel Island	
i.e.	Latin: <i>id est</i> , that is	
kg/yr	kilogram per year	
Massive i. b.	Massive ice body	
MGI	Massive ground ice	
Mt	megaton	10^9 kg
Mt/yr	megaton per year	
NaHCO ₃	Sodium hydrogen carbonate	
NaOH	Sodium hydroxide	
NW	Northwest	
ka	Latin: <i>kilo annus</i> , thousand years	3.1536×10^{10} s
m a.s.l.	meter above sea level	m
OC	Organic carbon	
POC	Particular Organic Carbon	
pH	potential of hydrogen	
ppm	Parts per million	
r. w.	references within	
SE	Southeast	
SOC	Soil Organic Carbon	
t	tons	10^3 kg
Tg/yr	teragram per year	10^9 kg/yr
TOC	Total Organic Carbon	
TU	Terrain unit	
Vol.	Volume/volumetric	
vol%	per cent by volume	
W	West	
w.b.i.	with barrier islands	
wt%	per cent by weight	
yr	year	3.1536×10^7 s

Abstract

Arctic regions are highly vulnerable to climatic change processes and are currently undergoing the most rapid environmental transition experienced on Earth, at a pace that is expected to increase over the coming decades. Changing environmental conditions affect the sensitive ice-rich permafrost coasts in northern Canada that erode due to warmer climate, longer open water seasons and stronger storms. Coastal erosion in the Canadian Arctic that is among the highest in the world releases terrestrial organic carbon stored in ice-rich permafrost into the Arctic Ocean, which fosters the feedback mechanisms between carbon cycle and climate.

The Yukon Coastal Plain is located in the western Canadian Arctic between the Mackenzie Delta and the Alaskan border and is characterized by the occurrence of ice-rich permafrost and large massive ground ice bodies. This ice contributes to facilitate coastal erosion, which is known to occur at a pace greater than in temperate regions during the short summer season. Erosion contributes to the release of large amounts of particulate organic carbon to the Arctic Ocean through the export of sediments. Additionally, large amounts of particulate and dissolved organic carbon (DOC) are released by rivers into the Arctic Ocean. Ground ice in permafrost also contains organic carbon in the dissolved state that will also be released to the ocean by coastal erosion, but the amounts of DOC present in the ground and eventually lost to the sea are unknown. It was therefore the objective of this thesis to quantify the amount of DOC present in massive ground ice and the amounts released by coastal erosion into the nearshore zone of the southern Beaufort Sea (Arctic Ocean).

Several massive ground ice bodies and ice wedges, exposed by coastal erosion or thermal denudation, were sampled on Herschel Island and along the mainland coast of the Yukon Territory. In total, 41 samples of ice blocks were obtained from these bodies and analyzed in the laboratories of the Alfred Wegener Institute. DOC concentrations were determined on the melted solutions accompanied by a series of sedimentological and hydrochemical analyses, including ice and sediment content, pH and electrical conductivity. These values were then combined with existing datasets on coastal erosion, morphometry, and stratigraphy to calculate annual DOC fluxes into the Beaufort Sea.

The DOC concentrations measured in massive ground ice bodies and ice wedges ranged between 1.0 and 19.5 mg/L. The calculated DOC stocks ranged between 0.09 and 0.24 g/m³ in massive ground ice for the whole Yukon Coastal Plain. The massive ground ice volume in coastal cliffs along the coastal plain was approximately 11 % and cliff heights ranged between 0.9 and 60.0 m. The average rate of erosion along the coastal stretch was 0.7 m/yr. Calculated DOC fluxes varied greatly, depending on the scenario of the computed DOC

fluxes (25%-quartile, 50%-quartile or 75%-quartile of all conducted DOC measurements). A low-case scenario revealed a DOC flux of 148 kg/yr, a moderate-case scenario yielded 274 kg/yr and a high-case scenario gave a DOC flux of 466 kg/yr for the whole coast.

DOC concentrations in ice wedges were up to eight times higher than in massive ground ice bodies. DOC in ice wedges was assumed to originate mainly from the presence of particulate organic carbon transported into polygon cracks during spring melt. For massive ground ice bodies, the origin of DOC seemed to depend on the genetic nature of the ice, as segregated ice or buried glacier ice. The DOC could have been introduced by water migration through the sediment and the interaction of basal glacier ice with subglacial sediments and/or could have been previously contained in glacier ice.

DOC fluxes from the erosion of massive ground ice at the coast are much lower than both DOC fluxes from arctic rivers and fluxes of particulate organic carbon derived from coastal erosion. However, DOC released by coastal erosion is assumed to be more labile and could therefore be more bioavailable in the nearshore zone.

DOC fluxes from massive ground ice seem to play only a minor role in the carbon budget of the Arctic Ocean. However, pore ice was not considered in this study and is assumed to be a greater source of DOC, because the interaction with the surrounding carbon-rich sediments due to freeze and thaw cycling is much stronger than for massive ground ice bodies.

Kurzfassung

Arktische Regionen reagieren besonders empfindlich auf Klimaänderungen und erfahren derzeit die schnellsten Umweltveränderungen auf der Erde, und zwar in einem Tempo, das voraussichtlich in den kommenden Jahrzehnten zunehmen wird. Veränderungen der Umweltbedingungen haben einen besonders starken Einfluss auf die eisreichen Permafrostküsten im Norden Kanadas, die durch wärmeres Klima, längere eisfreie Perioden arktischer Gewässer und stärkere Stürme erodieren. Die Küstenerosionsraten in der Arktis zählen zu den stärksten weltweit und führen zum Austrag von terrestrischem organischem Kohlenstoff aus dem eisreichen Permafrost in den Arktischen Ozean. Dieser Kohlenstoffeintrag ist möglicherweise in der Lage, die Rückkopplungs-Mechanismen zwischen Klima und Kohlenstoffkreislauf zu verstärken.

Die vorliegende Studie fand in Nordwestkanada entlang der Yukon-Küstenebene statt, die sich zwischen dem Mackenzie Delta und der Grenze zu Alaska erstreckt. Sie besteht aus eisreichem Permafrost, der große massive Grundeiskörper beinhaltet. Austauendes Grundeis in den gefrorenen Lockersedimenten führt zum Stabilitätsverlust der Sedimente und begünstigt Küstenerosion, die während des kurzen Sommers in der Arktis stärker als in gemäßigten Breiten voranschreitet. Durch den Abtrag der Sedimente werden große Mengen an organischem Kohlenstoff in den Arktischen Ozean exportiert. Zusätzlich werden große Mengen an partikulärem (4-6 Tg/a) und gelöstem organischem Kohlenstoff (18-33 Tg/a) durch Flüsse in den Arktischen Ozean eingetragen. Massives Grundeis enthält organischen Kohlenstoff in gelöster Form (DOC), der durch Küstenerosion in den Arktischen Ozean gelangt. Jedoch ist die Menge an DOC in massivem Grundeis, die potenziell in das Meer gelangen könnte, nicht bekannt. Ziel dieser Studie war daher, zum einen die DOC-Konzentrationen in massivem Grundeis zu quantifizieren und zum anderen die jährlichen Austragsraten in den küstennahen Bereich der südlichen Beaufort See infolge von Küstenerosion abzuschätzen.

Mehrere massive Grundeiskörper und Eiskeile, die durch Küstenerosion und thermische Abtragung freigelegt wurden, sind auf *Herschel Island* und entlang der Festlandsküstenebene des Yukon-Territoriums beprobt worden. Insgesamt wurden 41 Eisproben von diesen Eiskörpern genommen und am Alfred-Wegener-Institut in Potsdam analysiert. Die DOC-Konzentrationen wurde an den getauten Eisproben bestimmt und in Bezug zu sedimentologischen (volumetrischer Eis- und Sedimentgehalt) und hydrochemischen Untersuchungen (pH- und Leitfähigkeitsmessungen) gesetzt. Diese Werte wurden anschließend mit existierenden Datensätzen zu Küstenerosion, Morphometrie und

Stratigraphie kombiniert, um den jährlichen Austrag von gelöstem organischem Kohlenstoff in die Beaufort See zu berechnen.

Die Konzentrationen von gelöstem organischem Kohlenstoff, die in massiven Grundeiskörpern und Eiskeilen gemessen wurden, lagen zwischen 1,0 und 19,5 mg/L. Die berechneten Mengen an DOC in massivem Grundeis lagen zwischen 0,09 und 0,24 g/m³ entlang der Yukon-Küstenebene. Der volumetrische Gehalt an massivem Grundeis beläuft sich auf etwa 11 % und die Küstenhöhe liegt zwischen 0,9 und 60,0 m. Die durchschnittliche Erosionsrate beträgt 0,7 m/a. Die berechneten Austräge an DOC variieren stark, abhängig vom Szenario (25%-Quartil, 50%-Quartil oder 75%-Quartil aller DOC-Messungen), das für die Berechnung verwendet wurde. Ein minimales Austragsszenario ergab DOC-Austragsraten von 148 kg/a. Ein mittleres und maximales Austragsszenario ergaben jeweils Austragsraten von 274 beziehungsweise 466 kg/a für die gesamte Yukon-Küstenebene.

Die Konzentrationen von gelöstem organischem Kohlenstoff in Eiskeilen waren bis zu achtmal höher als in massiven Grundeiskörpern. Es wird angenommen, dass DOC in Eiskeilen zum Großteil von partikulärem organischem Kohlenstoff stammt, der während der Schneeschmelze im Frühling in die Frostspalten transportiert wurde. Der in den massiven Grundeiskörper gefundene gelöste organische Kohlenstoff ist vermutlich durch verschiedene Prozesse, abhängig von der Genese des Eiskörpers als Segregationeis oder begrabenes Gletschereis, in die Eiskörper gelangt. Dies vollzog sich zum einen durch Interaktionsprozesse während der Wassermigration durch das Sediment und zum anderen durch Austauschprozesse zwischen basalem Gletschereis und subglazialen Sedimenten. Zudem kann sich Kohlenstoff in gelöster Form bereits zuvor im Gletschereis befunden haben.

Der Austrag von DOC aus massivem Grundeis im Zuge von Küstenerosion ist bei weitem geringer als organische Kohlenstoffausträge durch Flüsse in partikulärer und gelöster Form, sowie Austräge von partikulärem organischem Kohlenstoff durch Küstenerosion. Dennoch wird vermutet, dass DOC, welches durch Küstenerosion ausgetragen wird, einen labilen Charakter aufweist und daher stärker für biogeochemische Stoffumsätze in der küstennahen Zone verfügbar ist.

Die Stoffflüsse von gelöstem organischem Kohlenstoff aus massivem Grundeis scheinen nur eine marginale Rolle im Kohlenstoffhaushalt des Arktischen Ozeans zu spielen. Dennoch ist anzunehmen, dass Poreneis, welches in dieser Studie nicht berücksichtigt wurde, eine sehr viel größere DOC-Quelle ist, da die Austauschprozesse zwischen Porenwasser und kohlenstoffhaltigen Sedimenten bei weitem stärker sind als in massiven Grundeis. Daher werden in kommenden Studien Analysen von Poreneis durchgeführt werden.

1 Introduction

1.1 State of the Art

The Arctic cryosphere is a fundamental component of the earth system. It stores and regulates the release of greenhouse gases and is therefore able to affect and change the global climate conditions (CALLAGHAN 2011). Since the 1800's, a warming trend in summer air temperatures began, that is by far greater than just the recovery from the Little Ice Age (KAUFMAN et al. 2009). From the beginning of the 19th century, there has been a continuous increase in global temperatures (JONES & MOBERG 2003), with most significant trends since the 1980's (ALLEY et al. 2003). From 1980 on, the annual average temperature has been twice as high over the arctic in comparison to the rest of the world (AMAP 2011). Over the past decade, global and arctic temperatures have reached record levels (BARINGER et al. 2010). Climate models predict the strongest temperature increase for the Arctic (KATTSOV & KÄLLÉN 2005), with some models forecasting a warming over land of 7 to 8°C by the end of the 21st century (IPCC 2007). Air temperatures in the Arctic will continue to rise faster than elsewhere in the world. Temperatures of 3 to 6°C warmer than today will have a strong impact on permafrost, which continues to thaw across vast areas (AMAP 2011, UNEP 2012). This temperature increase could result in an irreversible loss of 30 to 85 % of the near-surface permafrost, which is connected with a release of carbon dioxide between 43 to 135 Gt by 2100 (UNEP 2012). Changing global climatic conditions directly impact the arctic environmental system. According to contemporary arctic reports (AMAP 2011, FORBES et al. 2011), increasing temperature can cause significant changes in the Arctic such as:

- decline of sea-ice extent
- melting of ice caps and small glaciers
- thermal expansion of oceans
- thawing of permafrost
- influx of warm water into the Arctic Ocean

These in turn, could trigger or amplify processes in the Arctic at different scales, including:

- rise in sea-level
- longer open water seasons
- release of greenhouse gases from thawing permafrost
- occurrence of thermokarst
- stronger effects of storms on permafrost coasts
- changes of sediment and nutrient pathways into the nearshore zone

Alongside the physical and ecological consequences, cultural and socio-economical systems can also be strongly affected (MCGUIRE et al. 2009). The danger of permafrost degradation on infrastructure is well known, affecting buildings, streets, railroads, energy-, gas- and oil supply as well as industries and communication facilities (COUTURE et al. 2000, U.S. ARCTIC RESEARCH COMMISSION 2003, LANTUIT & SCHIRRMESTER 2011). The coast of the Arctic Ocean crystallizes many of the issues outlined above (FORBES et al. 2011, SCHAEFER et al. 2012). Coastal erosion leads to the destruction of extensive stretches of coast composed of ice-rich permafrost (LANTUIT et al. 2012). For this reason, cultural features, industrial or municipal infrastructure are at risk of destruction by incoming waves, like at the coastal community of Tuktoyaktuk (JOHNSON et al. 2003) or on Herschel Island, a cultural heritage site affected by erosion and sea level rise (LANTUIT & POLLARD 2008).

The coastal permafrost system is particularly vulnerable to changing environmental conditions. The following aspects play an important role in responding to environmental changes or driving the resulting consequences:

- Coastal erosion
- Organic carbon stocks
- Organic carbon fluxes
- Ground ice

Coastal erosion

Recent environmental changes have a strong impact on permafrost coasts (LANTUIT et al. 2012) and their sensitivity to erosion (SHAW et al. 1998, JONES et al. 2008, JONES et al. 2009b, COUTURE 2010, FORBES et al. 2011), especially due to the fact that 65 % of the arctic coastline consists of unconsolidated material (LANTUIT et al. 2012).

Since the 1950's, considerable research effort was made on Arctic coastal systems in Canada (e.g. MACKAY 1959, MCDONALD & LEWIS 1973, LEWIS et al. 1975, FORBES & FROBEL 1985, MACKAY 1986, FORBES & TAYLOR 1994). During the 1970's and 1980's, many studies were conducted, that were driven by engineering and regulatory requirements associated with offshore hydrocarbon exploration, and focused on shoreline sensitivity and coastal hazards in the southern Canadian Beaufort Sea (COUTURE 2010).

More recent studies have concentrated on the impact on heritage sites or community infrastructure (FORBES 1989, JOHNSON et al. 2003, FORBES et al. 2011). These studies resulted in a good knowledge of the rates of erosion along the coast and hence of the amount of sediment delivered to the Arctic Ocean.

First detailed erosion rates for the entire Yukon Coast were provided by MCDONALD & LEWIS (1973), who used aerial photographs from the 1950's and 1970's (HARPER et al. 1985b, HARPER 1990). They found wide-scale regional retreat with an average erosion rate of approximately 1.0 m/yr. More recent work was done by SOLOMON (2005), who calculated average coastal retreat rates of 0.6 m/yr for the time period from 1972 to 2000 for the southern Mackenzie Delta. A subsequent investigation by LANTUIT & POLLARD (2008), based on aerial and satellite imagery, determined erosion rates of 0.45 m/yr for the time period of 1970 to 2000 at the coast of the southern Beaufort Sea. Considering high local and regional variability, the average rate of coastal erosion for the whole arctic coastline is 0.5 m/yr. Alongside the Laptev and East Siberian Sea, coastal erosion rates in the Beaufort Sea rank among the highest on a circum-arctic scale (LANTUIT et al. 2012).

Recent research attempted to quantify material fluxes from coastal erosion. COUTURE (2010) calculated particular organic carbon (POC) fluxes of 0.04 Mt/yr and sediment fluxes of 2.66 Mt/yr, with an average coastal erosion rate of 0.7 m/yr for the Yukon Coastal Plain. These numbers are likely to increase, along with rates of coastal erosion in the Arctic, as some studies and reports indicate (RACHOLD et al. 2005a, AMAP 2011, LANTUIT et al. 2012, UNEP 2012).

Arctic coasts are subject to extensive coastal erosion. In some regions a significant correlation between frequency and intensity of storms, the duration of the open-water season and coastal erosion has already been documented (SOLOMON 2005, MANSON & SOLOMON 2007, OVEREEM et al. 2010), showing that erosion occurs mostly during extreme storm events (SOLOMON & COVILL 1995, ATKINSON 2005). Numerical model forecasts predict an increase in storm intensity (LAMBERT 1995), as well as an increase in the length of the open water season, especially in late summer and fall, the period during which the influence on coastal retreat is the strongest (MCGILLVRAY et al. 1993, ATKINSON 2005).

Organic carbon stocks

There are substantial organic carbon stocks in Arctic permafrost, but there are still many knowledge gaps associated with the amount of organic carbon contained in permafrost (MCGUIRE et al. 2009, STRAUSS et al. 2012). The estimated size of the permafrost carbon stock varies (STRAUSS et al. 2012), depending on the region under consideration and the depth of permafrost sediments considered. Much of the organic carbon in contemporary permafrost has been stored in the sediment column for millennia and could be released if permafrost thaws (OECHEL et al. 1993, GUO & MACDONALD 2006a, PETRONE et al.

2006, BOCKHEIM & HINKEL 2007) due to climate warming (SHUR & JORGENSEN 2007) or local degradation (HINZMAN et al. 2003, DOUGLAS et al. 2008, FORTIER et al. 2007).

Estimates of the global stock of soil organic carbon vary considerably. In the last decades the expected amount of soil organic carbon on a circum-arctic scale changed dramatically (MCGUIRE et al. 2009). In the 1980's, around 190 Gt organic carbon were expected in permafrost (POST et al. 1982), whereas studies at the beginning of the 20th century assumed 455 Gt (ANISIMOV & RENEVA 2006) or 900 Gt (ZIMOV et al. 2006b). Contemporary studies provide values with an organic carbon content of 1627 Gt (TARNOCAI et al. 2009). This carbon can be mobilized by thawing of permafrost and can become available for the carbon cycle by different pathways.

Organic carbon fluxes

Terrestrial organic carbon enters the Beaufort Sea in form of dissolved and particular organic carbon (DOC and POC) due to coastal erosion and river discharge. Table 1.1 summarizes these fluxes, which are complemented with known total organic carbon (TOC) fluxes.

For the Beaufort Sea, DOC fluxes from coastal erosion are 0.0018 Mt/yr, estimated by JORGENSEN & BROWN (2005) for the Alaskan Beaufort Sea. Organic carbon fluxes in form of POC (0.04 Mt/yr) have been calculated by COUTURE (2010) for the Yukon Coastal Plain. TOC fluxes have been estimated for the Alaskan Beaufort Sea and range between 0.15 Mt/yr (PING et al. 2011) and 0.18 Mt/yr (JORGENSEN & BROWN 2005). On a circum-arctic scale, no estimates of DOC and POC fluxes by coastal erosion have been derived so far. However, TOC fluxes of 6.7 Mt/yr have been estimated for the whole Arctic (RACHOLD et al. 2004 and r.w.).

DOC fluxes from Arctic rivers into the Beaufort Sea are better documented, especially for the Mackenzie River, where DOC fluxes range between 1.3 Mt/yr (MACDONALD et al. 1998), 1.4 Mt/yr (RAYMOND et al. 2007), and 1.7 Mt/yr (MCGUIRE et al. 2009). By incorporating DOC fluxes from smaller arctic rivers, like the Sag, Kuparuk and Colville, the DOC fluxes are 1.9 Mt/yr for the Beaufort Sea. POC fluxes from these rivers were summarized by RACHOLD et al. (2004) and r.w. with 2.15 Mt/yr. TOC fluxes of 4.1 Mt/yr yielding into the Beaufort Sea are documented for the Mackenzie River (RACHOLD et al. 2004). By incorporating smaller Alaskan and Canadian rivers, TOC fluxes are approximately 4.3 Mt/yr (RACHOLD et al. 2004 and r.w.). Circum-arctic DOC fluxes stemming from river discharge are relatively well known, ranging from 18.0 to 26.0 Mt/yr (DITTMAR & KATTNER 2003) and 33.0 Mt/yr (MCGUIRE et al. 2009). POC fluxes range between 4.0 to 6.0 Mt/yr (DITTMAR & KATTNER 2003) and TOC fluxes between 30.0 Mt/yr (RACHOLD et al. 2004) and 34.0 to 39.0 Mt/yr (MCGUIRE et al. 2009).

The transport and fate of dissolved organic carbon (DOC) released into the Arctic Ocean from land stocks is an important component of the Arctic carbon system that influences the global carbon cycling in the context of environmental changes significantly (SHAVER et al. 2000, NEFF & HOOPER 2002, COOPER et al. 2005). In comparison to POC stocks in peat and mineral soils, these amounts are small, but DOC is chemically labile (HOOD et al. 2009, WOODS et al. 2011, CORY et al. 2013) and may directly enter the food web or is quickly mineralized and returned to the atmosphere (BAUER & BIANCHI 2011). Intensified coastal erosion will lead to enhanced organic carbon fluxes into the Arctic Ocean (COUTURE 2010). Besides the fact that DOC fluxes from coastal erosion are unknown, the fate of DOC in the arctic near shore zone is enigmatic, as it is only subject to a few investigations (e.g. RACHOLD et al. 2000, DITTMAR & KATTNER 2003, RACHOLD et al. 2004). Values derived by DITTMAR & KATTNER (2003) were based on studies by TELANG et al. (1991), MACDONALD et al (1998), OPSAHL et al. (1999), LOBBES et al. (2000) and KÖHLER et al. (2003). The estimation of MCGUIRE et al. 2009 is based on a study by FINLAY et al. (2006).

Table 1.1: Organic carbon fluxes into the Beaufort Sea and the Arctic Ocean by coastal erosion and river discharge, modified after RACHOLD et al. (2004) and MCGUIRE et al. (2009).

	DOC flux [Mt/yr]	POC flux [Mt/yr]	TOC flux [Mt/yr]
Coastal erosion			
Beaufort Sea	0.0018	0.04	0.15 - 0.18
Total Arctic	-	-	6.7
River discharge			
Beaufort Sea	1.9	2.15	4.1
Total Arctic	18.0 - 33.0	4.0 - 6.0	30.0 - 39.0

Ground ice

Contemporary and future organic carbon fluxes depend on the composition and properties of the coast, and in particular its ground ice contents, as these govern the susceptibility to erosion. Several studies have shown a strong relationship between ground ice volume and erosion (DALLIMORE et al. 1996, WOLFE et al. 2001, LANTUIT & POLLARD 2008). In arctic coastal lowlands of Eurasia and North America ground ice can occupy a large proportion of the soil volume, with volumetric contents up to 90 % in coastal cliffs, which erode at rates up to 10.0 m/yr (LANTUIT et al. 2012). The southern Beaufort Sea region is one of the most ice-rich areas in the Canadian Arctic, with widespread massive ground ice (MACKAY 1966, POLLARD & FRENCH 1980, RAMPTON 1982, POLLARD 1990, LANTUIT & POLLARD 2005).

Only a few investigations have been attempted to calculate the importance of ground ice contribution to arctic carbon and nutrient budgets (DALLIMORE et al. 1996, WOLFE et al. 1998, COUTURE 2010, FRITZ et al. 2011a). No survey has so far provided values for the contribution of DOC contained in ground ice (nearly 30 % of the frozen ground along the Canadian Beaufort Sea) to the nearshore carbon budget (LANTUIT et al. 2012). Permafrost organic carbon stock quantifications usually subtract ground ice contents and disregard the organic carbon stored in massive ground ice. However, recent analysis from ice wedges yielded DOC concentrations between 1.6 and 28.6 mg/L (FRITZ et al. 2011a) and analysis of thermokarst cave ice gave DOC values of 8.7 up to 613.6 mg/L (DOUGLAS et al. 2011).

According to these assumptions, considerable amounts of DOC are expected to be stored in massive ground ice that is released by coastal erosion into the Arctic Ocean (FRITZ et al. 2011a). Consequently, the biogeochemistry and preservation history of frozen soils with may become highly significant for the future Arctic carbon cycle (DOUGLAS et al. 2011). This study provides first estimates of DOC fluxes from massive ground ice by coastal erosion.

Synthesis

Given the enormous stocks of organic carbon in northern high latitude and the equally enormous coastal erosion rates, the response of the carbon cycle of the Arctic to changes in climate, and specifically to the release of fresh organic carbon to the Arctic Ocean, is a major issue of global concern (ACIA 2004, 2005, MCGUIRE et al. 2006, AMAP 2011). The sensitivity of high latitude environments to global climate change has led researchers to speculate that changing temperatures in the Arctic will have a considerable impact on carbon cycling (FREY & SMITH 2005, STRIEGL et al. 2005, HOLMES et al. 2008). The changes in Arctic environmental systems may be irreversible on century time scales (CURRY et al. 1996, CHAPIN et al. 2005, MCGUIRE & CHAPIN 2006). Permafrost carbon release could lead to significant warming, even under less intensive emission projections (MACDOUGALL et al. 2012). The release of carbon stored in permafrost showed already 50 million years ago that it can trigger dramatic changes in the earth climate system (DeCONTO et al. 2012). Hence, there is a need to improve the understanding of the links between permafrost carbon and climate, and specifically to determine the contribution of dissolved organic carbon from coastal erosion (FRITZ et al. 2011, VONK et al. 2012).

1.2 Aims & Objectives

The purpose of this study is to calculate and update the carbon fluxes released by coastal erosion into the arctic near shore zone with specific regard to dissolved organic carbon (DOC) and its concentrations in massive ground ice. This goal leads to the following research questions:

- What amount of DOC is stored in massive ground ice and where it originates from?
- How much of the measured DOC from massive ground ice could be released (DOC flux) into the Beaufort Sea (Arctic Ocean) by coastal erosion?
- What role does the DOC play in the near-shore zone?

Stemming directly from these research questions the main objectives of this thesis are as follows:

- to determine the DOC concentrations in massive ground ice and
- to estimate the DOC fluxes into the nearshore zone.

1.3 Project framework

This thesis shall answer the research questions and objectives outlined above by focusing on the Yukon Coast in the southern Canadian Beaufort Sea. Since 1998 processes, along the arctic permafrost coasts are subject to investigations of the Alfred Wegener Institute for Polar- and Marine Research (AWI) in the Laptev Sea. In 2003, a research partnership on erosional processes in the Beaufort Sea was established between the AWI and the McGill University in Montréal. Both these activities are embedded into long-term international monitoring and research programs that have been initiated to investigate the changes of arctic permafrost coasts and are planned and coordinated by the AWI in Potsdam. The COPER project, which stands for “COastal Permafrost ERosion, organic carbon and nutrient release to the arctic nearshore zone”, is a scientific program investigating the pace and nature of sediment and organic matter transfer in the arctic coastal zone along the Yukon Coastal Plain and is the latest emanation of the German-Canadian partnership established in 2004. It focusses on recent coastal erosion in the southern Canadian Beaufort Sea and attempts to provide quantitative answers on the release of organic carbon by coastal erosion. The content of this master thesis is part of this project.

2 Geographical and geological background

2.1 The periglacial environment

The term “periglacial” was introduced by VON LOZINSKI (1909) to describe climatic and geomorphic conditions of areas peripheral to ice sheets. More recently, this term is used in the context of process description of cold, non-glaciated regions, independent of their proximity to glaciers and ice sheets (VAN EVERDINGEN 1998, FRENCH 2007). This environment is characterized by two major criteria, the presence of perennally frozen ground (i.e. permafrost) and frost action processes in association with water (HEGINBOTTOM et al. 2012). Typical frost processes that form the periglacial landscape are freeze and thaw cycles including frost cracking, frost heave and material sorting (FRENCH 2007).

2.2 Permafrost

Permafrost is defined as ground material (soil or rock and included ice and organic material), that remains at or below 0°C for at least two consecutive years (HARRIS et al. 1988, VAN EVERDINGEN 1998). The Earth’s land surface is underlain by approximately 25 % of permafrost (ZHANG et al. 1999). In Russia, about 65 %, in Canada about 50 % and in Alaska about 80 % of the land area is affected by permafrost (Figure 2.1). Besides the high latitude landscapes, sub-sea permafrost on the continental shelves of the Arctic Ocean and alpine permafrost areas are included (ROMANOVSKY et al. 2007). A negative heat balance at the surface between ground temperature and surface temperature is responsible for the thickness and growth of permafrost (POLLARD 1998). The heat balance is in turn controlled by air temperature and the geothermal gradient (FRENCH 2007). The most important environmental factors determining permafrost conditions are the regional climate, the topographic features, and the sediment composition and its moisture content (WASHBURN 1979). According to these parameters, permafrost can be classified into three major zones (Figure 2.1).

Continuous permafrost, that covers 90 to 100 % of an area, is detectable in high latitudes. The mean annual temperatures are smaller than or equal -8°C, supporting active formation of frozen ground. Mostly, a thin snow cover prevents isolation effects favorable for permafrost that either is actively aggrading or is in freeze-thaw equilibrium. In general, the genesis of continuous permafrost took place during and after the last glaciation (FRENCH 2007).

Discontinuous permafrost occurs towards lower latitudes and makes up 50 to 90 % of an area, which is separated by unfrozen ground. These unfrozen parts are mostly relic or in

process of degradation. It is mainly younger than continuous permafrost and formed within the last several thousand years.

Sporadic and isolated permafrost occupies 10 to 50 % of an area and is characterized predominantly by single patches of frozen ground separated by unfrozen ground. These areas are subject to advanced processes of degradation (WEISE 1983, FRENCH 2007, ROMANOVSKY et al. 2007).

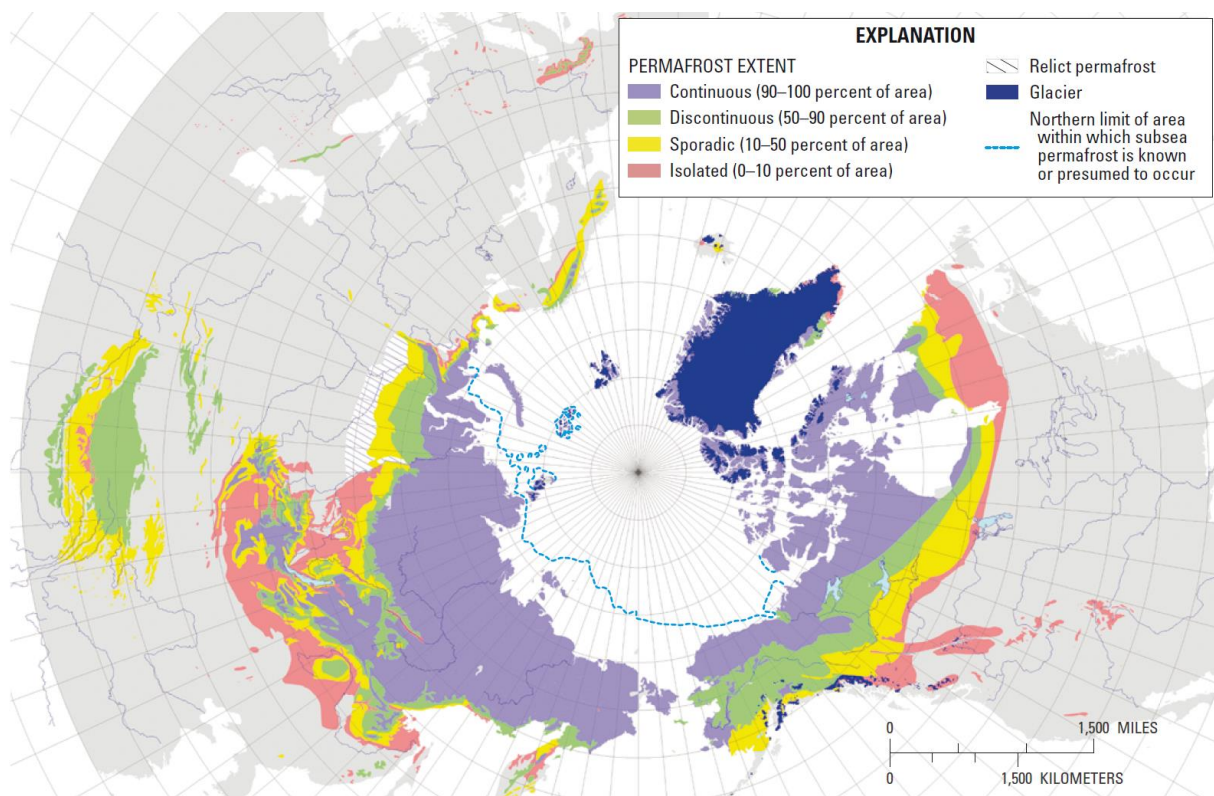


Figure 2.1: Permafrost map of the Northern Hemisphere, based on BROWN et al. (1997) in HEGINBOTTOM et al. (2012).

Permafrost is covered with an uppermost ground layer, known as “active layer”. This layer is exposed to periodic (decadal, seasonal or daily) cycles of freezing and thawing, depending on climate and weather conditions (FRENCH 2007). The active layer thickness can vary significantly from year to year and between locations (Figure 2.2) depending on the interaction of the control factors mentioned above. Between the active layer and the permafrost table, a transient layer is situated that can freeze or thaw on decadal and/or century timescales (FRENCH & SHUR 2010).

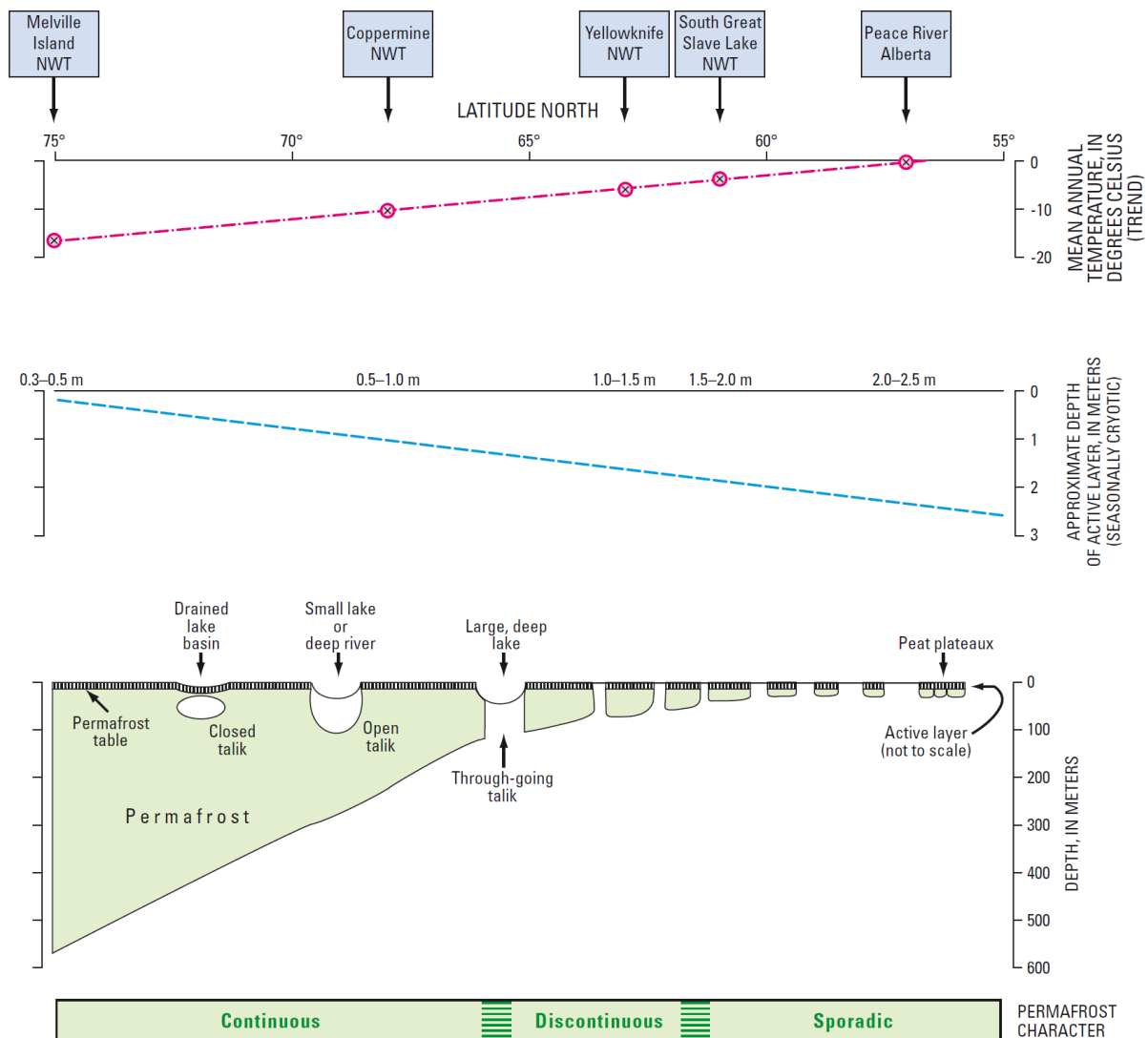


Figure 2.2: Idealized latitudinal distribution of permafrost characteristics from northwestern Canada, modified by BALLANTYNE & HARRIS (1994) in HEGINBOTTOM et al. (2012).

2.3 Ground ice

The main feature of permafrost in polar lowlands is the occurrence of ground ice that can comprise up to 50 % of the near-surface volume (MACKAY 1971), with extreme values up to 90 %. The mechanical strength of permafrost including ground ice is comparable with bedrock and contributes mainly to the stability of the Arctic ecosystem (ROMANOVSKY et al. 2007). Ground ice is defined as all types of ice formed in freezing and frozen ground (HARRIS et al. 1988). After MACKAY (1972b), it can be classified into four types: pore ice, segregated ice, vein ice, and intrusive ice. According to the origin of water prior to freezing and the water transfer process towards the freezing front, MACKAY (1972b) established ten classes of ground ice, where buried ice (glacier ice, snow bank ice, sea ice, river ice and lake ice) was excluded. To incorporate these ice features into existing classifications, MACKAY (1989) added a classification of massive ground ice (Figure 2.3). After HARRIS et al. (1988)

massive ground ice is a large mass of ground ice with a gravimetric water content exceeding 250 %.

In this study mainly two types of ground ice were investigated, massive ice bodies and ice wedges (vein ice) that are both after definition massive ground ice. According to the classification of MACKAY (1989), see Figure 2.3, massive ice bodies can be buried or intra-sedimental ice and ice wedges are intra-sedimental ice. Intra-sedimental ice is defined as ice bodies that originate from ice segregation (FRENCH 2007). In comparison to that, pore ice is ubiquitous, wherever moisture within permafrost occurs. The distinction between pore and segregated ice is related to the water content of the soil. The genesis of massive ground ice, especially from ice wedges is well studied (FRENCH 2007), whereas the question of the formation of massive ground ice cannot be entirely solved (FRITZ et al. 2011b, HEGINBOTTOM et al. 2012). Massive ice bodies are thick and broad ice lenses which can be more than ten meters thick with a horizontal extent of up to hundreds of meters (HEGINBOTTOM et al. 2012). Massive ice bodies are widespread in lowlands of the arctic coastal regions. Depending on its cryostratigraphical and geochemical characteristics, massive ice bodies can be assigned to different genesis, either as buried ice or as intra-sedimental ice (Figure 2.3).

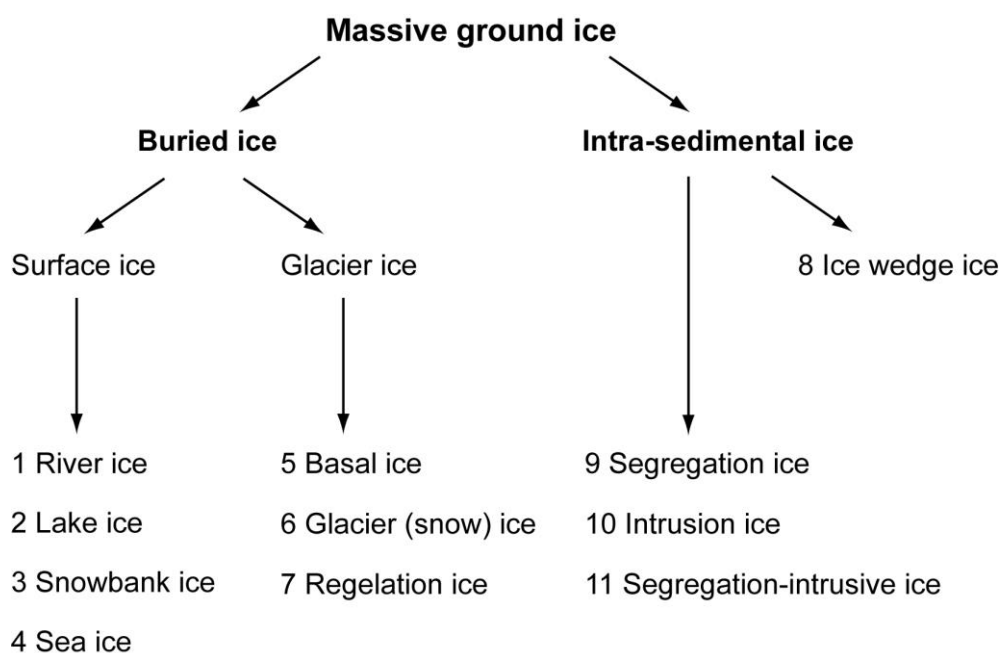


Figure 2.3: Classification of massive ground ice, modified after MACKAY (1989) in FRENCH (2007).

Ice wedge growth occurs during winter when thermally induced cracking of the ground causes vertical contraction cracks. In spring, meltwater from snow fills the cracks and forms single ice veins. From year to year, repeated cracking at the same place and filling with meltwater leads to the growth of the ice wedge (LACHENBRUCH 1962, MACKAY 1972b),

which is illustrated in Figure 2.4. Ice wedges form in two ways, syngenetically or epigenetically. Syngenetic ice wedges form at the same time with the accumulating sediment and a rising permafrost table. Epigenetic ice wedges form in already existing permafrost ground (FRENCH 2007).

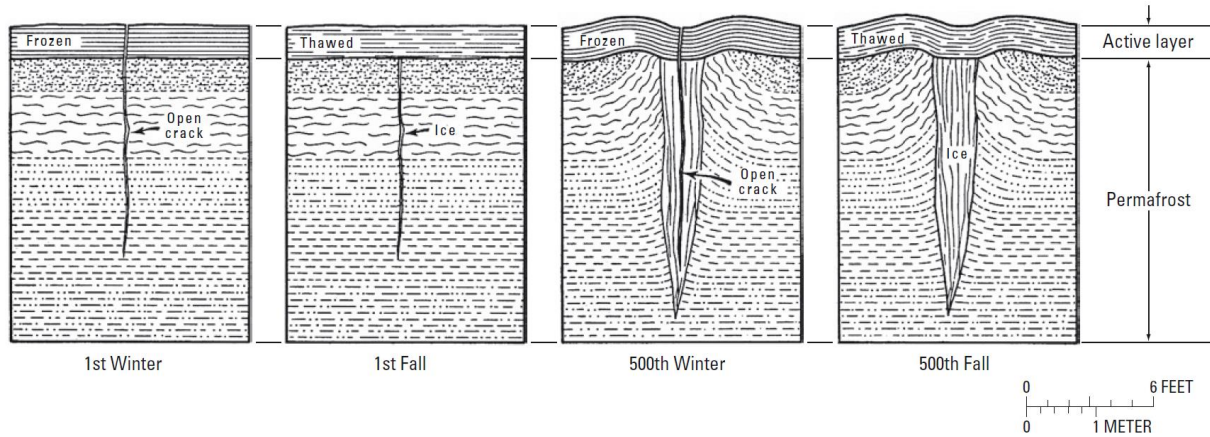


Figure 2.4: Idealized scheme of the evolution of an ice wedge, modified after LACHENBRUCH (1962) in HEGINBOTTOM et al. (2012).

2.4 Thermokarst and coastal erosion

The term thermokarst was first introduced by ERMOLAEV (1932) to describe the irregular terrain along the Siberian coastal lowlands. It defines the morphology of a surface area that formed by the melting of ground ice (ERMOLAEV 1932) due to disturbance of the thermal equilibrium of permafrost (FRENCH 2007). The term thermokarst applies to processes related with ground ice that lead to the instability of the ground surface (FRENCH 2007). Thermokarst forms wherever ice-rich permafrost thaws. With thawing permafrost surface subsidence starts (HEGINBOTTOM et al. 2012). An increasing active layer depth and thawing permafrost modifies the surface morphology profoundly. Thawing of permafrost with high ground ice contents can lead to massive surface subsidence along with the formation of characteristic thermokarst depressions (ULRICH et al. 2010). Thaw subsidence occurs by slow thawing in combination with drainage of meltwater (FRENCH 2007). Thermal erosion occurs on slopes where melting of exposed ground ice leads to the development of a steep slope face that retreats laterally. There are various reasons that lead to enhanced thermokarst processes, e.g. changing climate, lack of vegetation cover, fires, shifts of drainage channels, or human activities (GROSSE et al. 2011).

Very common expressions of thermal erosion are retrogressive thaw slumps (POLLARD 2005), which are subject of investigations in this study. Retrogressive thaw slumps are one of the most dynamic thermo-erosional landscape features in permafrost-affected environments (FRENCH 2007) and develop when massive ground ice bodies, underlying the ground

surface, become exposed due to terrain disturbance. Bowl-shaped thaw-structures are developing by backwasting of exposed ice-rich sediments. These structures can reach dimensions of up to 0.5 km inland and 1.0 km parallel to the coastline (LANTUIT & POLLARD 2008) or river banks. Retrogressive thaw slumps consist of three main elements (LEWKOWICZ 1987, DE KROM 1990), visible in Figure 2.5. The first element is a vertical or sub-vertical headwall (Figure 2.5 B), consisting of the active layer and ice-poor materials. In some cases 15 to 20 m of ice is exposed, depending on the thickness of the debris accumulating on the base of the headwall. The second element is a headscarp within the headwall (Figure 2.5 C). The angle of the headscarp varies between 20 and 50° and retreats by the ablation of ice-rich materials due to sensible heat fluxes and solar radiation. The third element is the slump floor (Figure 2.5 A), which is a mudflow that expand in a lobe pattern at the toe of the slump (LEWKOWICZ 1987, DE KROM 1990). At ice-rich coastal cliffs, thaw slumps are initiated by wave action and/or by active layer detachments. Active layer detachments occur on almost planar surfaces right up to steep slopes and are characterized by the downslope movement of seasonally thawed supersaturated material (DE KROM 1990). If massive ice melts faster than the coast retreats, a retrogressive thaw slump is initiated (LEWKOWICZ 1987).

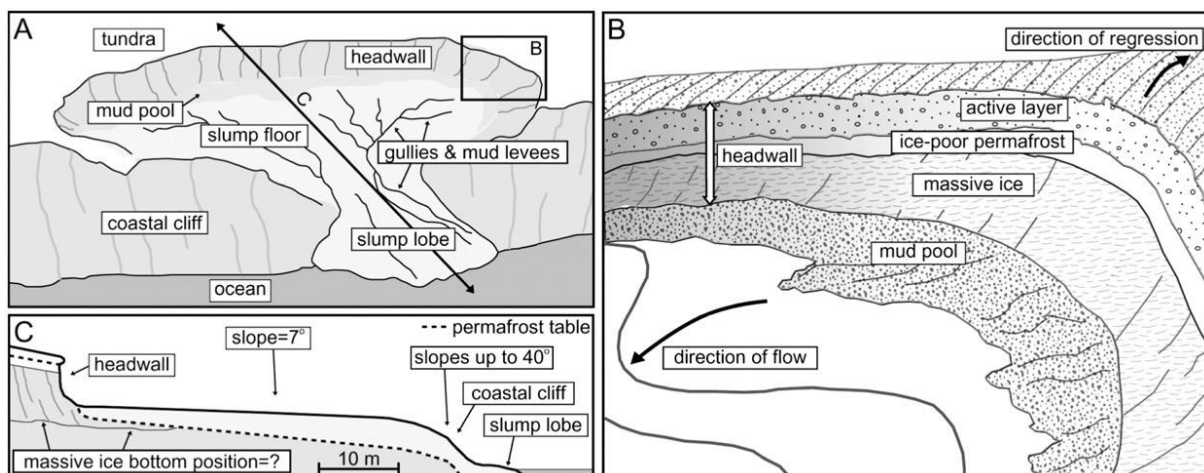


Figure 2.5: Scheme of a retrogressive thaw slump (A) with focus on the slump headwall (B) and a cross-section (C), in LANTUIT & POLLARD (2008).

Coastal retreat in the Arctic is well documented and an issue of major concern in recent scientific investigations (FORBES et al. 2011, LANTUIT et al. 2012). The coast is a key interface in the arctic environment (FORBES et al. 2011) and the interface of land-ocean interactions (RACHOLD et al. 2005a). In the Russian Arctic, measurements had been carried out for decades at various locations (VASILIEV 2003), whereas long-term records in the Canadian Arctic are rare (LANTUIT & POLLARD, 2008). For the first time, the Arctic Coastal Dynamics (ACD) Project provided a first circum-arctic assessment of coastal erosion

measurements. Arctic coastlines are highly variable and its dynamic character is controlled by environmental forcing (e.g. wind, wave action, sea-level changes, sea ice), geology, permafrost and its ground ice content as well as coastline morphometry (RACHOLD et al. 2005a). Environmental forcing triggers coastal processes like sediment transport and the degradation of permafrost by waves, currents and sea ice (Figure 2.6). During winter (7 to 9 months), a persistent sea-ice cover protects the coastline from waves and currents. In the ice-free season, which is only a minor part of the whole year, permafrost along the coast is rapidly eroded at rates of several meters per year (RACHOLD et al. 2005a). Storms, which are the main driver of erosion, occur throughout the year but have its strongest impact during the ice-free season (ATKINSON 2005). Besides the temporally variable coastal retreat, coastal erosion is also spatially highly variable due to variations in the (cryo)-lithology and geomorphology of coastal cliffs (SOLOMON 2005, JONES et al. 2008, LANTUIT & POLLARD 2008). Higher ground ice volumes support the thermal abrasion process (ARÉ 1988) as the coastal zone is more susceptible to erosion with melting of ground ice (HEQUETTE & BARNES 1990, KOBAYASHI et al. 1999), whereas higher cliffs protect the coastline to further erosion (LANTUIT et al. 2012)

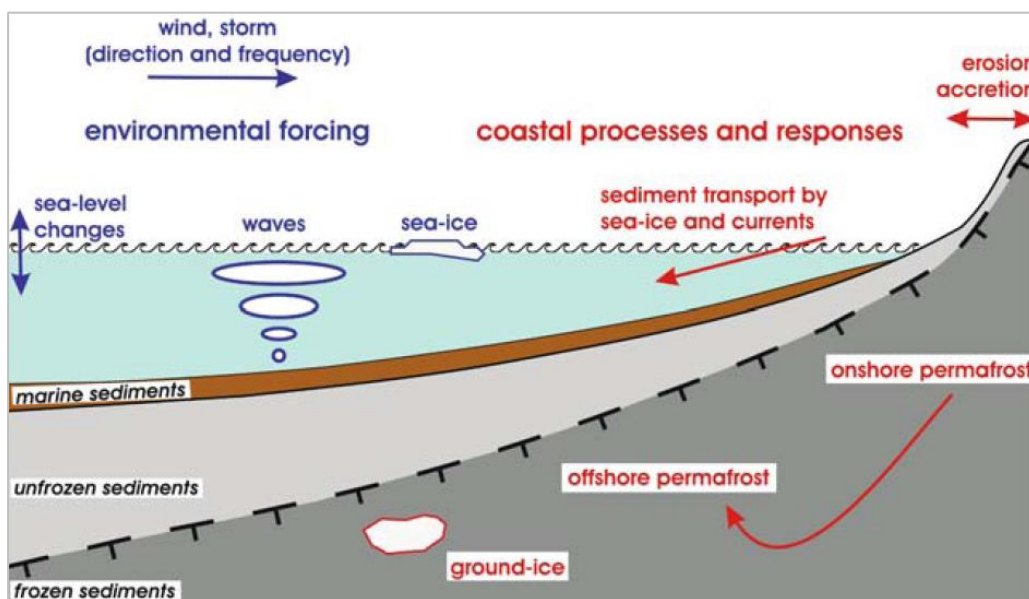


Figure 2.6: Environmental forcing processes and coastal processes and responses at arctic permafrost coasts, in RACHOLD et al. (2005a).

2.5 Dissolved organic carbon and the Arctic organic carbon cycle

Dissolved organic carbon (DOC) is defined as all organic compounds in solution smaller than $0.45\ \mu\text{m}$ (THURMAN 1985, POTTER & WIMSATT 2012) and describes the mass of organic carbon in dissolved state. The particle size and weight spectrum of DOC partly overlap with that of colloidal compounds (BLUME et al. 2010), visible in Figure 2.7. DOC is composed of various organic molecules and can be separated qualitatively into several fractions: humic substances, hydrophilic acids, and neutral compounds, like sugars, alcohols and ketones (Figure 2.7). The majority of dissolved organic carbon compounds on a molecular level (50 to 75 %) are composed of polymeric organic acids, called humic substances. The remaining part consists of fulvic acids and colloidal organic matter. The colloidal part consists of larger aggregates of humic acids and is commonly associated with clay minerals or oxides of iron and aluminum. DOC mainly originates from the leaching of humic substances from plants and soil organic matter (THURMAN 1985). Concentrations of DOC vary between different water types. In ground water a median DOC concentration of $0.7\ \text{mg/L}$, ranging from 0.2 to $15.0\ \text{mg/L}$ is common (LEENHEER et al. 1974, BARCELONA 1984). In interstitial waters of soil, DOC concentrations can range from 2.0 to $30.0\ \text{mg/L}$. DOC concentrations in snow and glacial water are slightly lower with 0.1 to $5.0\ \text{mg/L}$ (THURMAN 1985).

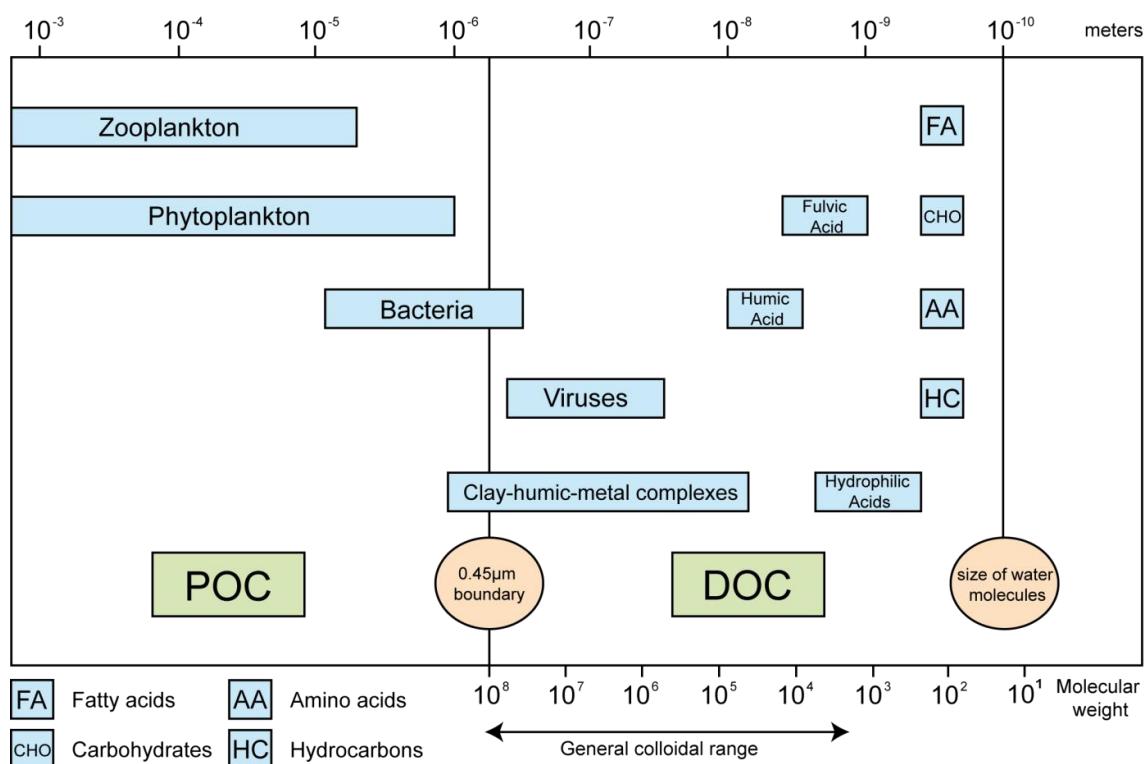


Figure 2.7: Continuum of dissolved organic carbon in natural waters, modified after THURMAN (1985).

Dissolved organic carbon is a substantial component of the global carbon cycle (HANSELL & CARLSON 2001, HEDGES 2002), which globally matches the amount of carbon in the atmosphere (AMON 2004). The Arctic carbon cycle consists of three major elements, the terrestrial part, the marine part and the atmosphere (Figure 2.8). The major reservoirs of organic carbon within land systems are contemporary terrestrial biomass, fossil terrestrial biomass or soil humus, and fossil kerogen from uplifted marine sedimentary rocks (BAUER & BIANCHI 2011). Organic carbon, in form of particular organic carbon (POC) and dissolved organic carbon (DOC), is transferred especially by river discharge and coastal erosion from Arctic land stocks to Arctic Ocean stocks. Once the organic carbon enters the Arctic Ocean it is either subject to bacterial degradation in the water column, buried in sediments or exported offshore.

If organic carbon is transported offshore it can be fractionally incorporated into Pacific and Atlantic water masses that enter and leave the Arctic Ocean by passing the Bering and/or the Fram Strait (MCGUIRE et al. 2009).

River discharge and coastal erosion are mainly responsible for the transfer of organic carbon in form of POC and DOC from the terrestrial to the marine system (RACHOLD et al. 2004, RACHOLD et al. 2005a) and substantially influence the carbon budget of the Arctic Ocean (MEYBECK 1982, ANDERSON et al. 1998, STEIN & MACDONALD 2004). The riverine transport of organic carbon is a major component of the global carbon cycle. The drainage basin of the Arctic ($\sim 24 \times 10^6 \text{ km}^2$) receives nearly 11 % of the global runoff (LAMMERS et al. 2001). Carbon fluxes from circum-arctic watersheds are therefore a key connection between the terrestrial and the marine components of the carbon cycle (GUO et al. 2007). Approximately 10 % of the global terrigenous DOC is delivered from arctic rivers to the Arctic Ocean (OPSAHL et al. 1999) and produces DOC concentrations in coastal waters that are twice as high as the corresponding concentrations in the Atlantic and Pacific Oceans (CAUWET & SIDOROV 1996).

Besides river discharge a huge amount of organic carbon is delivered by coastal erosion, mostly in form of POC. In total, the entry of POC to the Arctic Ocean from coastal erosion is equivalent to that from rivers (STEIN & MACDONALD 2004). The interactions of carbon cycling processes with changes in atmospheric CO_2 , climate, permafrost dynamics, and disturbance regimes (e.g. fire, logging) contribute to this complexity and makes it sensitive for predicted environmental changes (MCGUIRE et al. 2009). Even small changes in the oceanic dissolved organic carbon pool could lead to significant perturbations of the global carbon cycle on time scales of 1,000 to 10,000 years (HEDGES 1992, 2002, AMON 2004).

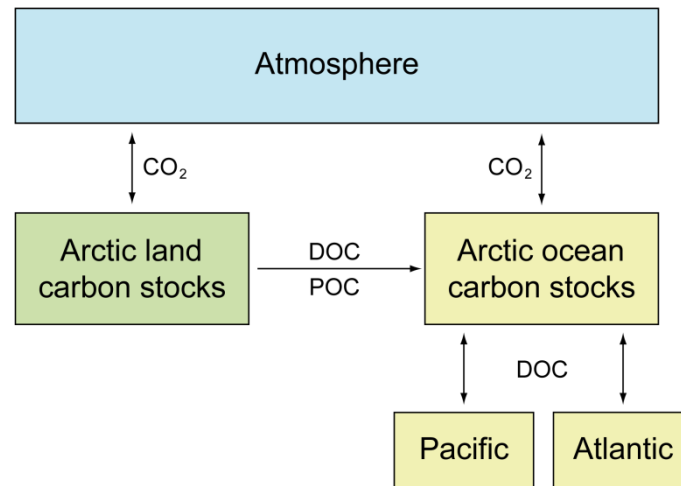


Figure 2.8: Dissolved organic carbon as major part of the Arctic carbon budget, modified after MCGUIRE et al. (2009).

2.6 Study area and regional setting

2.6.1 Yukon Coastal Plain

The Yukon Coastal Plain (Figure 2.9) is a landward expansion of the Beaufort Shelf (SMITH 1989) stretching approximately 300 km along the Canadian Beaufort Sea with a width of around 24 km (BOUCHARD 1974) from the Mackenzie Delta in the east to the Alaskan boarder in the west (RAMPTON 1982). It includes all flat and gently sloping land north of the Richardson, Barn and British Mountains and extends 80 km offshore onto the continental shelf up to a depth of about 100 m (BOSTOCK 1970). The Mackenzie Trough, north-east of Herschel Island, and Herschel Basin, south-east of Herschel Island, are the only depressions interrupting the otherwise gentle surface on the shelf. Herschel Island is part of the Yukon Coastal Plain and was connected to the mainland when sea level was lowered (RAMPTON 1982, BURN 2009).

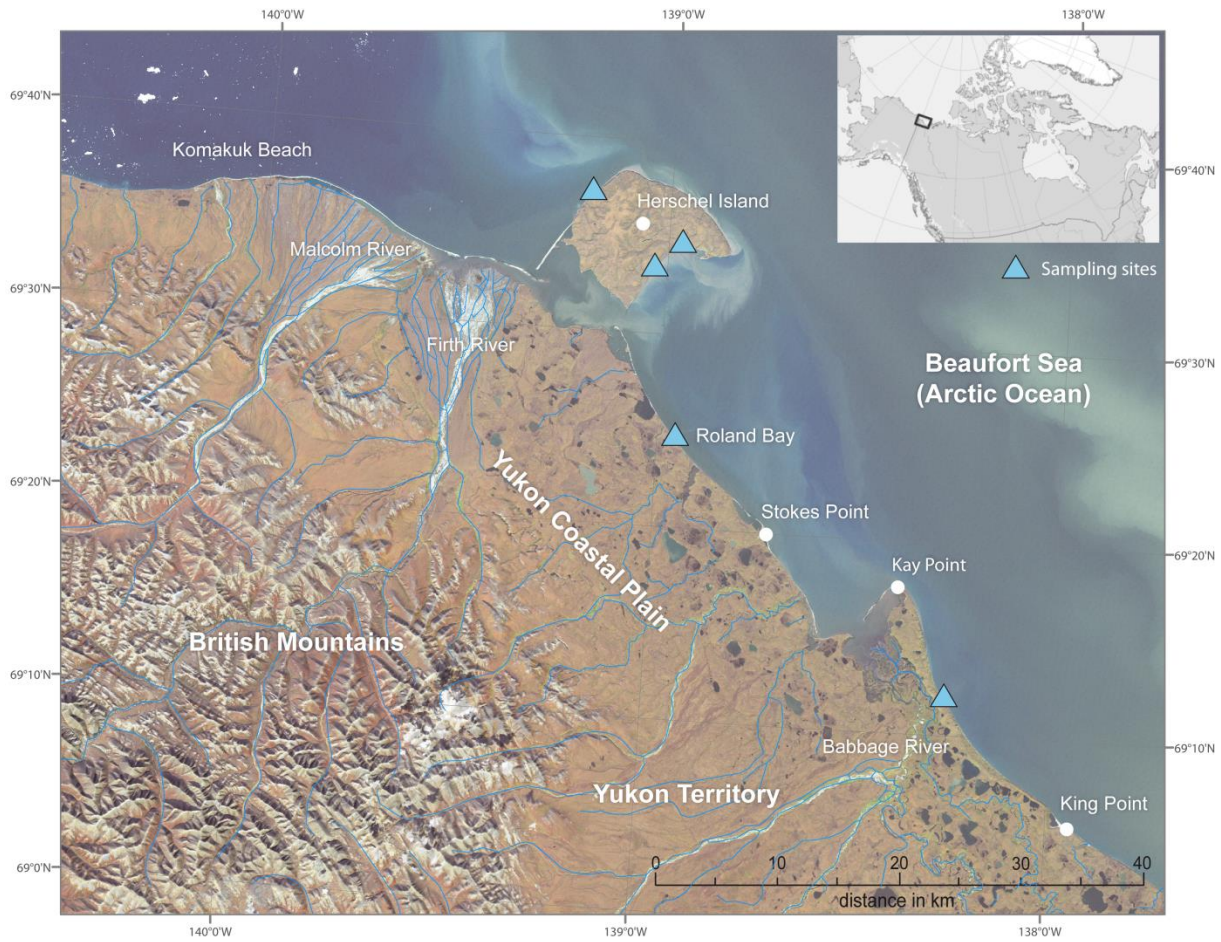


Figure 2.9: Map showing the Yukon Coastal Plain and study sites.

2.6.2 Permafrost and geomorphology

The Yukon Coastal Plain is situated in an area of continuous permafrost (RAMPTON 1982) with a thickness of several hundred meters (SMITH et al. 2001) and a narrow fringe of sub-sea permafrost beneath the shallow shelf part (JORGENSEN & BROWN 2005).

The deeper bedrock of the Yukon Coastal Plain is composed of Jurassic and Lower Cretaceous shale and sandstone. Erosional processes during the Late Tertiary, probably formed the pediment structures under non-periglacial climate conditions (SMITH et al. 1989). Pleistocene and holocene marine and fluvial deposits cover this erosional surface that is subject to periglacial processes (RAMPTON 1982). During the Late Wisconsinan, the coastal plain from Shingle Point to Herschel Island was covered by the Laurentide Ice Sheet (FRITZ et al 2012). Approximately 40,000 a BP the Yukon Coastal Plain was deglaciated (MACKAY 1972a, RAMPTON 1982).

The Yukon Coastal Plain is composed of five major geological units, including fluvial, lacustrine, glaciofluvial, morainal and marine deposits, visible in Figure 2.10. Fluvial deposits

had been deposited either by channel flow or overbank flooding. Lacustrine sediments predominantly originate from thermokarst and occur in morainal areas. Most extensive forms of glaciofluvial deposits can be found south of Herschel Island as outwash plains and fans. Morainal deposits are common within the glacial limit, in form of ice-thrust moraines at Herschel Island and Kay Point. Marine deposits are present in form of sand and gravel beaches and spits, and clayey intertidal deposits. Beaches stretch nearly along the whole Yukon Coastal Plain and are predominantly up to 15 m wide. Spits can reach lengths of up to 150 m at the distal edge of the Malcolm and Firth River alluvial fans and south and east of Herschel Island.

Most prominent thermo-erosional features are retrogressive thaw slumps, active layer detachment slides and large block failures in combination with thermo-erosional niches at coastal cliffs (DE KROM 1990). Active thermokarst proceeds mainly in form of retrogressive thaw slumps (BROWN & KUPSCH 1974). Coastal slopes on Herschel Island are subject to intense thermokarst and thermo-erosional activity (LANTUIT & POLLARD 2008).

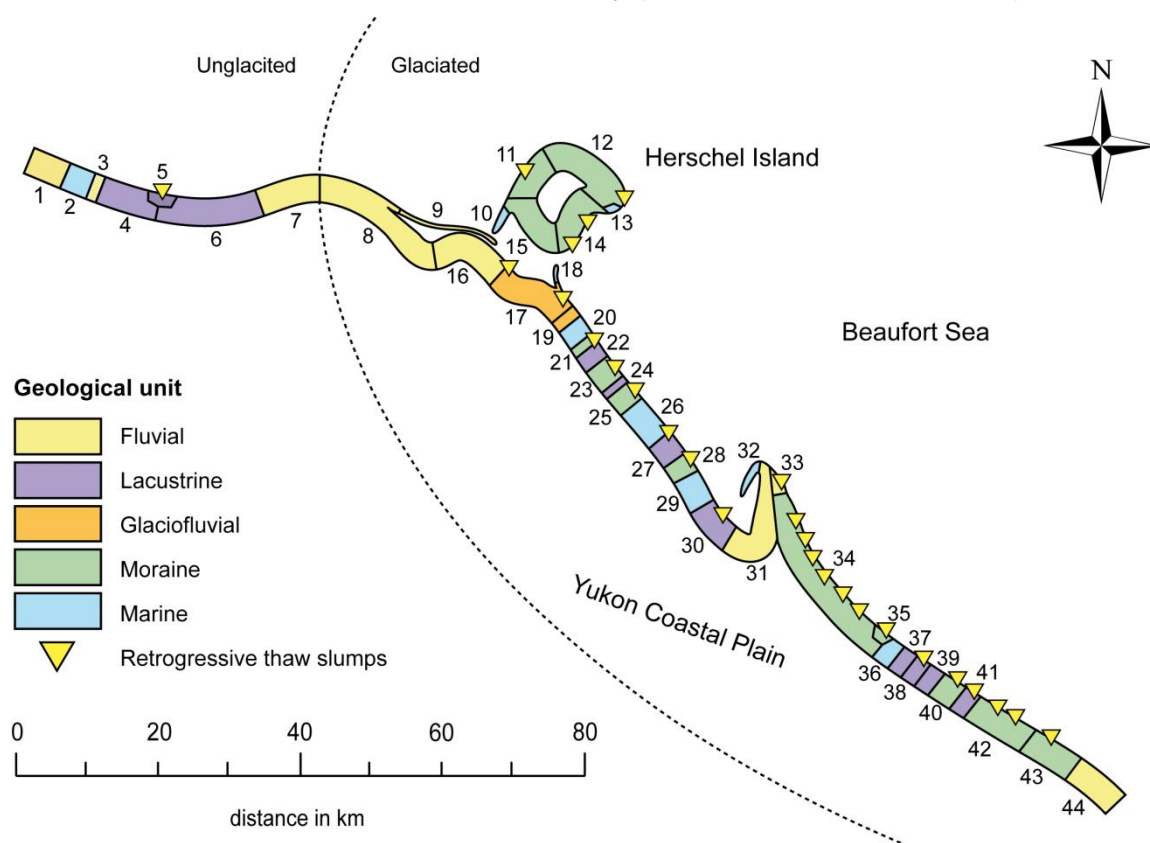


Figure 2.10: Distribution of pleistocene and holocene sediments along the Yukon Coastal Plain, modified after COUTURE (2010), bases on RAMPTON (1982).

2.6.3 Climate

The climate of the Yukon Coastal Plain is dominated by continental arctic air in winter and maritime arctic air in summer. As winters are long with 250 days below zero degrees, the study area is characterized by a polar tundra climate with harsh and cold conditions. The average temperatures of the warmest months not exceed 10°C (RAMPTON 1982). The sea ice that covers the Southern Beaufort Sea region most of the year is responsible for a more continental instead of maritime climate (SMITH et al. 1989).

Since the 1950's temperature and precipitation data have been collected at Komakuk Beach (Figure 2.11) Shingle Point and in Inuvik. The METEOROLOGICAL SURVEY OF CANADA provides temperature and precipitation datasets of Komakuk Beach (figure 2.11) and Shingle Point for the time period from 1971 to 2000. The Yukon Coastal Plain is characterized by a south-easterly temperature gradient. Mean annual temperatures range from -11°C at Komakuk Beach to -9.9°C at Shingle Point and -8.8°C in Inuvik (Mackenzie Delta). Summer temperatures (July mean daily temperatures) are in the range of 7.8°C at Komakuk Beach to 11.2°C at Shingle Point, and 14.2°C in Inuvik. Winter temperatures (January mean daily temperatures) vary from -24°C at Komakuk Beach to -23.7°C at Shingle Point, and -27.6°C in Inuvik. Precipitation is low and falls mainly in form of rain or drizzle during summer. For Komakuk Beach the average annual precipitation is 154 mm. Slightly higher values have been observed at Shingle Point with 253 mm and Inuvik with 250 mm. The snow cover can reach average maximum values of 50 cm on the plain (RAMPTON 1982). With warmer temperatures in late May, the snow starts to melt. Most of the meltwater is retained until river breakup in early June. In this short period, most of the annual water supply is discharged (REIMNITZ & WOLF 1998).

Wind plays an important role in the study area, especially with regard to sediment transport and coastal erosion. The dominant wind direction along the Yukon Coastal Plain is north-west leading to an easterly drift of surface waters (HILL 1990). In spring and summer (May to August), the wind mainly blows from the east (BOUCHARD 1974), which leads to a western drift of surface waters (HILL et al. 1991). Sea ice is dominating the landscape for nearly three-quarters of the year. Only for a brief period of 3 to 4 months in summer, sea ice is absent along the coastal plain and the open water mainly covered by fog and cloud (HILL et al. 1991).

2.6.5 Study sites

Samples have been taken at four parts of the Yukon Coastal Plain, at the west- and southeastern side of Herschel Island, at Roland Bay in the central part and at Kay Point in the eastern part of the coastal plain (Figure 2.12). For the western part it was not possible to attain ice samples. At the southeastern side of Herschel Island four ice wedges (TSA12-IW, TSC12-IW, TSD12-IW1, TSD12-IW2) and one massive ice body (TSD12-MI) were objects of investigations. At Roland Bay in the central part, a series of nine ice wedges (RB12-IW) and in the eastern part at Kay Point, one massive ice body (KP12-MI) and one ice wedge (KP12-IW) were sampled.

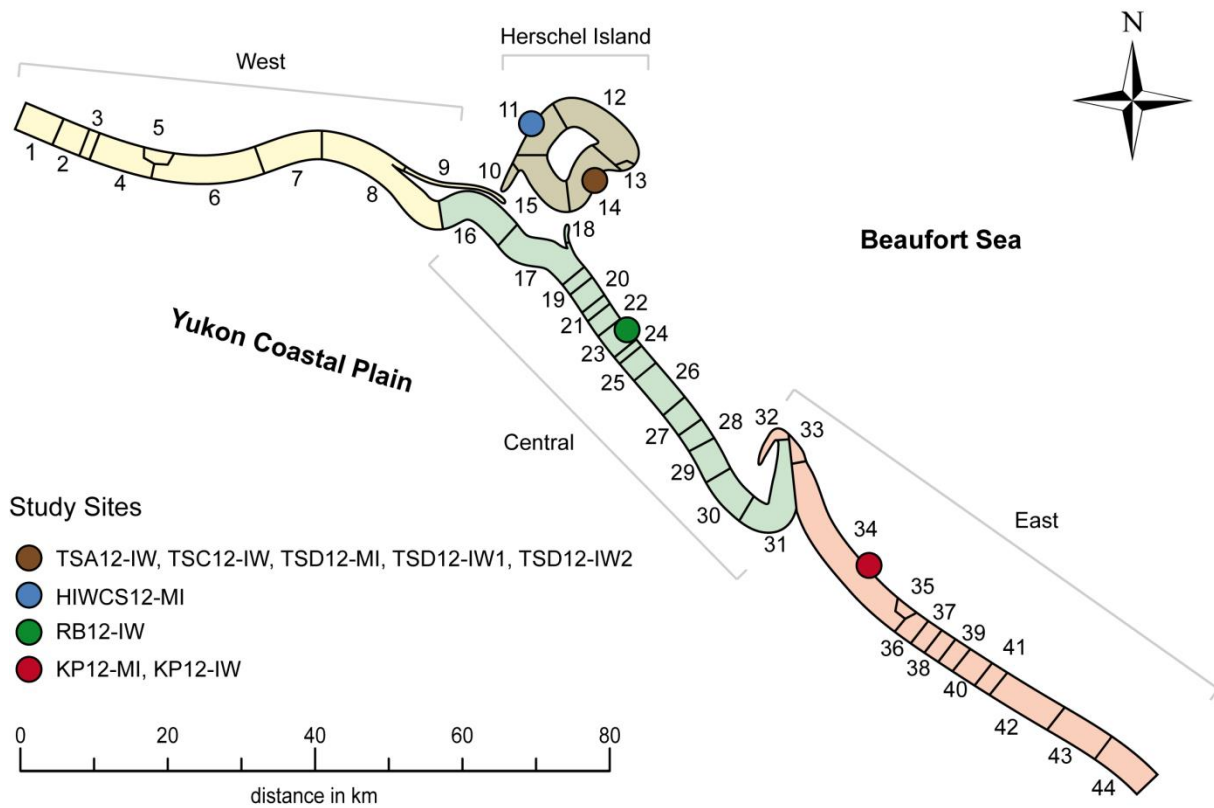


Figure 2.12: Coastal divisions of the Yukon Coastal Plain and study sites.

3 Methods

This chapter describes the methods used to estimate DOC fluxes from coastal erosion, the object of this study. The work flow structure and methodological procedure is depicted in Figure 3.1. The first part of this chapter describes the work conducted in the field and the laboratory to determine the DOC concentrations in massive ground ice. The second part includes the methods for the determination of coastal erosion rates and ground ice volumes. Methods used for the estimation of DOC fluxes from massive ground ice by coastal erosion are presented in the third part.

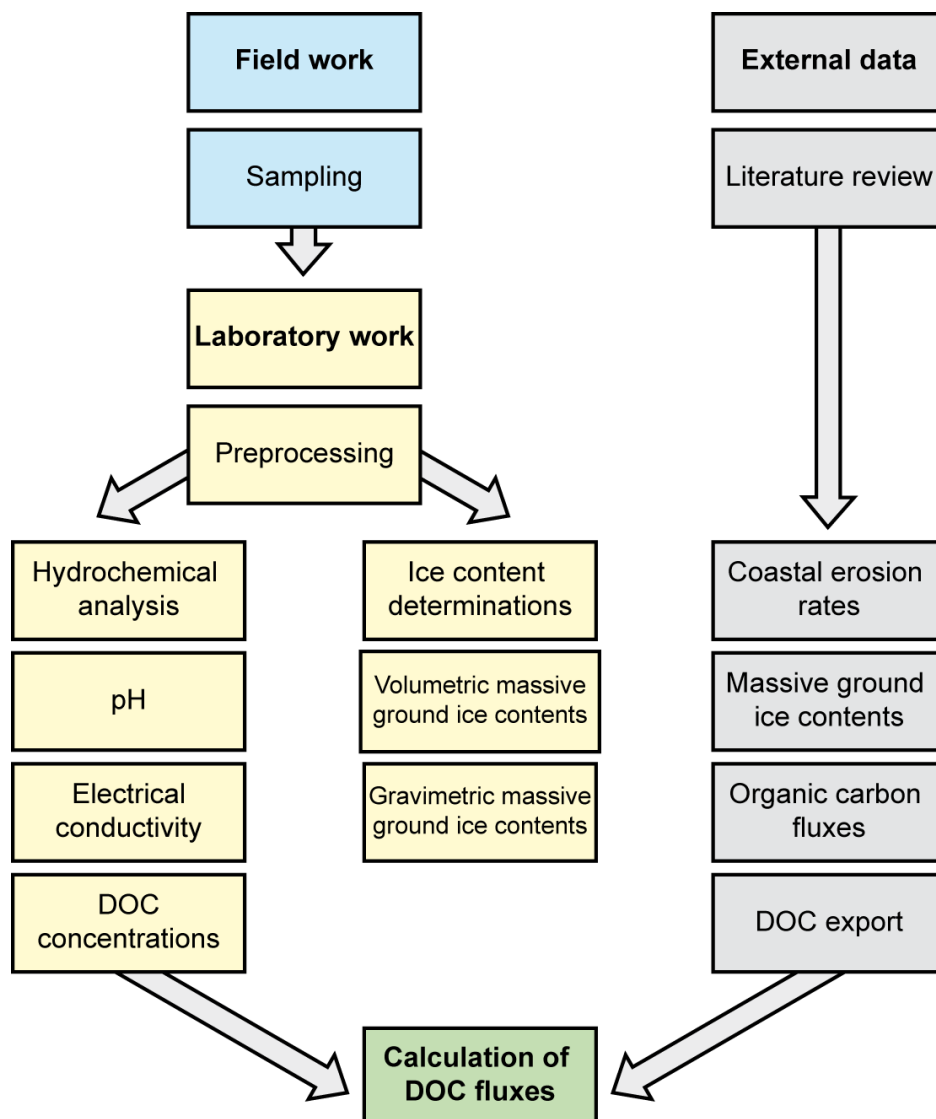


Figure 3.1: Flow chart illustrating the work flow in the thesis.

3.1 Field Work

Field work took place on Herschel Island and on the Yukon Coastal Plain during the Arctic Expedition “Yukon Coast 2012”, in cooperation of the Alfred Wegener Institute for Polar and Marine Research (AWI Potsdam, Germany), the McGill University (Montréal, Canada), the Geological Survey of Canada (Dartmouth, Canada), and the Aurora Research Institute (Inuvik, Canada). The expedition lasted 42 days and included studies on coastal erosion, thermokarst activity, vegetation, and paleolimnology. The results will be documented in an upcoming report to be published in *Berichte zur Polar und Meeresforschung*.

Field sampling targeted massive ice body and ice wedge exposures in five retrogressive thaw slumps. The selection of these slumps was based on three main criteria. The first criterion was to find an accessible site and limit risks associated with sampling. The second criteria was to select massive ice ground ice exposures, which height and width were large enough to obtain an adequate and representative number of samples, and the third criteria was to select sampling sites that covered a wide stretch of the Yukon Coastal Plain, including Herschel Island, to achieve reasonable spatial representativeness. The three slumps located on Herschel Island were reached with a Zodiac inflatable boat. The other two slumps on the Yukon Coastal Plain were reached by helicopter.

Each sampling site was thoroughly documented at different scales. Initially, field descriptions noted topography, aspect, relief, height of the exposure, elevation and dimensions of the slump, surrounding vegetation, as well as an interpretation of landform and geomorphological processes. A Garmin etrex LEGEND HCx handheld GPS was used to record geographic coordinates. Then, the whole exposure was photographed with a digital camera. The documenting was complemented with a detailed sketch of the exposure, along with a comprehensive description of the cryostratigraphy. Cryostratigraphic nomenclature of MACKAY (1989), FRENCH & SHUR (2010) and KANEVSKIY et al. (2011) was used. The information obtained was entered into a database. Sampling commenced only after these metadata were obtained.

To ensure pristine samples, the first 5 to 10 cm of the weathered ice surface was removed before the samples were taken. Samples of massive ground ice were either chiseled out, or cut with a chainsaw. A volume of 15 cm³ was stored in plastic bags. A naming convention was used to identify samples, using the sampling site designation, year, permafrost feature, and sample number. For example, sample TSD12-MI-01 was taken in thaw slump D, in year 2012 (12), from massive ice (MI) with sample number one (01). The abbreviation IW was used for ice wedges. Location abbreviations RB and KP stand for Roland Bay and Kay Point.

After sampling, the ice blocks were immediately transferred to a thermally isolated box and transported to an ice house, a subterranean chamber built in the permafrost to keep goods and food frozen. After leaving Herschel Island, the samples were transferred to the Aurora Research Institute in Inuvik and stored at -20°C . A temperature data logger monitored the sample boxes for the journey from Inuvik (Canada) to Potsdam (Germany). Upon arrival, the samples were transferred to the institute and stored in a freezer at -20°C , where they remained until the laboratory analyses were about to be carried out.

3.1.1 Preprocessing at the Cold lab

The samples were transferred to a cold lab at the German Research Centre for Geosciences (GFZ Potsdam), where they were prepared for hydrochemical analyses. A common ice processing procedure was followed (e.g. used by LACHNIET et al. 2012). The melted and contaminated margins of the frozen samples were cut away at -15°C with a band saw. The cut samples fit in a 250 ml glass beaker. To avoid contamination until further processing in the hydrochemical lab, samples were wrapped in aluminum foil. The aluminum foil was pre-combusted at 550°C to dispose all organic carbon. Sample surplus was put into plastic bags and archived in a cold storage at AWI Bremerhaven. After cutting, the surfaces of the samples were cleaned with a knife (wearing nitrile laboratory gloves). The samples were then examined in the cold laboratory to describe the following characteristics:

- Cryostructure
- Content, orientation and size of gas bubbles
- Existence (or non-existence) of organic matter
- Sediment content and color

This information was referenced in the sample database.

3.1.2 Hydrochemical analyses

Hydrochemical measurements were carried out on all samples in order to analyze pH, electrical conductivity, and DOC concentrations. After un-wrapping the aluminum foil, the processed ice samples were transferred into 250 ml glass beakers and allowed to thaw at room temperature for five days. These beakers were pre-cleaned with ultrapure water. Aluminum foil was used to cover the glass beakers to prevent contamination during thawing. Then, the liquid samples were stored for seven days at 4°C in a fridge to allow suspended matter to settle. A syringe was then used to transfer 8 ml of each sample for pH and electrical conductivity measurements and 40 ml for DOC measurements. Between each analysis, the melted subsamples were stored at 4°C to prevent bacterial decomposition.

3.1.3 pH measurement

The concentration of hydrogen ions in a solution is a measurement for acidity or alkalinity and is recorded with a pH value between 0 and 14. pH measurements were carried out with a pH meter (MultiLab 540, WTW), which calculates the pH using the voltage between a glass and a reference electrode (HANDBOOK WTW 1989) when the electrode is inserted into the solution. A total of 41 unfiltered subsamples were measured and the results were recorded in the sample database.

3.1.4 Electrical conductivity measurement

Nearly all solutions possess a certain content of dissolved and dissociated electrolytes. This sum parameter of soluble anions and cations can be assumed to be responsible for the electrical conductivity (K) of a liquid sample (HÖLTING 1996), which is defined as the reciprocal of the electric resistance (R). The higher the concentration of ions, the higher is the electrical current created by the movement of ions between two electrodes (HANDBOOK WTW 1993). The electrical conductivity is applied to the reference temperature of 25°C and recorded in $\mu\text{S}/\text{cm}$ (HANDBOOK WTW 1993). All 41 unfiltered subsamples were measured and the results transferred to the sample database.

3.1.5 Determination of DOC

The first step to quantify DOC is filtering the liquid sample to eliminate the particulate fraction. DOC is defined after DIN EN 1484 as all organic compounds in water that can pass a membrane filter with a pore size of 0.45 μm (THURMAN 1985, POTTER & WIMSATT 2012). The size of the filters used in marine and geochemical studies varies between 0.2 and 0.7 μm . The most valid method is to process the samples using membrane filters with a pore size of <0.2 μm , but these are not typically used for particle-rich waters (BAUER & BIANCHI 2011). DOUGLAS et al. (2011) used a 0.45 μm acid-washed polypropylene filter for measurements of DOC in cave ice. More common is the use of binder-free glass fiber filters of which 0.7 μm is the smallest nominal pore size available (GUO et al. 2004, GUO & MACDONALD 2006a, WURL & HOLMES 2008, LETSCHER et al. 2012). Since thawed massive ground ice potentially contains a large amount of sediments in comparison to sea or river water (FRENCH 2007), a glass fiber filter of 0.7 μm filter size was used in this study.

There are three main types of measurement techniques used to quantify the DOC concentration in the remaining filtrate (BAUER & BIANCHI 2011):

- high-temperature catalytic combustion
- low-temperature chemical oxidation
- photochemical oxidation.

In this study, DOC concentration was obtained using high-temperature catalytic combustion. This measurement technique is a standard used at the US Environmental Protection Agency (EPA) (POTTER & WIMSATT 2005). Within this technique, there are following ways to determine the DOC content (MANUAL SHIMADZU/TOC-V 2008):

- difference method
- direct method
- addition method.

In this study the direct method was used to determine the DOC concentration.

Long-term evaluation processes and inter-comparisons of DOC analyzing methods led to standardized reference material with agreed-upon DOC concentrations (HANSELL & CARLSON 2001). Standard samples have a known concentration of organic carbon compounds. Standard samples are used to provide an independent verification of the method and the instrument (POTTER & WIMSATT 2012), and to monitor and control the quality of the measurements. Standards used in this study are listed in Table 3.1.

Table 3.1: List of used quality control standards and their features.

Standard	Origin	Producer	DOC conc.
HURON-98	Natural lake water, Lake Huron	National Laboratory for Environmental Testing, Canada	1.50 mg/L
PERADE-20	Natural river water, St. Anne River	National Laboratory for Environmental Testing, Canada	3.95 mg/L
US-QC-Standard I	Synthetic product	Ultra Scientific Analytical Solutions, USA	10.0 mg/L
US-QC-Standard II	Synthetic product	Ultra Scientific Analytical Solutions, USA	25.0 mg/L

Blank samples (ultrapure water with a DOC concentration <0.25 mg/L) were added to the measurement cycle and used to monitor and validate the required quality of the analytical system (POTTER & WIMSATT 2012). Furthermore, four laboratory reagent blanks were used to reconstruct possible contaminations during the preprocessing (Table 3.2). These

blanks consist of ultrapure water and were treated exactly the same way as the ice samples. They were exposed to all glassware, equipment, solvents and reagents that were used to process the ice samples. To evaluate possible influences in the analytical procedure blanks were processed in two different ways: with and without filtration, and with and without acidification, as illustrated in Table 3.2. The ultrapure water used for the blanks was provided by a Milli-Q[®] Advantage A10[®] water treatment system that is able to produce organic carbon free, ultrapure deionized water with a TOC concentration smaller or equal than 5 µg/L.

Table 3.2: List of the laboratory reagent blanks and their processing procedure.

Blank-ID	Filtration	Acidification
Blank 1	No	No
Blank 1-2	Yes	Yes
Blank 2	No	No
Blank 2-2	yes	Yes

All 41 subsamples were processed for analyses in the hydrochemical lab. The measurements of the samples were executed in several steps, illustrated in Figure 3.2. First, 20 ml of the subsample was passed through a 0.7 µm glass fiber filter. Afterwards, another 20 ml were transferred through the same filter into head space vials and acidified (<pH 2) with hydrochloric acid (HCl 30 % suprapure), to prevent microbial alteration, and capped with a crimp cap. DOC concentrations were measured by a SHIMADZU TOCVCPH[®] Total Organic Carbon Analyzer. The device is able to detect carbon in a range of 0 to 25,000 mg/L, with a device specific theoretical detection limit of 0.4 µg/L. As the ice samples were cut in the preprocessing, and contamination could possibly occurred, the detection limit was upgraded to 1.0 mg/L and the device calibrated for measurements in the range of 0 to 10 mg/L and from 0 to 100 mg/L. A possible analytical measurement error can range between +/-15 to 20 % in the lower measuring range and +/-10 % in the higher measuring range. For each sample, two measurement cycles were made.

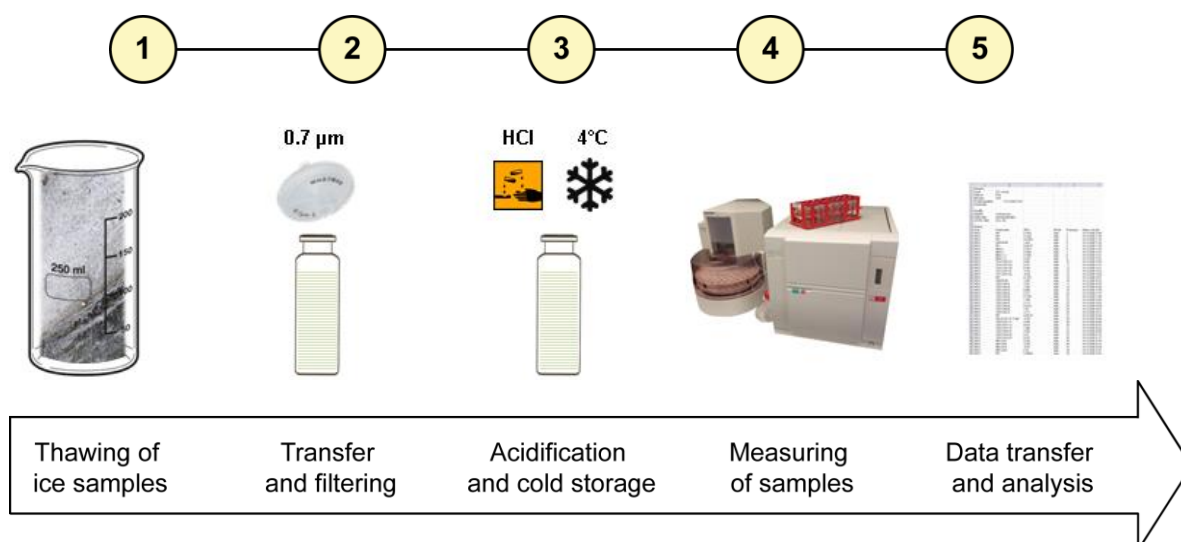


Figure 3.2: Flow chart illustrating the dissolved organic carbon measurement procedure.

In this study the direct method was used to determine the DOC concentration (MANUAL SHIMADZU/TOC-V 2008). This direct method is also called non-purgeable-organic-carbon-method (NPOC-method). As the device needs special vials for the measurement, the acidified samples were transferred from the head space vials into thin 9 ml glass vials, which were pre-combusted at 550°C. Once the samples entered the measurement cycle (Figure 3.3), 5 ml of the samples were acidified with diluted 2 mol hydrochloric acid to pH 2-3 at processing step A. Then, the sample was sparged with oxygen gas. The sparge gas was bubbled through the sample to eliminate the inorganic carbon (IC) component at processing step B. The total inorganic carbon (TIC) was then converted into carbondioxide (CO₂) and purged out for five minutes after chemical reaction 1 (MANUAL SHIMADZU/TOC-V 2008).



The remaining, non-purgeable organic carbon was then combusted on a catalyst bed of platinum-coated alumina spheres by catalytic oxidation at 680°C to carbondioxide at processing step C, and measured by a non-dispersive-infrared detector (NDIR-detector) at processing step D. This process is described by chemical reaction 2 (MANUAL SHIMADZU/TOC-V 2008).



Each measurement lasted 15 to 25 minutes, and the results were automatically saved in the device-associated software. The detected DOC was reported as mg/L or ppm in the data processor at processing step E. The obtained results were recorded and exported to the sample database.

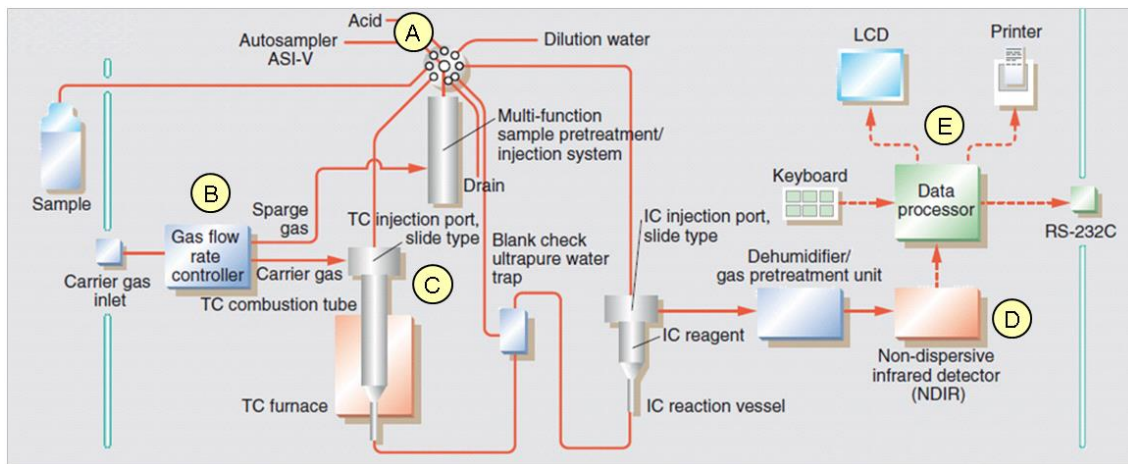


Figure 3.3: Dissolved organic carbon measurement procedure.

3.2 Ice content

The ice contents were estimated by determining the absolute, gravimetric and volumetric ice contents of the samples. As mentioned in section 3.1.1, the ice samples were transferred into 250 ml glass beakers for thawing. After melting, all 41 samples were weighted and the volume was read. Subsequently, the samples were dried in an oven for seven days at 55°C to evaporate the water. Once the subsamples were fully evaporated, the glass beakers with the leftovers of sediment were weighted again. With the weights of the fresh sample and the dry sample the absolute ice content was estimated (Eq. 1).

$$\text{Absolute ice content [g]} = \text{Fresh sample weight [g]} - \text{Dry sample weight [g]} \quad (\text{Eq. 1})$$

From the absolute ice content the gravimetric ice content was determined after VAN EVERDINGEN (2005) in Eq. 2:

$$\text{Gravimetric ice content [wt\%]} = \frac{\text{Absolute ice content [g]}}{\text{Dry sample weight [g]}} \times 100 \quad (\text{Eq. 2})$$

For the calculation of the volumetric ice content it is necessary to determine the bulk density of the ice and the containing sediment (ROWELL 1994). For this study a standard bulk density of quartz with 2.65 g/cm³ for sediment (SCHROEDER 1992, HINTERMAIER-ERHARD & ZECH 1997), and a density of 0.91027 g/cm³ for ice at -10°C (LIDE et al. 2008) was assumed. To estimate the volumetric ice and sediment content, the term for the calculation of density ($\rho = m/V$) was converted according to the volume ($V = m/\rho$) and transformed after equation 3 and 4.

$$\text{Volumetric sediment content [vol\%]} = \frac{\text{Dry sample weight [g]}}{\text{Standard density of quartz } \left[\frac{\text{g}}{\text{cm}^3}\right]} \times 100 \quad (\text{Eq. 3})$$

$$\text{Volumetric ice content [vol\%]} = \frac{\text{Absolute ice content [g]}}{\text{Ice density } \left[\frac{\text{g}}{\text{cm}^3}\right]} \times 100 \quad (\text{Eq. 4})$$

3.3 Mapping and spatial distribution of massive ground ice

Since the 1970's, several studies described ground ice contents on the Yukon Coast at selected locations (MACKAY 1966, HARPER et al. 1985b, HARRY et al. 1988, POLLARD 1990). Recently, a morphological model was developed by COUTURE (2010) to assess the ice content along the entire Yukon Coastal Plain. This model is based on methods developed in a former study by COUTURE et al. (1998) and calculates the volume and type of ground ice for different terrain units. These terrain units were drawn along the coastline of the Yukon according to predominant landforms, surficial materials, permafrost conditions, and coastal processes (RACHOLD et al. 2005b, OVERDUIN & COUTURE 2006). Initially, 21 terrain units were determined. With the help of direct field observations and data from RAMPTON (1982), WOLFE et al. (2001) and HARPER et al. (1985b) the segmentation was refined to account for massive ground ice occurrence. In the end, this resulted in the determination of 44 terrain units (Figure 3.4 and Table 3.3).

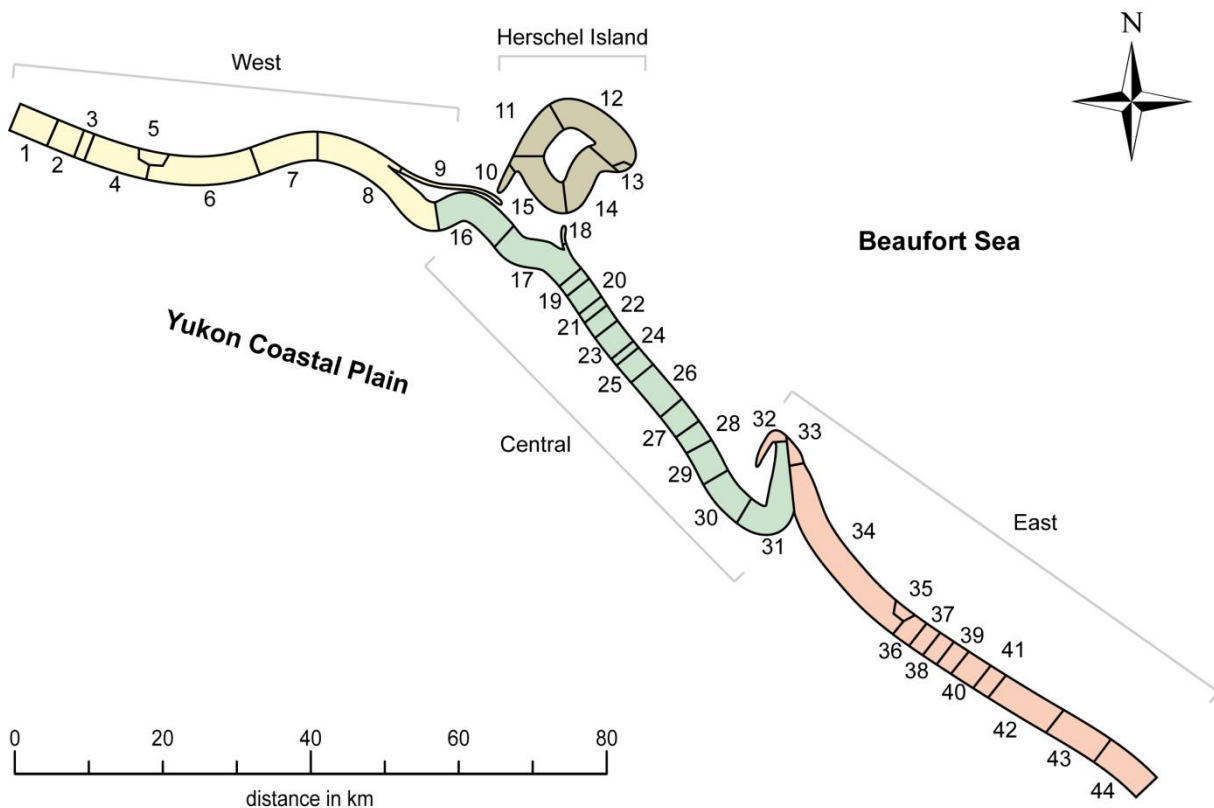


Figure 3.4: Terrain units along the Yukon Coastal Plain, altered after COUTURE (2010).

Table 3.3: Terrain units and location names of the Yukon Coastal Plain, after COUTURE (2010).

Terrain unit	Segment name
1	Clarence Lagoon W
2	Clarence Lagoon
3	Clarence Lagoon E
4	Komakuk Beach W2
5	Komakuk Beach W1
6	Komakuk Beach
7	Malcolm River fan
8	Malcolm River fan with barrier islands
9	Nunaluk Spit
10	Avadlek Spit
11	Herschel Island W
12	Herschel Island N
13	Simpson Point
14	Herschel Island E
15	Herschel Island S
16	Workboat Passage W
17	Workboat Passage E
18	Catton Point
19	Whale Cove W
20	Whale Cove
21	Whale Cove E
22	Roland Bay NW
23	Roland Bay W
24	Roland Bay E
25	Stokes Point W
26	Stokes Point
27	Stokes Point SE
28	Phillips Bay NW
29	Phillips Bay W
30	Phillips Bay
31	Babbage River Delta
32	Kay Point spit
33	Kay Point
34	Kay Point SE
35	King Point NW
36	King Point lagoon
37	King Point
38	King Point SE
39	Sabine Point W
40	Sabine Point
41	Sabine Point E
42	Shingle Point W
43	Shingle Point E
44	Running River

For each of these terrain units, the volume of ground ice was determined by COUTURE (2010) for ice wedges and massive ice bodies, which is used for the calculation of DOC fluxes in this study. At first, the percentage of ice content for each ice type was estimated by COUTURE (2010). Afterwards, the volumetric massive ice content for each terrain unit was calculated. For each terrain unit, 17 input variables were used to generate variables and volumes by using the programming software R, which were required to obtain a total ground ice volume.

The thickness of the terrain units depends on the coastline height, which are based on direct measurements or are derived from the Canadian Ice Service (CIS) database by COUTURE (2010). As ground ice contents are typically higher near the surface (POLLARD & FRENCH 1980), two layers were established to account for ground ice contents, which are based on the vertical sediment structure. Layer 1 extends in general down to the most obvious sedimentary break and layer 2 from the base of layer 1 to the base of the cliff. Furthermore, an average active layer thickness was subtracted as the calculations are only made for permafrost material for each terrain unit. Moreover, each segment reaches 100 m back from the coast. This segmentation was initiated to consider the three dimensional variations in ice types, to allow proper representations of different sized ice wedge polygons and not to overestimate the size of ground ice bodies (COUTURE 2010).

3.3.1 Volume of ice wedges

The volumetric calculations presume that ice wedges have a surface expression. For that reason all values are conservative estimates. A default of 88 % was taken into consideration as limited data exist on volumetric ice contents of ice wedges. This default based on a measurement at one location within the study area (COUTURE 2010).

The volumetric content of ice wedges was quantified by estimating the total length of ice wedge troughs in a terrain unit (L_W) by dividing the total area of a terrain unit (A) by the mean ice wedge spacing (W_S) (Eq. 5). The factor 2 was integrated into the equation to account for the two different stratigraphic units. The volumetric content of ice wedges is based on the size of the polygons, and therefore the spacing of the ice wedges. Ice wedges meet at right angles and form a tetragonal network in plain view (FRENCH 2007, FRENCH & SHUR 2010).

$$L_W = \frac{A \times 2}{W_S} \quad (\text{Eq. 5})$$

The total volume of ice wedges in a terrain unit was calculated after equation 6. As ice wedges are considered to be triangular in cross-section, a factor of 0.5 was integrated. The mean ice wedge width (W_T) and depth above sea level (D_{WT}) was derived by direct measurements. The length of the ice wedge troughs (L_W) was determined by equation 5.

$$V_W = 0.5 \times W_T \times D_{WT} \times L_W \quad (\text{Eq. 6})$$

3.3.2 Volumes of massive ice bodies

The presence of massive ice bodies accompanies the presence of retrogressive thaw slumps. Usually, massive ice bodies underlie a terrain unit only if it or a significant number of retrogressive thaw slumps have been positively identified in a coastal unit, indicated by remote sensing imagery. The lower parts of the massive ice bodies are usually not visible as there are buried in slump debris. In calculations, it is assumed that massive ice bodies extend to the base of a terrain unit as the thickness of massive ice bodies is difficult to determine (COUTURE 2010). The mean depth to the top (D_M) and bottom (D_{BM}) of massive ice bodies was derived from direct measurements, or estimated from published values. For the upper stratigraphic unit the volume of massive ice bodies is estimated by equation 7.

At first, the beginning of the massive ice body was determined by subtracting the thickness of the uppermost soil layer (D_1) by the depth to the top of the massive ice body (D_M). Secondly, this value was projected on the whole terrain unit by multiplying the total surface area of a terrain unit (A). And thirdly, the value was subtracted by the volume of ice wedges in massive ice bodies (V_{WM}) to incorporate the possible presence of ice wedges.

$$V_{M1} = [(D_1 - D_M) \times A] - V_{WM} \quad (\text{Eq. 7})$$

The same calculation procedure was applied for the lower stratigraphic unit by equation 8. The only difference is that instead of the thickness of the uppermost soil layer (D_1), the depth to the bottom of the massive ice (D_{BM}) was subtracted by the depth to the top of the massive ice body (D_M).

$$V_{M2} = [(D_{BM} - D_M) \times A] - V_{WM} \quad (\text{Eq. 8})$$

The total volume of massive ice in a terrain unit was estimated after equation 9 by the addition of volumes of massive ground ice in stratigraphic units 1 (V_{M1}) and 2 (V_{M2}).

$$V_{MT} = V_{M1} + V_{M2} \quad (\text{Eq. 9})$$

3.4 Estimation of dissolved organic carbon stocks

The estimation of dissolved organic carbon stocks is based on the results of the DOC concentration measurements. The median of all 41 samples was used to derive an average DOC concentration value for the whole coast. The median was used instead of the mean to account for samples with DOC concentrations below the detection limit, so that no overestimation occurs. The samples, representative for four terrain units (TUs, Figure 3.4 and Table 3.3) were taken at Herschel Island W (TU 11), Herschel Island E (TU 14), Roland Bay W (TU 23) and Kay Point SE (TU 33). The median value of DOC concentration was extrapolated to all terrain units (n=44). To obtain the DOC stock (DOC_{stock}) for all terrain units in g/m^3 , following input parameters were required and calculated after equation 10:

$$DOC_{stock} = \sum_{j=1}^n \theta_j \times \rho \times DOC_{conc.j} \quad (\text{Eq. 10})$$

where:

θ = volumetric massive ground ice content for a terrain unit in vol%

ρ = density of pure ice at -10°C (0.917 g/cm^3)

$DOC_{conc.}$ = median DOC concentration in massive ground ice in mg/L.

Three scenarios had been set up to give a range of possible DOC stocks in massive ground ice that includes quartiles and median as followed:

- Scenario I: 25 %-quartile DOC concentration of all samples
- Scenario II: 50%-quartile (median) DOC concentration of all samples
- Scenario III: 75 %-quartile DOC concentration of all samples.

Scenario I is the 25%-quartile of all 41 measured DOC concentrations multiplied with the specific volumetric massive ice content for each terrain unit and the density of pure ice. The same procedure was conducted for scenario II (Median of all 41 measured samples) and scenario III (75%-quartile of all 41 measured samples). Subsequently, a terrain unit specific DOC stock in g/m^3 was conducted (Appendix).

3.5 Calculation of DOC fluxes

The calculation of DOC fluxes, the annual release of dissolved organic carbon by coastal erosion, was conducted for each terrain unit of the Yukon Coastal Plain ($n=44$). The estimation was based on an equation provided by LANTUIT et al. (2009) originally used for the estimation of POC fluxes, excluding massive ground ice. This equation was adapted and simplified by FRITZ et al. (2011a) to determine DOC fluxes from ice wedges. In this study, this equation was modified and expanded to include massive ice bodies. The estimated DOC flux is given in kg/yr and was calculated by equation 11.

$$\text{DOC}_{\text{flux}} = \sum_{j=1}^n l_j \times h_j \times R_j \times \text{DOC}_{\text{stock}_j} \quad (\text{Eq. 11})$$

where:

l = length of the coastline of a terrain unit in m

h = coastline height of a terrain unit in m

R = mean annual coastal erosion rate for a terrain unit in m/yr

$\text{DOC}_{\text{stock}}$ = DOC concentration in massive ground ice for a terrain unit in g/m^3 .

The length of the coastline (l) of all terrain units was provided by COUTURE (2010). The coastline height (h) originates from a variety of sources (MCDONALD & LEWIS 1973, LEWIS & FORBES 1975, RAMPTON 1982, GILLIE 1987, HARRY et al. 1988, FORBES et al. 1995, FORBES 1997, COUTURE 2010). The coastal erosion rates (R) for all segments were derived from HARPER et al. (1985b).

Three scenarios, corresponding to the scenarios of the estimated DOC stocks (section 3.4), were set up to give a range of possible DOC fluxes:

- Scenario A: Estimation with DOC stocks of scenario I
- Scenario B: Estimation with DOC stocks of scenario II
- Scenario C: Estimation with DOC stocks of scenario III

For the estimation of DOC fluxes presented by scenario A, DOC stocks from scenario I (section 3.4) has been multiplied with the terrain unit specific parameters coastline length, coastline height and mean annual coastal erosion rate. The same procedure was conducted for DOC fluxes of scenario B by using DOC stocks of scenario II and for DOC fluxes of scenario C by using DOC stocks of scenario III. Subsequently, a terrain unit specific DOC flux in kg/yr was derived (Appendix).

4 Results

The results are divided in two sections. The first section includes a qualitative description of the cryolithology, the sediment characteristics of the samples and the results of the hydrochemical analyses (DOC concentration, pH, electrical conductivity). It is supported by figures illustrating the stratigraphic profiles and sampling locations. These are presented following an east to west gradient on Herschel Island (TSA12-IW1, TSC12-IW1, TSD12-MI, TSD12-IW1, TSD12-IW2, HIWCS12-MI) and from west to east along the coastal plain (RB12-IW, KP12-MI, KP12-IW). Given thicknesses of the active layer have been measured in mid August. The second section gives an overview of the volumetric massive ground ice contents, coastal erosion rates, coastline heights, DOC stocks and the estimated DOC fluxes. Adjectives used in the following, like low, moderate and high, are used to distinguish the results and are not absolute. To compare fluxes on a regional basis, the Yukon Coastal Plain was segmented further into four parts (Figure 3.4 and Table 3.3), the western part (TU 1-9), Herschel Island (TU 10-15), the central part (TU 16-31) and the eastern part (TU 33-44).

4.1 Permafrost profiles and hydrochemical characteristics

4.1.1 Ice wedge TSA12-IW1

Ice wedge TSA12-IW is located 43.0-48.0 m a.s.l. on the south-eastern coast of Herschel Island in thaw slump A and has a width of 4.5 m in the middle part. The sampling was performed from the bottom of the slump headwall and samples were taken from the left, the middle and the right side of the ice wedge to get a comprehensive coverage. The results of laboratory analysis and volumetric ice content determination are summarized in Table 4.1.

The profile is divided into three different stratigraphic units (Figure 4.1) and has a height of approximately 5.0 m. At the bottom of the headwall, the slump debris (unit I) forms the lower end of the profile, which consists of mud originating from thawed permafrost sediments. The sediments surrounding the ice wedge (unit II) are 4.0 m thick and consist of clayey frozen material. The ice wedge has a visible height of 4.0 m and reaches up to the lower part of the active layer (unit III), which is in average 37 cm thick. It is likely that the ice wedge extends below the slump debris material. The upper part of the profile is made of the active layer and the tussock tundra vegetation.

The ice sample *TSA12-IW-01* taken from the left part of the ice wedge consisted of clear ice containing few sediment inclusions. These inclusions were fine-grained and greyish. The volumetric ice content was estimated to be 99.97 %. The pH and electrical conductivity were

6.88 and 43.4 $\mu\text{S}/\text{cm}$. The measured DOC concentration was 8.08 mg/L. The ice sample *TSA12-IW-02* taken from the middle part of the ice wedge was clear and bubble rich with sediment inclusions. The sediment was brownish-reddish and fine-grained. The volumetric ice content was 99.99 % with a pH of 7.25 and an electrical conductivity of 62.3 $\mu\text{S}/\text{cm}$. The measured DOC concentration was 8.28 mg/L. The ice sample *TSA12-IW-03* was taken in the right part of the ice wedge. The ice sample contained larger sediment inclusions and sediment veins. The volumetric ice content was 99.97 %. The pH was 7.45, electrical conductivity 68.3 $\mu\text{S}/\text{cm}$ and the DOC concentration 6.26 mg/L.

Table 4.1: Volumetric ice contents and hydrochemical parameters of ice wedge TSA12-IW.

	Ice content [vol%]	DOC conc. [mg/L]	pH	Electrical cond. [$\mu\text{S}/\text{cm}$]
TSA12-IW1-01	99.97	8.08	6.88	43.4
TSA12-IW1-02	99.99	8.28	7.25	62.3
TSA12-IW1-03	99.97	6.26	7.45	68.3
Range	99.97 – 99.99	6.26 – 8.08	6.88 – 7.45	43.4 – 68.3
Arithmetic mean	99.98	7.54	7.19	58.0

TSA12-IW

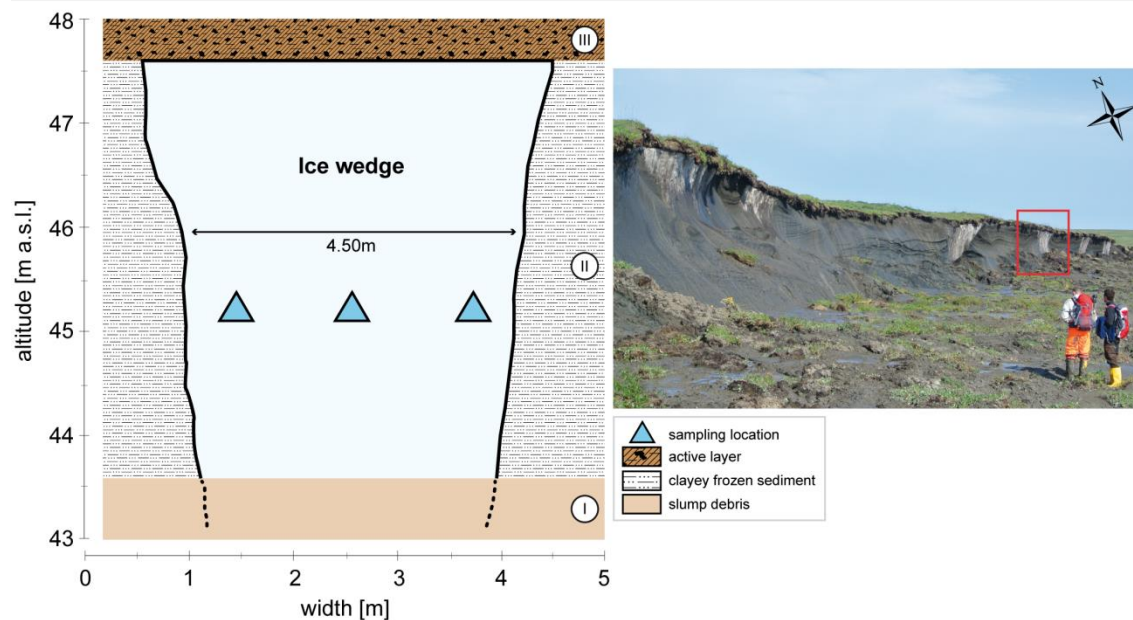


Figure 4.1: Cryostratigraphic profile of ice wedge TSA12-IW and sampling locations.

4.1.2 Ice wedge TSC12-IW1

Ice wedge TSC12-IW is located in the headwall of thaw slump C at the south-eastern coast of Herschel Island, close to thaw slump A, with an exposition of the profile towards the south-east. The sampling was performed at a height of 36.0 m a.s.l. at the bottom of the slump headwall. Two samples were taken from the upper and the middle part of the ice wedge. The results of the laboratory analyses and volumetric ice content determination are summarized in Table 4.2.

The profile is divided into six different stratigraphic units (Figure 4.2) and has a height of approximately 4.0 m. The bottom part of the profile (unit I) is composed of slump debris, originating from thawed sediments. Above the slump debris, is a 2.0 m thick layer of clayey frozen sediment (unit II) that surrounds the ice wedge. The ice wedge has a maximal width of 0.5 m and a visible height of 2.0 m (as the lower part is truncated by slump debris). Above the ice wedge and layer II, a sediment layer of poorly sorted greyish loam with cobbles and no visible organic (unit III) follows. It has a lens-like irregular reticulated cryostructure with ice lenses of 2 to 10 mm width. Unit III has a height of 0.5 m and is separated from unit IV by an ice lens up to 30 cm thick. Unit IV is a permanently frozen brownish sediment layer with a prismatic structure, which contains roots and cobbles, but no visible ice. It has a fissured, irregular reticulated cryostructure and peaty inclusions. The thickness of this layer ranges between 0.5 and 1.0 m. The upper end of the profile is formed by the active layer (unit I), which has an average thickness of 36 cm and is topped by tussock tundra vegetation.

The ice sample *TSC12-IW-01* was taken in the upper part of the profile and contained large sediment inclusions and small air bubbles (<1 mm). The volumetric ice content was 99.96 %. The sediment was brown-beige and fine-grained. The determined DOC concentration was 13.2 mg/L. The pH was 7.20 and the electrical conductivity 92.7 $\mu\text{S}/\text{cm}$. The ice sample *TSC12-IW-02* was taken from the lower part of the ice wedge. The sediment was yellow-greyish and fine grained. The volumetric ice content was 99.70 %. The derived DOC concentration was 19.5 mg/L. The pH and electrical conductivity were 7.20 and 92.7 $\mu\text{S}/\text{cm}$, respectively.

Table 4.2: Volumetric ice contents and hydrochemical parameters of ice wedge TSC12-IW.

	Ice content [vol%]	DOC conc. [mg/L]	pH	Electrical cond. [μ S/cm]
TSC12-IW1-01	99.96	13.2	7.20	92.7
TSC12-IW1-02	99.70	19.5	7.65	230.2
Range	99.70 – 99.96	7.20 – 7.65	7.20 – 7.65	92.7 – 230.2
Arithmetic mean	99.83	16.36	7.43	161.45

TSC12-IW**Figure 4.2:** Cryostratigraphic profile of ice wedge TSC12-IW and sampling locations.

4.1.3 Ice wedge TSD12-IW1

Ice wedge TSD12-IW1 is located in a height of 47.0 m a.s.l. in the headwall of thaw slump D on the south-eastern coast of Herschel Island. Three samples were taken from the left side, the middle and the right side of the ice wedge to cover its entire width. The sampling was performed from the top of the ice wedge. The results of laboratory analyses and volumetric ice content determination are summarized in Table 4.3.

The profile is divided into five different stratigraphic units (Figure 4.3) and has a height of approximately 8.0 m. At the base of this profile is a massive ground ice body (unit I), which downward dimensions are unknown as it is truncated by slump debris (not visible on the figure). The ice wedge TSD12-IW1 is embedded in this massive ice and is exposed sub-vertically in north-eastern direction. It has a height of 4.0 to 5.0 m and a width of 3.0 m. At the upper left (unit IIa) and right side (unit IIb), the ice wedge is bordering at clayey-silty sediment with a fine lens-like cryostructure with a thickness of 1.5 m. This unit is dark-grey with grey-brown layers up to 1 cm thick. At the left side, the border between unit I and unit IIa is not sharp and has been drawn with a white dotted line. At the right side, the sediment close to the ice wedge is stratified sub-vertically. The ice wedge is cut by unit III at approximately 60.0 m a.s.l. just above it. Unit III has a thickness of 1.0 m and is characterized by silty-clayey sediment with sandy layers (1 to 20 mm thick) and a fine lens-like cryostructure. It is greyish-brown with isolated pebbles. In the lower part of unit III, towards the ice wedge macro-organic compounds (possibly roots) and ice lenses up to 15 mm thick occur. The gradual transition between unit III and unit IV is characterized by pure, vertical laminated ice with small (~2 mm) and vertically aligned air bubbles. The upper part of this transition zone shows sediment inclusions in ice and a coarse lens-like cryostructure, between 15 and 70 cm thick. Unit IV is characterized by ice-rich silty-clayey sediments with a coarse lens-like cryostructure. It is diamictic with scattered pebbles, which are partially rounded and up to 8 cm wide. The top of the profile is represented by the active layer (unit V). It is grey-brown and is terminated at the top by tussock tundra vegetation.

The ice sample *TSD12-IW1-71* was taken from the left side of the ice wedge and consisted of pure ice with oval rounded air bubbles up to 1 mm size. The volumetric ice content was 99.98 %. The enclosing sediment was greyish-brown and sandy. The hydrochemical parameters pH and electrical conductivity yielded values of 7.85 and 173.1 $\mu\text{S}/\text{cm}$. The concentration of DOC was 5.85 mg/L. The ice sample *TSD12-IW1-72*, from the middle of the ice wedge, was sediment-poor and had a brown color after thawing. The enclosing sediment had a grey color and was fine-grained. The volumetric ice content was 99.75 %. A pH of 7.76 and electrical conductivity of 359.0 $\mu\text{S}/\text{cm}$ were measured. The DOC concentration was 9.02 mg/L. The ice sample *TSD12-IW1-73* was taken from the right side of the ice wedge and

featured a few sediment clusters. The sample had a greyish-brown color. The enclosing fine-grained and sandy sediment had a greyish color. The volumetric ice content was 99.91 %. The parameters pH and electrical conductivity showed values of 7.68 and 161.8 $\mu\text{S}/\text{cm}$. The DOC concentration was 7.89 mg/L.

Table 4.3: Volumetric ice contents and hydrochemical parameters of ice wedge TSD12-IW1.

	Ice content [vol%]	DOC conc. [mg/L]	pH	Electrical cond. [$\mu\text{S}/\text{cm}$]
TSD12-IW1-71	99.98	5.85	7.85	173.1
TSD12-IW1-72	99.75	9.02	7.76	359.0
TSD12-IW1-73	99.91	7.89	7.68	161.8
Range	99.75 – 99.98	5.85 – 9.02	7.68 – 7.85	161.8 – 359.0
Arithmetic mean	99.88	7.58	7.76	231.0

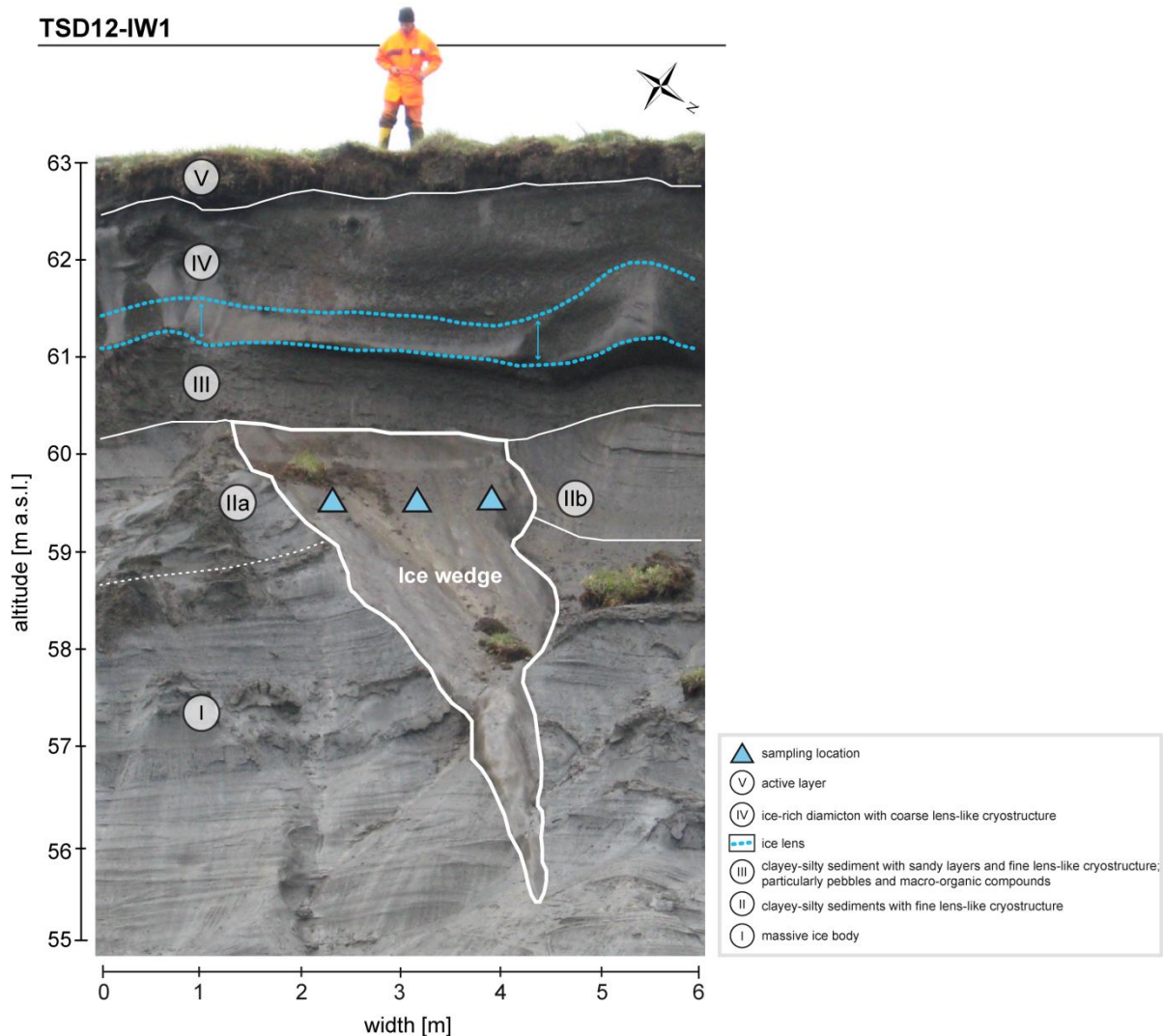


Figure 4.3: Cryostratigraphic profile of ice wedge TSD12-IW1 and sampling locations.

4.1.4 Ice wedge TSD12-IW2

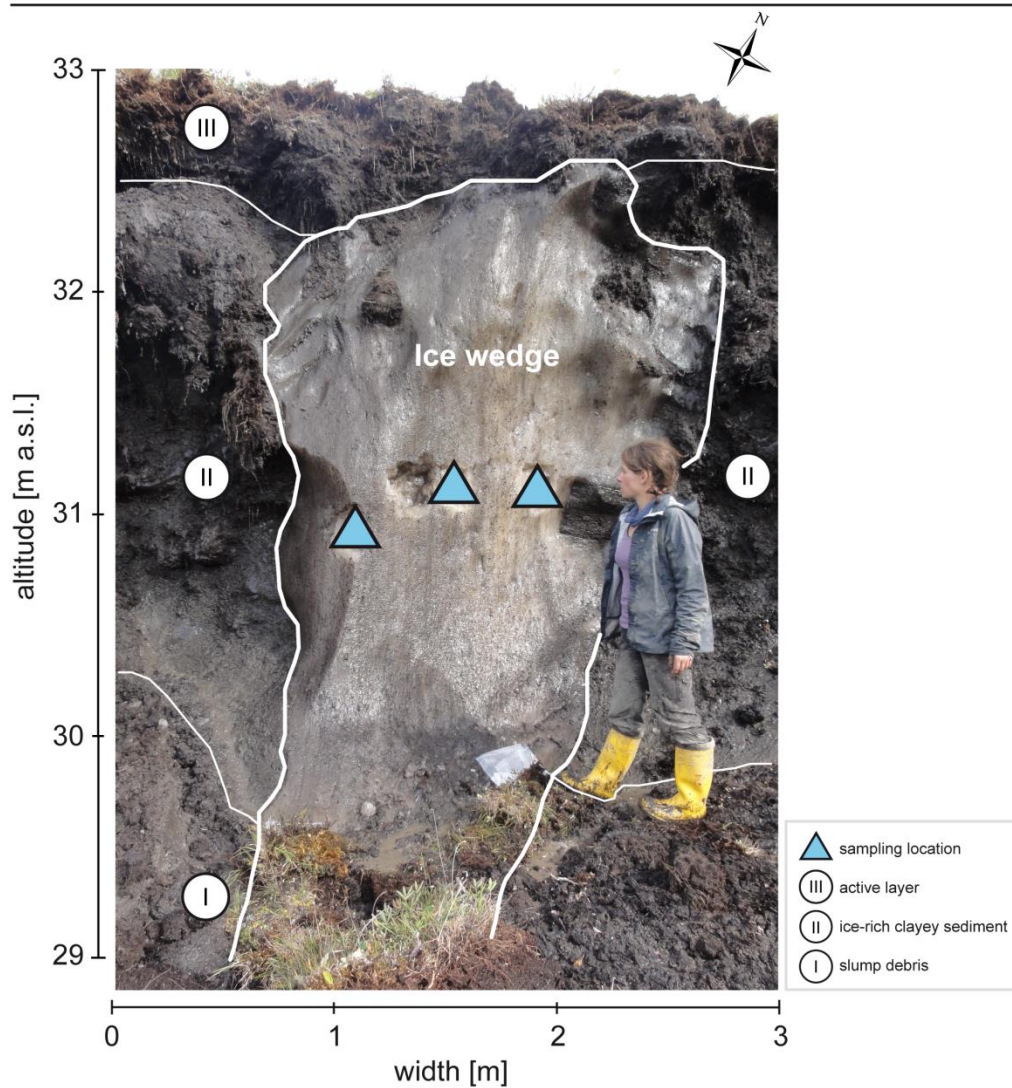
Ice wedge TSD12-IW2 is located in the headwall of thaw slump D at the south-eastern coast of Herschel Island. The ice wedge is exposed in southern direction. The sampling was executed at a height of 30.0 m a.s.l. at the bottom of the slump headwall. Three samples were taken from the left side, the middle and the right side at the upper part of the ice wedge to cover the whole exposed surface of the ice wedge. The results of laboratory analyses and volumetric ice content determination are summarized in Table 4.4.

The profile is divided into three different stratigraphic units (Figure 4.4) and has a height of approximately 4.0 m. At the bottom of the profile, is the slump debris (unit I) of thawed sediments. Unit II, which surrounds the ice wedge, is characterized by ice-rich clayey sediment with lens-like cryostructure and is characterized by a thickness of approximately 2.0 to 3.0 m. The ice wedge has a width of 1.0 to 1.5 m and a visible height of 3.0 m. The actual size is unknown as the ice wedge is truncated at the bottom by slump debris. On top, the active layer (unit III) has an average thickness of 45 cm and is overlain by tussock tundra vegetation.

The ice sample *TSD12-IW2-01* was taken from the left side of the ice wedge. The volumetric ice content was 100 %. The values obtained for pH and electrical conductivity were 7.3 and 44.3 $\mu\text{S}/\text{cm}$. The DOC concentration was 2.94 mg/L. The ice sample *TSD12-IW2-02* was taken from the middle part of the ice wedge and was a thin piece of ice. The enclosing sediment was reddish-brown and sandy. The volumetric ice content was 99.99 % and the pH and electrical conductivity were 7.25 and 47.2 $\mu\text{S}/\text{cm}$. The value for DOC concentration was 4.25 mg/L. The ice sample *TSD12-IW2-03* was taken from the right part of the ice wedge and contained small air bubbles and linear sediment inclusions. The sediment found after thawing was reddish-brown and sandy. The volumetric ice content was 99.99 %. The pH and electrical conductivity were 6.8 and 50.2 $\mu\text{S}/\text{cm}$. The DOC concentration was 6.03 mg/L.

Table 4.4: Volumetric ice contents and hydrochemical parameters of ice wedge TSD12-IW2.

	Ice content [vol%]	DOC conc. [mg/L]	pH	Electrical cond. [μ S/cm]
TSD12-IW2-01	100.00	2.94	7.30	44.3
TSD12-IW2-02	99.99	4.25	7.25	47.2
TSD12-IW2-03	99.99	6.03	6.80	50.2
Range	99.99 – 100.00	2.94 – 6.03	6.80 – 7.30	44.3 – 50.2
Arithmetic mean	99.99	4.41	7.12	47.23

TSD12-IW2**Figure 4.4:** Cryostratigraphic profile of ice wedge TSD12-IW2 with sampling locations.

4.1.5 Massive ice body TSD12-MI

The massive ice body TSD12-MI is located in thaw slump D on the south-eastern coast of Herschel Island. The massive ice body is exposed in south-eastern direction. The sampling was performed at a height of 37.0 to 46.0 m a.s.l. by climbing the ice body with crampons and sampling ice blocks every 3.0 m. In total, ten samples were taken orthogonally to the stratigraphy of the massive ice to cover the body comprehensively. The results of laboratory analyses and volumetric ice content determination are summarized in Table 4.5.

The profile is divided into five different stratigraphic units (Figure 4.5) and has a height of approximately 16.0 m. The slump debris (unit I) forms the base of the profile and covers the lower part of the massive ice body (unit II). The massive ice body consists of bubble-rich white ice with sediment inclusions. It is sediment rich at the top and in selected layers throughout the profile. Two linear layers of pure and milky ice up to 2.0 m in thickness occur vertically in the massive ice body. The visible thickness of the ice body is up to 14.0 m. The exact downward extension of the body is unknown as the ice is buried by slump debris. Above the massive ice body, an ice-rich clayey diamictic layer (unit III) with a thickness of approximately 4.0 m, which is characterized by ice wedges (unit IV), is situated just below the active layer (unit V).

Ice sample *TSD12-MI-01* was clear and air bubble-rich with sediment inclusions. The air bubbles were elongated with sizes greater than 1 mm. The sediment obtained after thawing was greyish and sandy. The sample had a volumetric ice content of 99.99 %, a pH of 7.7 and an electrical conductivity of 77.7 $\mu\text{S}/\text{cm}$. The DOC concentration was 1.06 mg/L. The ice sample *TSD12-MI-02* contained sediment inclusions. The sediment was bright greyish-brown. The sample had a volumetric ice content of 99.97 %, a pH of 7.65 and an electrical conductivity of 87.9 $\mu\text{S}/\text{cm}$. The DOC concentration was 1.03 mg/L. The ice sample *TSD12-MI-03* contained fine sediment layers more than 2 cm thick as well as gravel. The air-bubbles were not elongated. The enclosing sediment was grey and was made of clay, silt and sand with pieces of gravel. The volumetric ice content was 93.40 %, the pH 8.09 and the electrical conductivity 386.0 $\mu\text{S}/\text{cm}$. The DOC concentration was 6.07 mg/L. The ice sample *TSD12-MI-04* contained up to 4 cm thick sediment layers and several thinner sediment layers. The enclosed air-bubbles were not elongated and were greater than 1 mm in size. The sample had a volumetric ice content of 92.65 %, a pH of 8.1 and an electrical conductivity of 504.0 $\mu\text{S}/\text{cm}$. The DOC concentration was 5.72 mg/L. The ice sample *TSD12-MI-05* was clear and air bubble-rich. The air-bubbles were not elongated their size was greater than 1 mm in diameter. The sample had a volumetric ice content of 100 %, a pH of 7.24 and an electrical conductivity of 47.7 $\mu\text{S}/\text{cm}$. There was no DOC concentration available as the value obtained was below the device specific detection limit. The ice sample *TSD12-MI-06* contained

sediment layers and air bubbles. The enclosing sediment was greyish, clayey-silty and formed conglomerates upon thawing. The sample had a volumetric ice content of 99.52 %, a pH of 8.01 and an electrical conductivity of 236.5 $\mu\text{S}/\text{cm}$. The DOC concentration was 1.8 mg/L. The ice sample *TSD12-MI-07* was air bubble rich with bubbles greater than 1 mm in diameter and several sediment inclusions. The sediment was greyish, clayey-silty and formed conglomerates upon thawing. The sample revealed a volumetric ice content of 99.09 %, a pH of 7.92 and an electrical conductivity of 206.5 $\mu\text{S}/\text{cm}$. The DOC concentration was 2.17 mg/L. The ice sample *TSD12-MI-08* was air bubble-rich with bubble sizes greater than 1 mm in diameter. The sample had a volumetric ice content of 100 %, a pH of 7.18 and an electrical conductivity of 26.5 $\mu\text{S}/\text{cm}$. The DOC concentration was not available as the concentration in the sample was below the device specific detection limit. The ice sample *TSD12-MI-09* included several sediment layers from 1 to 10 mm thickness. The sediment was dark-brown and clayey-silty. The sample had a volumetric ice content of 99.16 %, a pH of 7.79 and an electrical conductivity of 175.6 $\mu\text{S}/\text{cm}$. The DOC concentration was 1.85 mg/L. The ice sample *TSD12-MI-10* contained a high visible sediment content. The sediment layers were up to 5 mm thick, laminated and had a reddish-dark-brown color. The fine, silty-clayey sediment formed smaller conglomerates. The liquid was sediment-rich upon thawing. The sample had a volumetric ice content of 98.24 %, a pH of 8.01 and an electrical conductivity of 379.0 $\mu\text{S}/\text{cm}$. The DOC concentration was 3.12 mg/L.

Table 4.5: Volumetric ice contents and hydrochemical parameters of massive ice body TSD12-MI
 (* The median was used instead of the arithmetic mean for values below the detection limit [b. d. l.]).

	Ice content [vol%]	DOC conc. [mg/L]	pH	Electrical cond. [μ S/cm]
TSD12-MI-01	99.99	1.06	7.70	77.7
TSD12-MI-02	99.97	1.03	7.65	87.9
TSD12-MI-03	93.40	6.07	8.09	386.0
TSD12-MI-04	92.65	5.72	8.10	504.0
TSD12-MI-05	100.00	b. d. l.	7.24	47.7
TSD12-MI-06	99.52	1.80	8.01	236.5
TSD12-MI-07	99.09	2.17	7.92	206.5
TSD12-MI-08	100.00	b. d. l.	7.18	26.5
TSD12-MI-09	99.16	1.85	7.79	175.6
TSD12-MI-10	98.24	3.12	8.01	379.0
Range	92.65 – 100.00	1.03 – 6.07	7.18 – 8.10	26.5 – 504.0
Arithmetic mean	98.20	1.80*	7.77	212.74

TSD12-MI

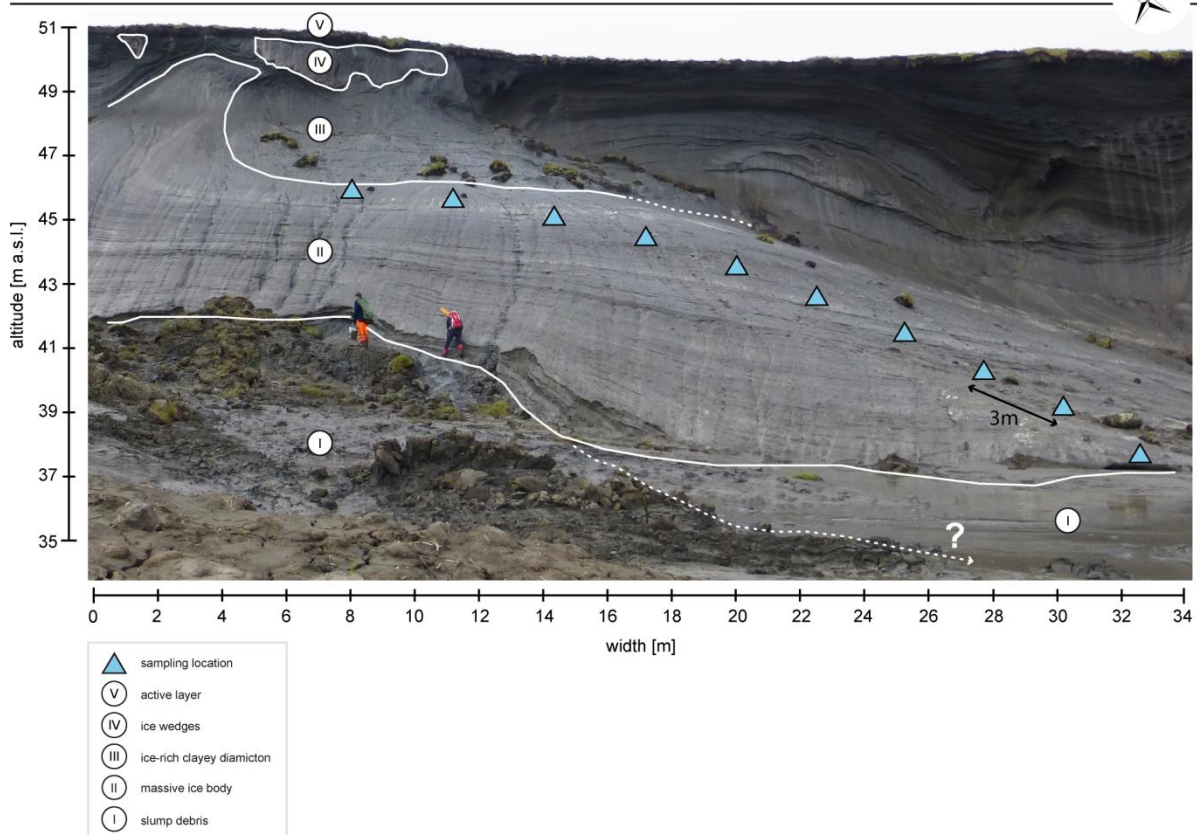


Figure 4.5: Cryostratigraphic profile of massive ice body TSD12-MI with sampling locations.

4.1.6 Massive ice body HIWCS12-MI

The massive ice body HIWCS12-MI is located in a thaw slump on the west coast of Herschel Island and exposed in south-western direction. The sampling was performed at a height of 35.0 to 47.0 m a.s.l. by climbing the ice body with crampons. Two blocks of ice were obtained and the results of the hydrochemical analysis are displayed in Table 4.6.

The profile is divided into four different stratigraphic units (Figure 4.6) and has a height of approximately 14.0 m. The lower part of the profile is covered by slump debris (unit I), which buries the lower part of the massive ice body (unit II). The visible thickness of this ice body is 10.0 m. The slump headwall starts just above the ice body. Unit III consists of an ice-rich clayey diamicton with a thickness of 2.0 to 3.0 m. The upper end of the profile is made of the active layer (unit I) and the overlying tussock tundra vegetation. The mean active layer depth at this location is 50 cm.

The ice sample *HIWCS12-MI-02* contained sediment layers with thicknesses greater than 2 mm, which include gravel and small (<1 mm) and rounded air-bubbles. The sediment was yellow-brown to dark-brown and made of very fine material in largest part. The sample had a volumetric ice content of 98.63 %, a pH of 7.99 and an electrical conductivity of 201.9 $\mu\text{S}/\text{cm}$. The DOC concentration was 2.14 mg/L. The ice sample *HIWCS12-MI-03* contained sediment clusters, macro-organic and small (<1 mm) not-elongated air-bubbles. The sediment was very fine and of a dark-brown to yellow-brown color. The sample had a volumetric ice content of 99.62 %, a pH of 8.32 and an electrical conductivity of 125.3 $\mu\text{S}/\text{cm}$. The DOC concentration was 2.86 mg/L.

Table 4.6: Volumetric ice contents and hydrochemical parameters of massive ice body HIWCS12-MI.

	Ice content [vol%]	DOC conc. [mg/L]	pH	Electrical cond. [μ S/cm]
HIWCS12-MI-02	98.63	2.14	7.99	201.9
HIWCS12-MI-03	99.62	2.86	8.32	125.3
Range	98.63 – 99.62	2.14 – 2.86	7.99 – 8.32	125.3 – 201.9
Arithmetic mean	99.12	2.50	8.16	163.6

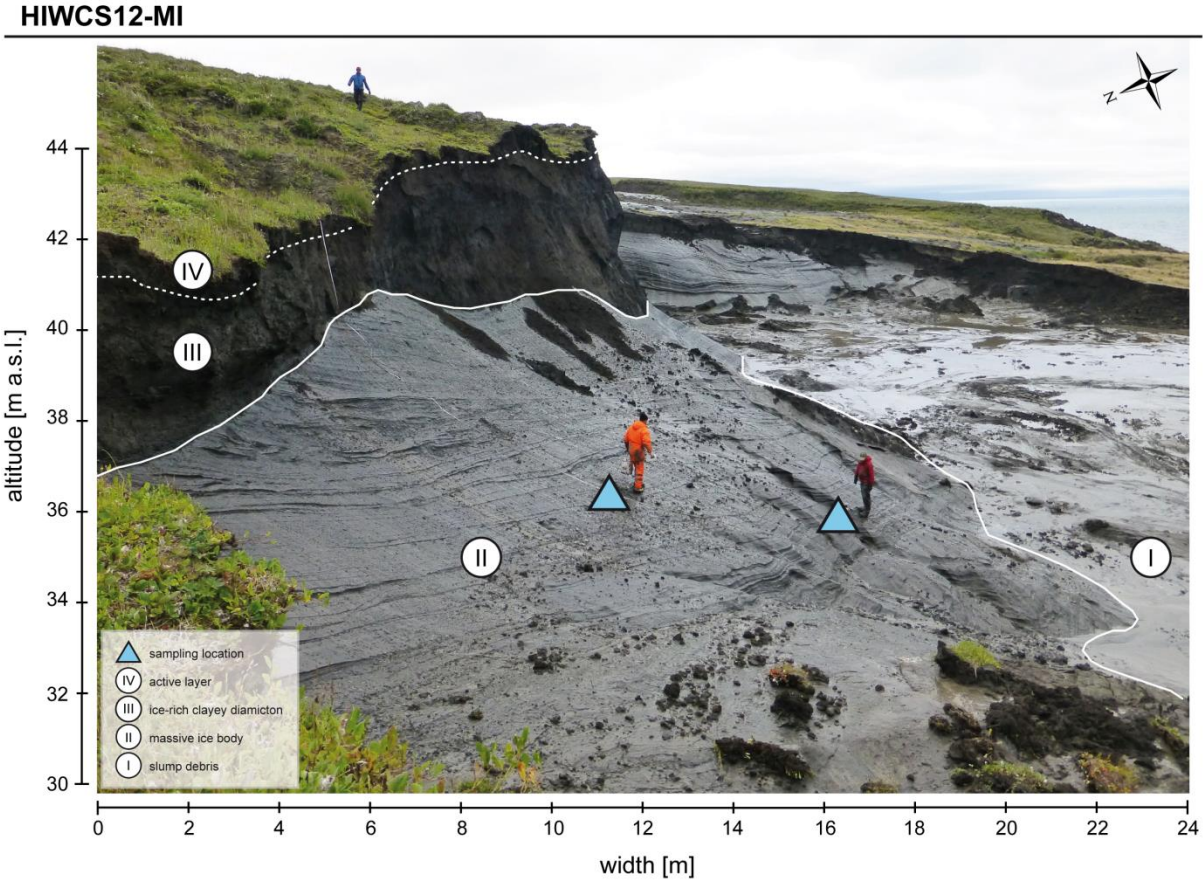


Figure 4.6: Cryostratigraphic profile of massive ice body HIWCS12-MI with sampling locations.

4.1.7 Ice wedge series RB12-IW

The series of ice wedges RB12-IW is located in thaw slump Roland Bay on the Yukon Coastal Plain, 15 km south-east of Herschel Island. The thaw slump is exposed in north-eastern direction and has a width of 208.0 m. The sampling was executed at a height of 27.0 m a.s.l. from the bottom of the headwall. In the following section, at first, the focus is on the stratigraphy of the slump headwall (Figure 4.7) and secondly on the results of the analysis of ice blocks samples from the ice wedges (Table 4.7).

The profile is divided into five different stratigraphic units (Figure 4.7) and has a height of approximately 6.0 m consisting of thawed permafrost sediment. Unit II above the ice is a diamictic layer of 2.0 m thickness with linear ice inclusions. It is surrounded by ice wedges of 4.5 m visible height. The extension of the ice wedges downward is unknown as it is covered by slump debris. Above unit II, follows a frozen blackish sediment layer (unit III) with a lens-like cryostructure. It has a thickness of approximately 1.0 m. Above this layer, is an ice-rich sediment layer (unit IV) with lens-like cryostructure with a thickness of 1.5 m. Unit IV is overlain by the active layer (unit V) with an average thickness of 0.5 m and is topped by tussock tundra vegetation.

The ice sample *RB12-IW1* contained greyish silty-clayey sediment. The sample had a volumetric ice content of 98.92 %, a pH of 7.62 and an electrical conductivity of 444.0 $\mu\text{S/cm}$. The DOC concentration was 2.43 mg/L. The ice sample *RB12-IW2* contained thin sub-linear sediment layers and several sediment clusters. The sediment was silty-clayey and greyish. The sample had a volumetric ice content of 99.98 %, a pH of 7.12 and an electrical conductivity of 73.4 $\mu\text{S/cm}$. The DOC concentration was 12.66 mg/L. The ice sample *RB12-IW3* was sediment-poor. The sediment was silty-clayey with a reddish-brown color and contained some dark-brown accumulations. The sample had a volumetric ice content of 99.97 %, a pH of 7.18 and an electrical conductivity of 75.5 $\mu\text{S/cm}$. The DOC concentration was 10.87 mg/L. The ice sample *RB12-IW4* was sediment-rich and formed sediment clusters after thawing. The sediment was of yellow-brown color and was clayey to sandy and contained angular gravel. The sample had a volumetric ice content of 99.54 %, a pH of 7.53 and an electrical conductivity of 366.0 $\mu\text{S/cm}$. The DOC concentration was 6.38 mg/L. The ice sample *RB12-IW5* contained few sediment clusters. The sediment was sandy and greyish with dark organic accumulations. The sample had a volumetric ice content of 100 %, a pH of 7.21 and an electrical conductivity of 56.1 $\mu\text{S/cm}$. The DOC concentration was 15.77 mg/L. The ice sample *RB12-IW6* contained thin sediment layers and several sediment clusters. The ice contained lens-like air bubbles. The sample had a volumetric ice content of 99.95 %, a pH of 6.94 and an electrical conductivity of 39.1 $\mu\text{S/cm}$. The DOC concentration was 16.29 mg/L. The ice sample *RB12-IW7* contained few sediment. The sediment was

greyish, silty-clayey with several dark-brown clusters. The sample had a volumetric ice content of 99.94 %, a pH of 6.95 and an electrical conductivity of 39.3 $\mu\text{S}/\text{cm}$. The DOC concentration was 15.54 mg/L. The ice sample *RB12-IW8* contained few sediment. The sediment was sandy with a brown color. The sample had a volumetric ice content of 99.97 %, a pH of 7.37 and an electrical conductivity of 64.4 $\mu\text{S}/\text{cm}$. The DOC concentration was 6.62 mg/L. The ice sample *RB12-IW9* was sediment-poor and the sediment was sandy and yellow-brown. The sample had a volumetric ice content of 99.97 %, a pH of 7.76 and an electrical conductivity of 98.6 $\mu\text{S}/\text{cm}$. The DOC concentration was 6.62 mg/L.

Table 4.7: Volumetric ice contents and hydrochemical parameters of ice wedge series RB2-IW.

	Ice content [vol%]	DOC conc. [mg/L]	pH	Electrical cond. [μ S/cm]
RB12-IW1	98.92	2.43	7.62	444.0
RB12-IW2	99.98	12.66	7.12	73.4
RB12-IW3	99.97	10.87	7.18	75.5
RB12-IW4	99.54	6.38	7.53	366.0
RB12-IW5	100.00	15.77	7.21	56.1
RB12-IW6	99.95	16.29	6.94	39.1
RB12-IW7	99.94	15.54	6.95	39.3
RB12-IW8	99.97	8.57	7.37	64.4
RB12-IW9	99.97	6.62	7.76	98.6
Range	98.92 – 100.00	2.43 – 16.29	6.94 – 7.76	39.1 – 444.0
Arithmetic mean	99.80	10.57	7.30	139.60

RB12-IW

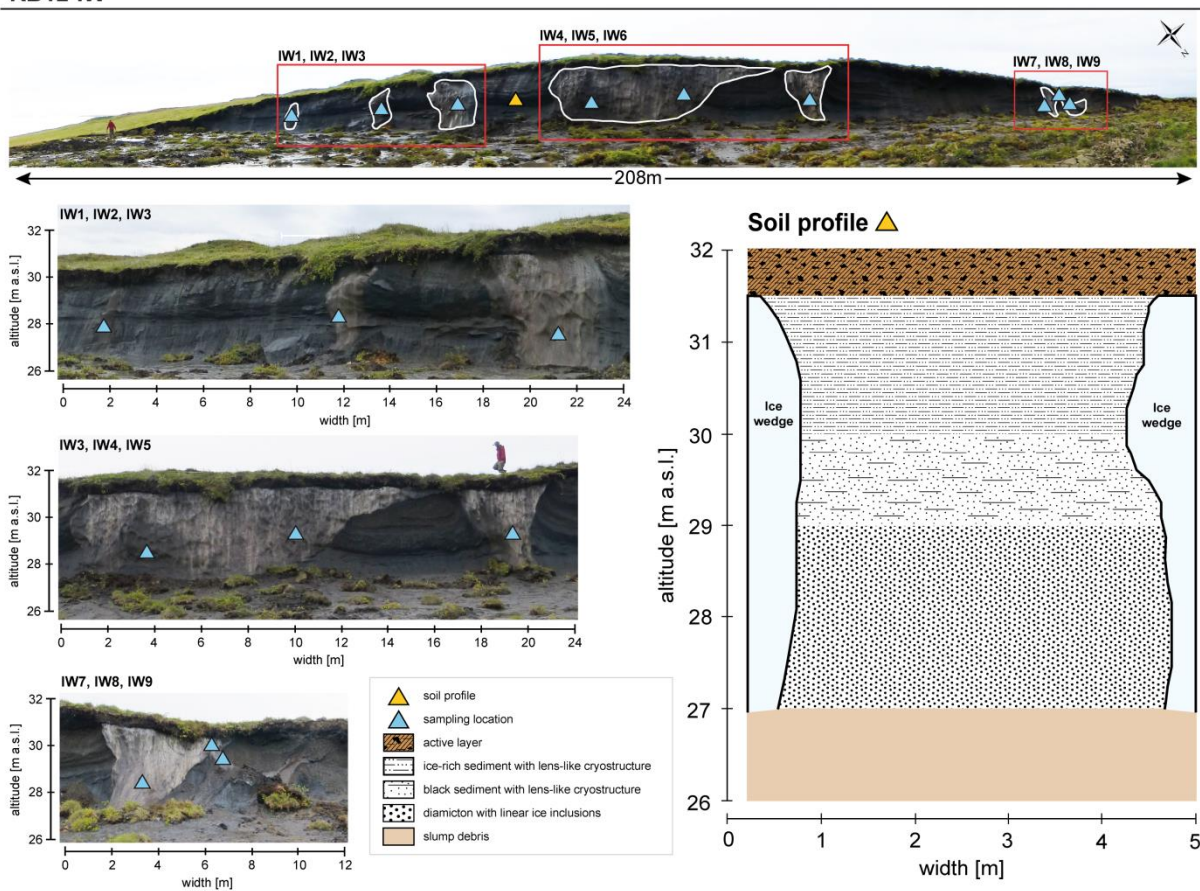


Figure 4.7: Exposure description and cryostratigraphic profile of ice wedge series RB12-IW with sampling locations in the exposure and the profile.

4.1.8 Massive ice body KP12-MI

The massive ice body KP12-MI is located in a thaw slump at Kay Point along the Yukon Coastal Plain, 40 km south-east of Herschel Island. The massive ice body is exposed in northern direction. The sampling was executed in a height of 47.0 to 51.0 m a.s.l. by climbing the ice body with crampons and sampling seven ice blocks in different cryostratigraphic features of the ice body. The results of laboratory analysis and volumetric ice content determination are summarized in Table 4.8.

The profile is divided into six different main stratigraphic units (Figure 4.8) and has a height of approximately 10.0 m. Three sub-units are used to describe different ice characteristics within the massive ice body. The lowest part of the profile is presented by slump debris (unit I). The main part of the profile is formed by the massive ground ice body (unit II) with a visible thickness of 8.0 m as the lower part is buried by slump debris. The massive ground ice body consists of different types of ice: milky white ice (unit IIa), clear blue ice (unit IIb) and sediment-rich grey ice (unit IIc). Above the massive ice body, the slump headwall begins. It is segmented into four different units. Unit III, which directly forms the border between massive ice and frozen sediment, is characterized by diamictic sediment with micro-lenticular cryostructure. It is 0.5 to 1.0 m thick. Unit IV is an ice-rich loamy diamicton with lens-like cryostructure with a thickness of approximately 1.0 m. Units III and IV are characterized by an ice wedge that reaches down into the massive ice layer (unit II). The upper end of the profile is presented by the active layer (unit VI) that has a thickness of 55 cm in average and is topped by tussock tundra vegetation.

The ice sample *KP12-MI-01* consisted of pure ice with numerous air-bubbles that were not directed with sizes of greater than 1 mm. The sample had a volumetric ice content of 100 % with a pH of 6.32 and an electrical conductivity of 14.8 $\mu\text{S}/\text{cm}$. The DOC concentration was not available as the value was below the device specific detection limit. The ice sample *KP12-MI-02* consisted of pure clear ice with a few air-bubbles greater than 1 mm. The sample had a volumetric ice content of 100 % with a pH of 7.09 and an electrical conductivity of 18.0 $\mu\text{S}/\text{cm}$. The DOC concentration was not available as the value was below the device specific detection limit. The ice sample *KP12-MI-03* was pure and clear ice without any air-bubbles. The sample had a volumetric ice content of 100 % with a pH of 6.75 and an electrical conductivity of 5.4 $\mu\text{S}/\text{cm}$. The DOC concentration was not available as the value was below the device specific detection limit. The ice sample *KP12-MI-04* was pure ice with linear layers of air-bubbles. The sample had a volumetric ice volume of 100 % with a pH of 6.91 and an electrical conductivity of 51.8 $\mu\text{S}/\text{cm}$. The DOC concentration was not available as the value was below the device specific detection limit. The ice sample *KP12-MI-05* consisted of pure ice with numerous small air-bubbles greater than 1 mm. The sample had a

volumetric ice content of 99.99 % with a pH of 7.93 and an electrical conductivity of 332.0 $\mu\text{S}/\text{cm}$. The DOC concentration was 1.06 mg/L. The ice sample *KP12-MI-06* consisted of pure and clear ice with numerous air-bubbles with sizes of approximately 1 mm. The sample had a volumetric ice content of 100 % with a pH of 7.25 and an electrical conductivity of 107.1 $\mu\text{S}/\text{cm}$. The DOC concentration was not available as the value was below the device specific detection limit. The ice sample *KP12-MI-07* contained several thin sediment layers and numerous partially directed air-bubbles. The sediment was grey-yellow-brown and made of sandy to silty-clayey particles. The sample had a volumetric ice content of 99.92 % with a pH of 7.95 and an electrical conductivity of 378.0 $\mu\text{S}/\text{cm}$. The DOC concentration was 2.46 mg/L.

Table 4.8: Volumetric ice contents and hydrochemical parameters of massive ice body KP12-MI
 (* The median was used instead of the arithmetic mean for values below the detection limit [b. d. l.]).

	Ice content [vol%]	DOC conc. [mg/L]	pH	Electrical cond. [μ S/cm]
KP12-MI-01	100.00	b. d. l.	6.32	14.8
KP12-MI-02	100.00	b. d. l.	7.09	18.0
KP12-MI-03	100.00	b. d. l.	6.75	5.4
KP12-MI-04	100.00	b. d. l.	6.91	51.8
KP12-MI-05	99.99	1.06	7.93	332.0
KP12-MI-06	100.00	b. d. l.	7.25	107.1
KP12-MI-07	99.29	2.46	7.95	378.0
Range	98.92 – 100.00	1.06 – 2.46	6.32 – 7.93	5.4 – 378.0
Arithmetic mean	99.90	1.76*	7.17	129.59

KP12-MI

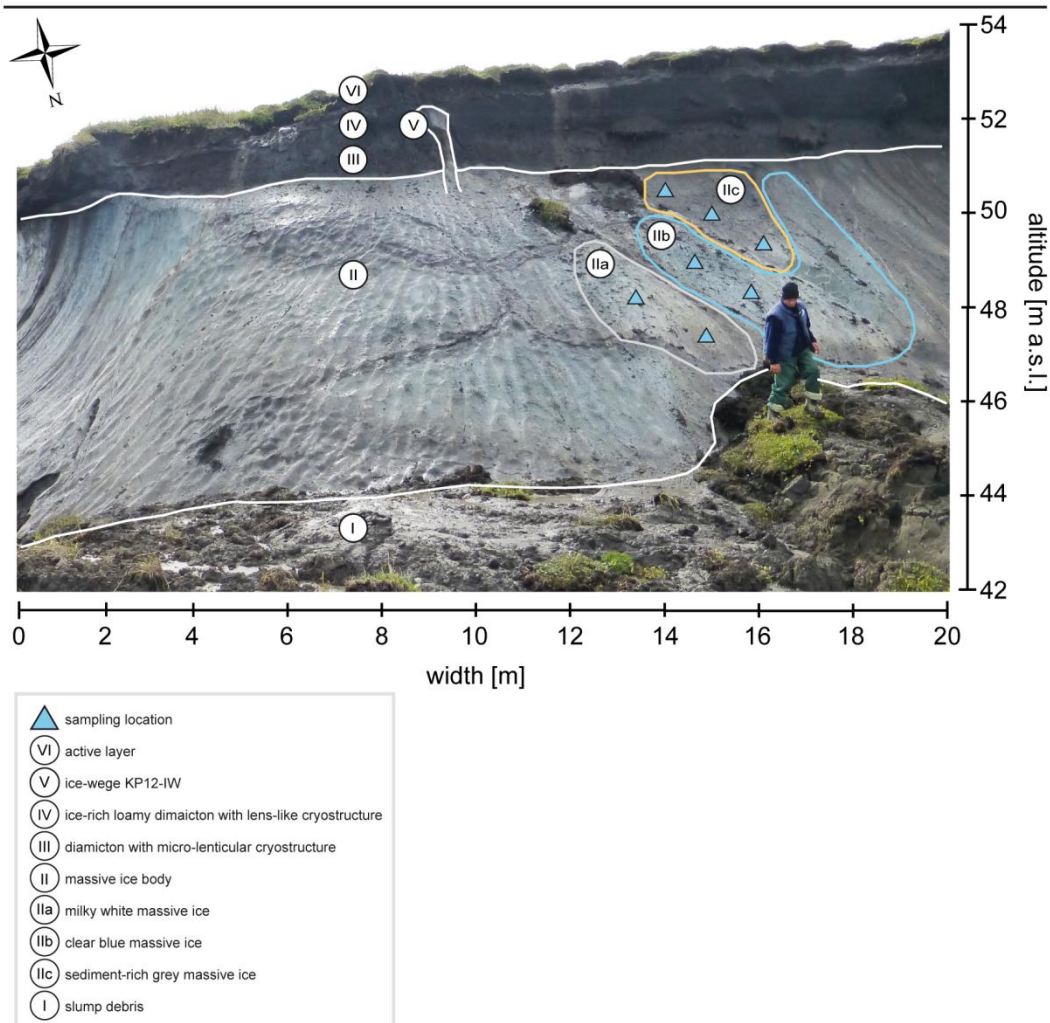


Figure 4.8: Cryostratigraphic profile of massive ice body KP12-MI with sampling locations.

4.1.9 Ice wedge KP12-IW

The ice wedge KP12-IW in the headwall of thaw slump Kay Point is located on the Yukon Coastal Plain, 40 km south-east of Herschel Island. The ice wedge is exposed in northern direction. The sampling was executed in a height of 51.0 m a.s.l. from top of the massive ice body KP12-MI. Two ice samples have been taken. The results of laboratory analysis and volumetric ice content determination are summarized in Table 4.9.

The profile is divided into six different stratigraphic units (Figure 4.9) and has a height of approximately 4.0 m. The lower part is formed by the massive ice body KP12-MI that is described in detail in section 4.1.8. The layer directly above the massive ice is characterized by ice-rich sediment with a lens-like vertical to sub-vertical cross-linked cryostructure and layers of clay and sand. The sandy layers have grey, the clayey layers a brown color. The sediment of the layer that has a thickness of 20 cm is grey-brown. Subsequently above, follows a diamictic layer with fine lens-like cryostructure, organic-rich intrusions and gravel enclosures. The ice-lenses and ice-layers are very thin (<1 cm). The contained gravel is small with sizes of 1 to 3 cm and well-rounded. The thickness of the layer is approximately 30 cm. The transition to the layer above is presented in form of a bright sediment layer. The layer above is characterized by loamy diamictic sediment with a lens-like cryostructure and gravel intrusions with a thickness of approximately 1.0 m. The ice-lenses have a thickness of 1 to 5 mm. The peat intrusions have sizes up to 10 cm in width. The gravel particles are well rounded with sizes between 1 and 12 cm. The ice wedge, with a width of 30.0 to 40.0 m and a visible height of 3.5 m, intersects the described units. The fate of the lower part is unknown as it penetrates the massive ice body and is not visible. The upper part of the profile is presented by the active layer with a depth of 55 cm and tussock tundra vegetation on top.

The ice sample *KP12-IW1-01* is taken from the left side of the ice wedge. The sediment was very fine (silty-clayey) with a yellow-brown color. The sample had a volumetric ice content of 99.96 % with a pH of 7.81 and an electrical conductivity of 90.0 $\mu\text{S}/\text{cm}$. The DOC concentration was 3.14 mg/L. The ice sample *KP12-MI-02* from the right part of the ice wedge was sediment-poor. The sediment was sandy with a yellow-brown color. The sample had a volumetric ice content of 99.97 % with a pH of 8.61 and an electrical conductivity of 105.3 $\mu\text{S}/\text{cm}$. The DOC concentration was 4.81 mg/L.

Table 4.9: Volumetric ice contents and hydrochemical parameters of ice wedge KP12-IW.

	Ice content [vol%]	DOC conc. [mg/L]	pH	Electrical cond. [μ S/cm]
KP12-IW1-01	99.96	3.14	7.81	90.9
KP12-IW1-02	99.97	4.81	8.61	105.3
Range	99.96 – 99.97	3.14 – 4.81	7.81 – 8.61	98.10 – 105.3
Arithmetic mean	99.96	3.97	8.21	98.10

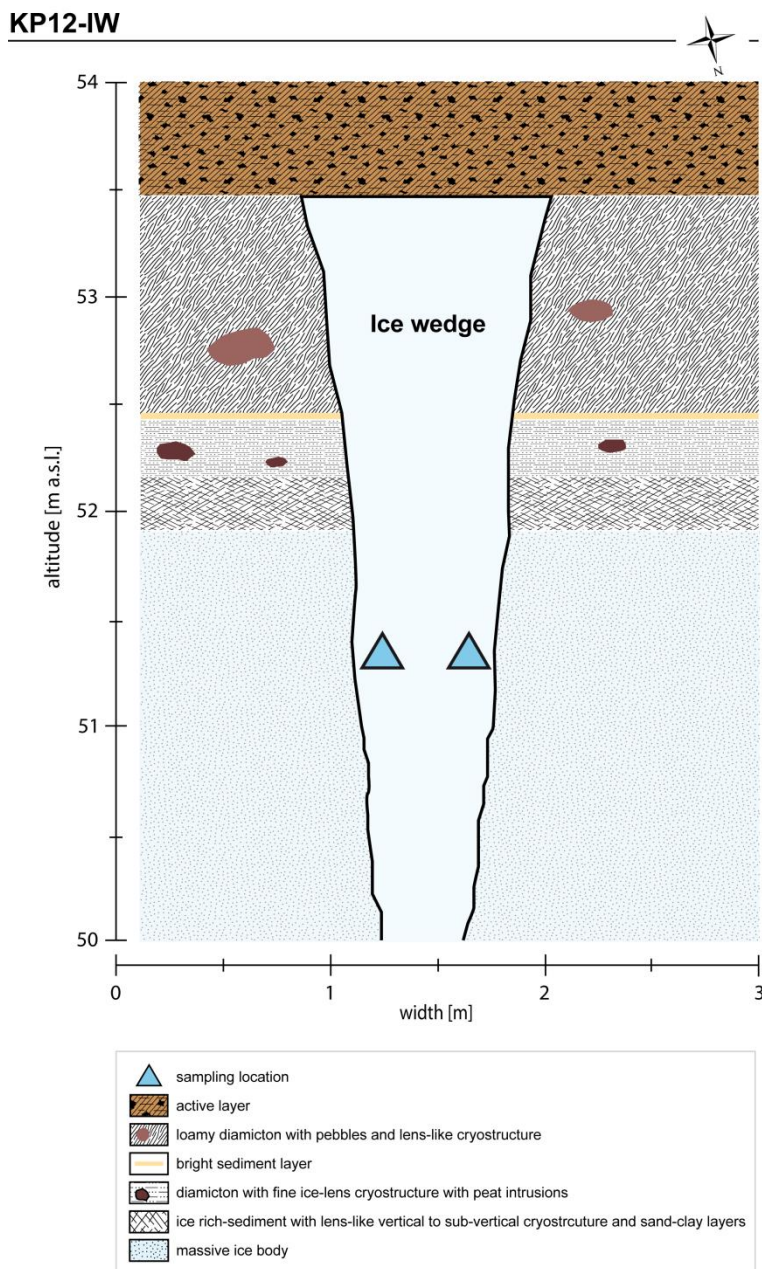


Figure 4.9: Cryostratigraphic profile of massive ice body KP12-IW with sampling locations.

4.2 Synthesis hydrochemistry

Table 4.10 gives an overview of the results from the hydrochemical analyses. Almost all samples were sediment-poor with volumetric ice contents greater than 98 %. Only two samples taken from massive ground ice at thaw slump D (TSD12-MI12) had lower ice contents, between 92.56 vol% and 93.40 vol%. Overall, volumetric ice contents ranged between 92.56 and 100.00 % with an arithmetic mean of 99.43 % (Table 4.10).

The values for DOC concentration are in the range of 1.03 and 19.48 mg/L (Figure 4.10) with a median of 4.30 mg/L. The median was used instead of the arithmetic mean because of the presence of samples with DOC concentrations below the detection limit. That was the case for seven samples, two from massive ice body TSD12-MI and five from massive ice body KP12-MI. The DOC concentrations were at the highest in ice wedges TSC12-IW and RB12-IW (Figure 4.10).

The pH was in the range of 6.32 and 8.61 (Table 4.10) with an arithmetic mean of 7.5. The lowest pH values were found in KP12-MI and TSD12-IW2, the highest values in KP12-IW and HIWCS12-MI (Figure 4.11). The values for electrical conductivity ranged between 5.4 and 504.0 $\mu\text{S}/\text{cm}$ (Table 4.10). The lowest values were found in KP12-MI and TSD12-MI and the highest values in TSD12-MI and RB12-IW (Figure 4.12). The arithmetic mean was 149.9 $\mu\text{S}/\text{cm}$.

Table 4.10: Synthesis of hydrochemical analyses (* The median was used instead of arithmetic mean because of values below the detection limit [b. d. l.]).

Samples in total	Ice content [vol%]	DOC conc. [mg/L]	pH	Electrical cond. [$\mu\text{S}/\text{cm}$]
Range	92.65 – 100.0	1.03 – 19.48	6.32 – 8.61	5.4 – 504.0
Arithmetic mean	99.43	4.30*	7.50	149.9

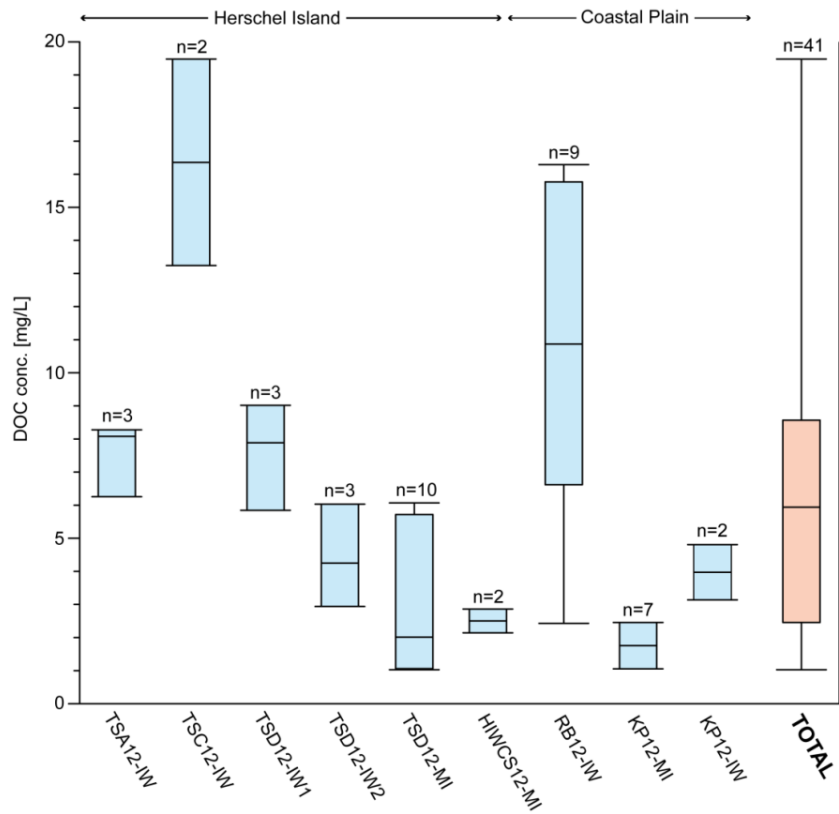


Figure 4.10: Box plot diagram showing the results of DOC concentration measurements.

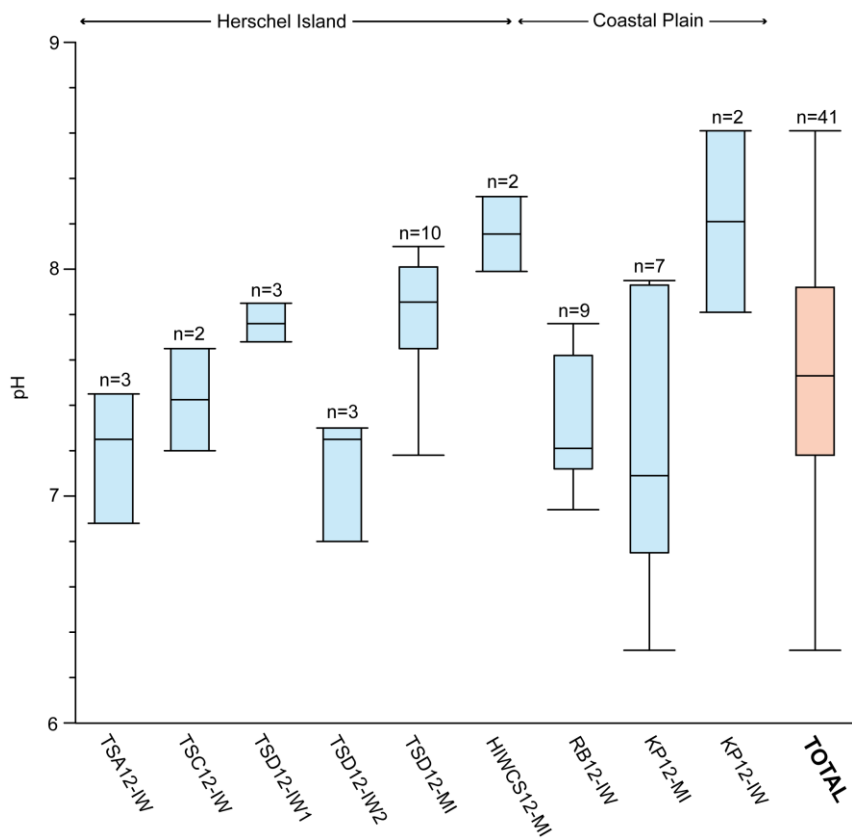


Figure 4.11: Box plot diagram showing the results of pH measurements.

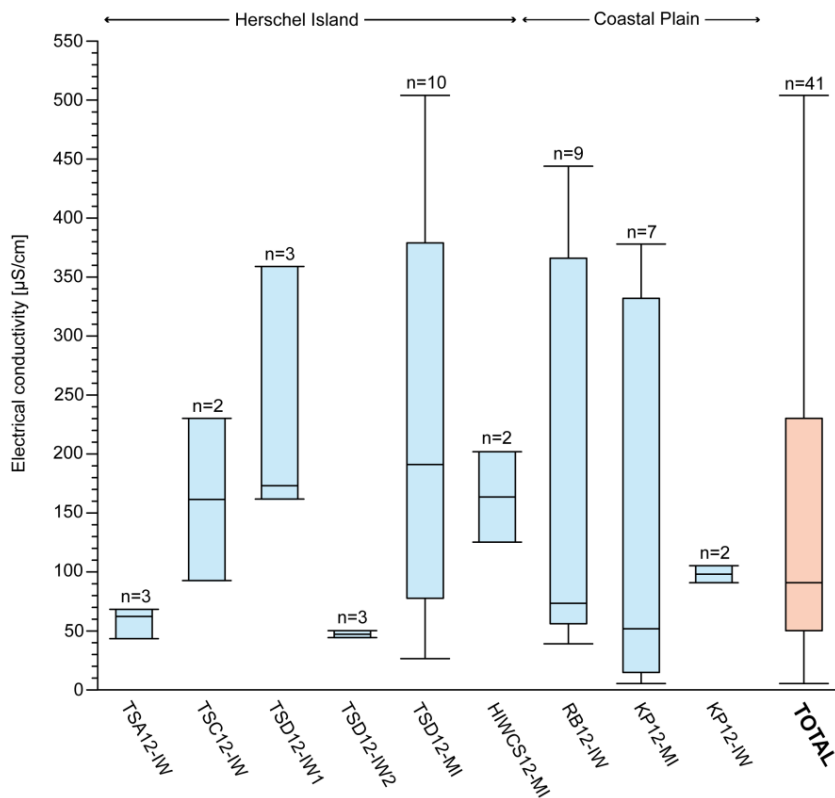


Figure 4.12: Box plot diagram showing the results of electrical conductivity measurements.

4.3 Massive ground ice contents

Volumetric massive ground ice contents along the Yukon Coastal Plain have been compiled by COUTURE (2010). Figure 4.13 gives an overview of the terrain units and their volumetric massive ground ice contents.

Massive ground ice contents ranged between 0 vol% (no massive ground ice) and 47 vol%. The average massive ground ice content for the entire Yukon Coastal Plain was 11 vol%. The lowest values, with no ground ice contents, were found in fourteen terrain units (TU 2, 3, 7, 8, 9, 10, 13, 18, 20, 26, 29, 31, 32 and 36) and the highest value of 47 vol% at King Point SE (TU 38).

The western coastal part is generally ice-poor with an average massive ground ice content of 10 vol%. In two terrain units, massive ground ice contents were higher. At Clarence Lagoon W (TU 1), massive ground ice contents were 35 vol% and at Komakuk Beach W1 (TU 5) 40 vol%. The remaining terrain units at Komakuk Beach (TU 4 and 6) had values of 7 and 8 vol%. No massive ground ice was found at Clarence Lagoon and Clarence Lagoon E (TU 2 and 3) as well as at the river fan (TU 7), Nunaluk Spit (TU 8) and Avadlek Spit (TU 10).

Massive ground ice volumes on Herschel Island can reach up to 28 vol% in the east (TU 14) but are in general low with an average of 10 vol%. The spits Avadlek Spit (TU 10) and

Simpson Point (TU 13) contain no massive ground ice. The cliffs at the west side (TU 11) and the north side (TU 12) have values of 9 to 10 vol% and the southern coast (TU 15) 14 vol%.

The central coastal part has an average massive ground ice content of 10 vol%. Contents are at the highest at Whale Cove E (TU 36) with 36 vol% and Workboat Passage W (TU 16) with 22 vol%. No massive ground ice contents can be found at spits like Catton Point (TU 18) and Stokes Point (TU 26). Furthermore, the western part of Phillips Bay (TU 29) and the delta of Babbage River (TU 31) contain no massive ground ice. In the other terrain units, the massive ground ice content not exceeds 10 vol% (TU 19, 24, 27 and 30), except Roland Bay NW and W (TU 22 and 23) and Stokes Point W (TU 25) with 12 vol%.

In the eastern coastal part, massive ground ice contents of up to 47 vol% at King Point SE (TU 38) can be reached. The average content along this coastal part is 12 vol%. No massive ground ice can be found at Kay Point spit (TU 32) and King Point Lagoon (TU 36). In some terrain units values reach more than 10 vol%. This is the case for Kay Point (TU 33) with 14 vol%, King Point NW (TU 35) with 13 vol%, King Point (TU 37) with 14 vol% and Sabine Point, Sabine Point E and Sabine Point W (TU 40, 41 and 42) with 18, 14 and 15 vol%, respectively.

The remaining terrain units do not exceed a value of 10 vol%, like Kay Point SE (TU 34) with 9 vol%, Shingle Point E (TU 43) with 5 vol% and Running River (TU 44) with 1 vol%. Retrogressive thaw slumps, which appearance is connected with thawing underlying massive ground ice, can be found ubiquitously along the whole Yukon Coastal Plain, except for the western coastal part where massive ground ice can be found only in a small thaw slump at Komakuk Beach.

In conclusion, massive ground ice contents are on average nearly the same in all coastal parts with 10 vol% except the eastern part with 12 vol%. The highest ground ice contents can be found at Clarence lagoon (TU 1), Komakuk Beach (TU 5), the east side of Herschel Island (TU 14), Workboat passage (TU 16), Whale Cove (TU 21) and King Point (TU 38). The lowest values, as well as the segments for which no massive ground ice occurs, are found at spits, river fans and most lagoons.

In general, the highest volumetric massive ground ice contents can be found in rolling moraine (17 vol%) and lacustrine sediments (16 vol%). A slightly lower value had been found in glacial outwash (12 vol%) and ice-thrust moraine sediments (14 vol%). An absence of massive ground was already determined in marine and fluvial deposits by COUTURE (2010).

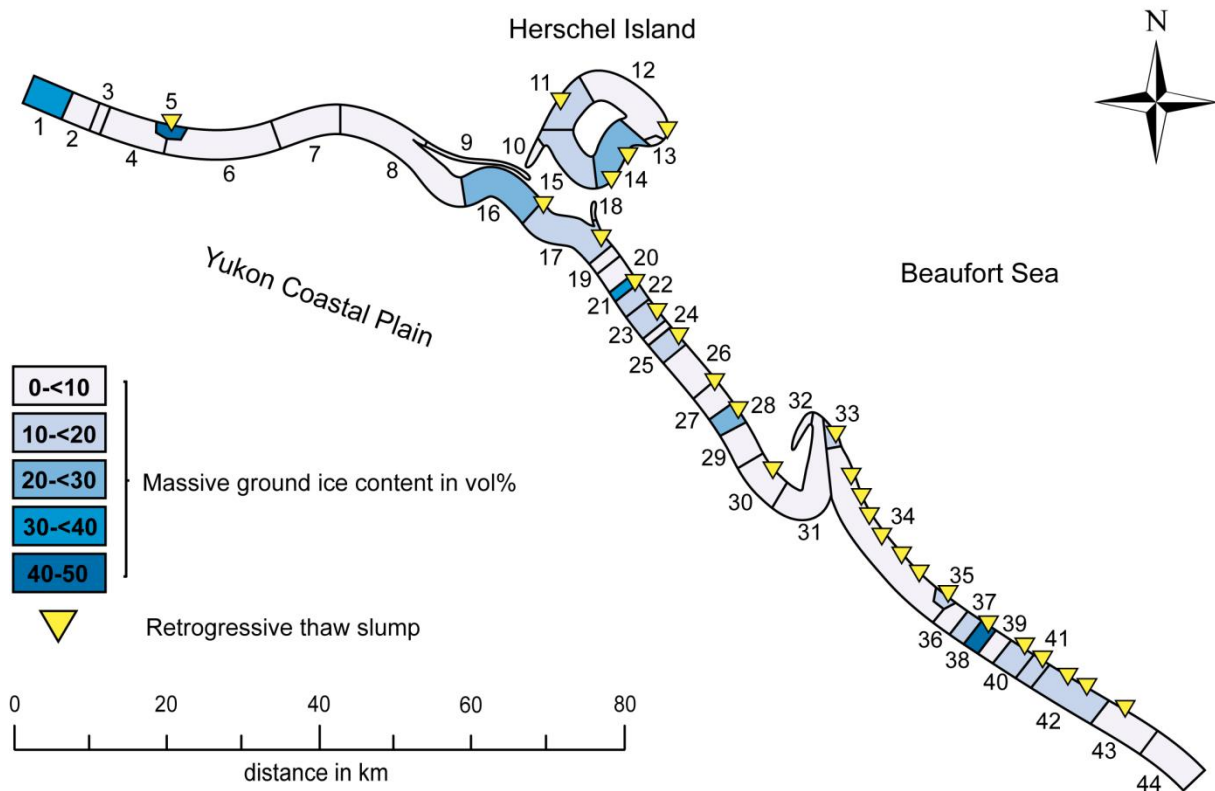


Figure 4.13: Volumetric massive ground ice contents along the Yukon Coastal Plain.

4.4 Coastal erosion rates

Coastal erosion rates along the Yukon Coastal Plain have been classified in seven classes from no erosion to greater than 3.0 m/yr (Figure 4.14). Coastal erosion rates range between 0.0 m/yr (no erosion) and 3.13 m/yr at King Point lagoon (TU 36). The average coastal erosion along the Yukon Coastal Plain is 0.73 m/yr. Figure 4.14 gives an overview of these rates for each terrain unit.

In the western part of the coast, erosion rates reach up to 1.83 m/yr at Malcolm River fan (TU 7) and are lowest at Clarence lagoon (TU 1, 2 and 3) with 0.44 to 0.62 m/yr and at the Malcolm River fan (TU 8), where no erosion occurs. At Komakuk Beach (TU 4, 5 and 6), coastal erosion rates between 0.68 and 1.40 m/yr occur. At Nuneluk Spit (TU 9), close to Herschel Island, the erosion rate is 0.95 m/yr.

Herschel Island is dominated by coastal erosion rates smaller than 1 m/yr. The highest erosion rates can be found at the west side of Herschel Island (TU 11) with 0.95 m/yr, while no erosion occurs at the south side of the island (TU 15) and the spit Simpson Point (TU 13). Annual coastal retreat at the northern (TU 12) and eastern (TU 14) part are 0.77 and 0.71 m/yr. On average, the coastal erosion rate at Herschel Island is 0.53 m/yr.

The central part of the coastal plain is composed of terrain units with variable coastal erosion rates that range from class 0.0-0.5 m/yr to 1.5-2.0 m/yr. No coastal erosion occurs at four terrain units: Catton Point (TU 18), Whale Cove E (TU 21), Phillips Bay NW (TU 28) and Babbage River Delta (TU 31). The highest coastal erosion rate can be found at Whale Cove (TU 20) with 1.5 m/yr. Strongest erosion rates greater than 1.0 m/yr are detected at Stokes Point (TU 26) with 1.36 m/yr and Phillips Bay (TU 30) with 1.3 m/yr. On average the coastal erosion rate in the central part is 0.43 m/yr.

The eastern part of the coastal plain is characterized by a scattered range of erosion ranging from 0.0 m/yr (no erosion) to 3.13 m/yr. At Kay Point (TU 33) and Kay Point lagoon (TU 36), erosion rates are high with values of 2.65 and 3.13 m/yr. No erosion occurs at Kay Point Spit (TU 32) and King Point NW (TU 28). Erosion rates exceeding 1.0 m/yr can be found at King Point (TU 37) with 2.44 m/yr, King Point SE (TU 38) with 1.6 m/yr and Sabine Point E (TU 41) with 1.43 m/yr. On average the coastal erosion is 1.15 m/yr in this coastal part.

In conclusion, erosion rates are at the highest in the eastern part of the coastal plain with an average value of 1.15 m/yr. The central part and Herschel Island are characterized by lower erosion rates of 0.43 and 0.53 m/yr. The western part has moderate erosion rates of 0.82 m/yr.

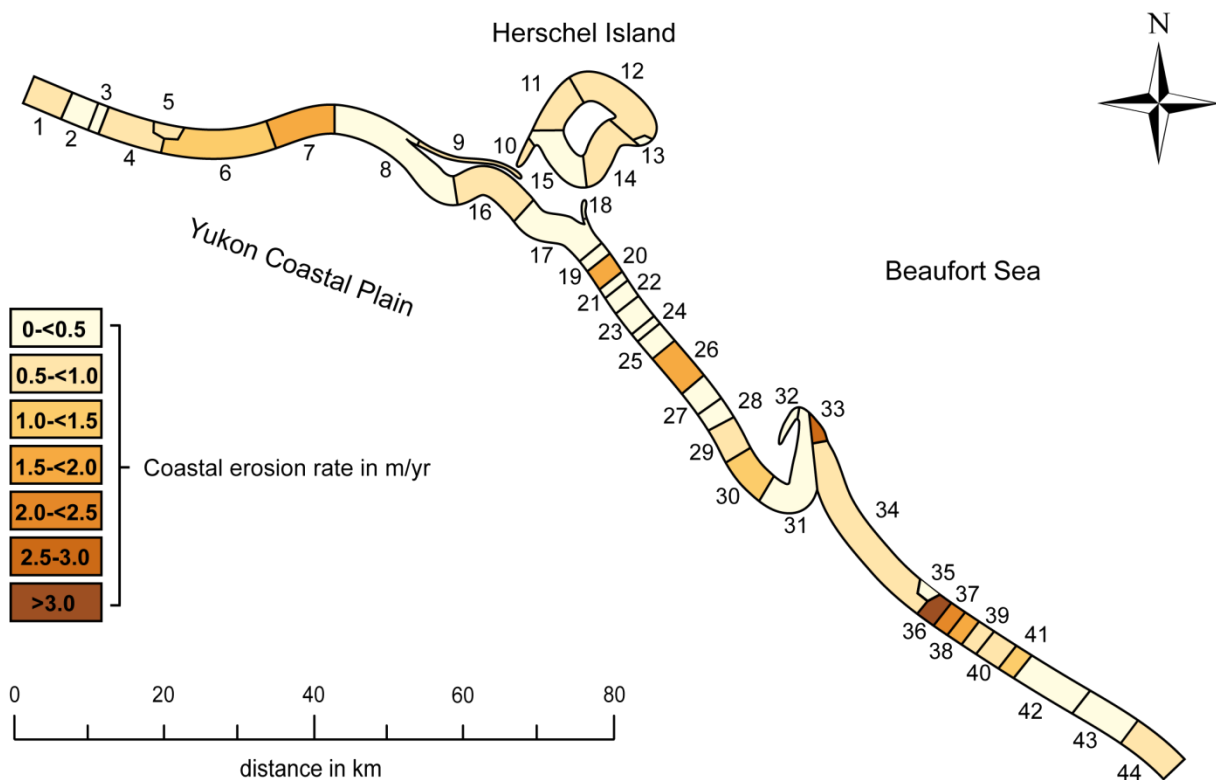


Figure 4.14: Coastal erosion rates along the Yukon Coastal Plain.

4.5 Coastline height

The coastline height varies along the Yukon Coastal Plain (Figure 4.14) between 0.9 and 60.0 m. The lowest coastline heights can be found at Kay Point Spit (TU 32) with 0.9 m and the highest at the north side of Herschel Island (TU 12) with 60.0 m. The average coastline height is 12.2 m.

The western part of the Yukon Coastal Plain is relatively flat (average 2.5 m) with the highest coastline height at Komakuk Beach (TU 4, 5, 6) with 3.5 to 5.3 m and the lowest coastline heights at the Malcolm River fan (TU 7 and 8), Clarence Lagoon (TU 2 and 3) and Nunaluk Spit (TU 9) between 1.0 and 1.2 m, respectively.

Herschel Island is dominated by a high coastline height (average 24.7 m). Especially in the western and northern part of the island the coastline height can reach up to 56.0 m (TU 11) and 60.0 m (TU 12). The south-eastern part of the island is flatter ranging from 5.5 m at Herschel Island S (TU 15) to 24.5 m at the east side of the island (TU 14 and 15). The coastline of Avadlek Spit has a height of 1.0 m.

The central part of the coastal plain is characterized by moderate coastline heights (average 6.9 m) between 1.0 and 22.0 m. The lowest coastline heights, not exceeding 5.0 m, can be found at Workboat Passage (TU 16 and 17), Whale Cove (TU 19, 20 and 21) and the north-western part of Roland Bay (TU 22). At Catton Point, coastline height is 1.4 m. At Roland Bay (TU 23 and 24), the coastline height can reach values of 19.0 m in the west (TU 23) and 19.0 m in the east of Roland Bay (TU 24). At units Stokes Point and Phillips Bay, the coastline height varies between 1.0 m in Phillips Bay W (TU 29) and 10.0 m at Stokes Point SE (TU 27). At Babbage River delta, the coastline height is 3.0 m.

The eastern part of the coastal plain is characterized by a moderate to high coastline height with a lowest value of 0.9 m at Kay Point spit (TU 32) and highest value of 40.0 m at King Point NW (TU 35) and Sabine Point (TU 40). At Kay Point spit (TU 32), the coastline height is very low with 0.9 m but increases in the eastern direction to 7.0 m at Kay Point (TU 33) and 30.0 and 40.0 m at Kay Point SE (TU 34) and King Point NW (TU 35), respectively. A similar increasing trend in eastern direction can be found from King Point lagoon (TU 36) with 1.0 m height through King Point (TU 37) and King Point SE (TU 34), with 7.0 and 12.0 m, respectively, to Sabine Point W (TU 43) and Sabine Point (TU 40), with 25.0 and 40.0 m, respectively. The remaining terrain units further east from Sabine Point E (TU 41) to Running River (TU 44) are in the range of 20.0 to 26.0 m coastline height. On average the western part of the coastline is 19.8 m high.

To summarize, Herschel Island has the highest coastline with 24.7 m on average, followed by the eastern part with 19.8 m. The central and western parts have smaller coastline heights of 2.5 to 6.9 m, respectively.

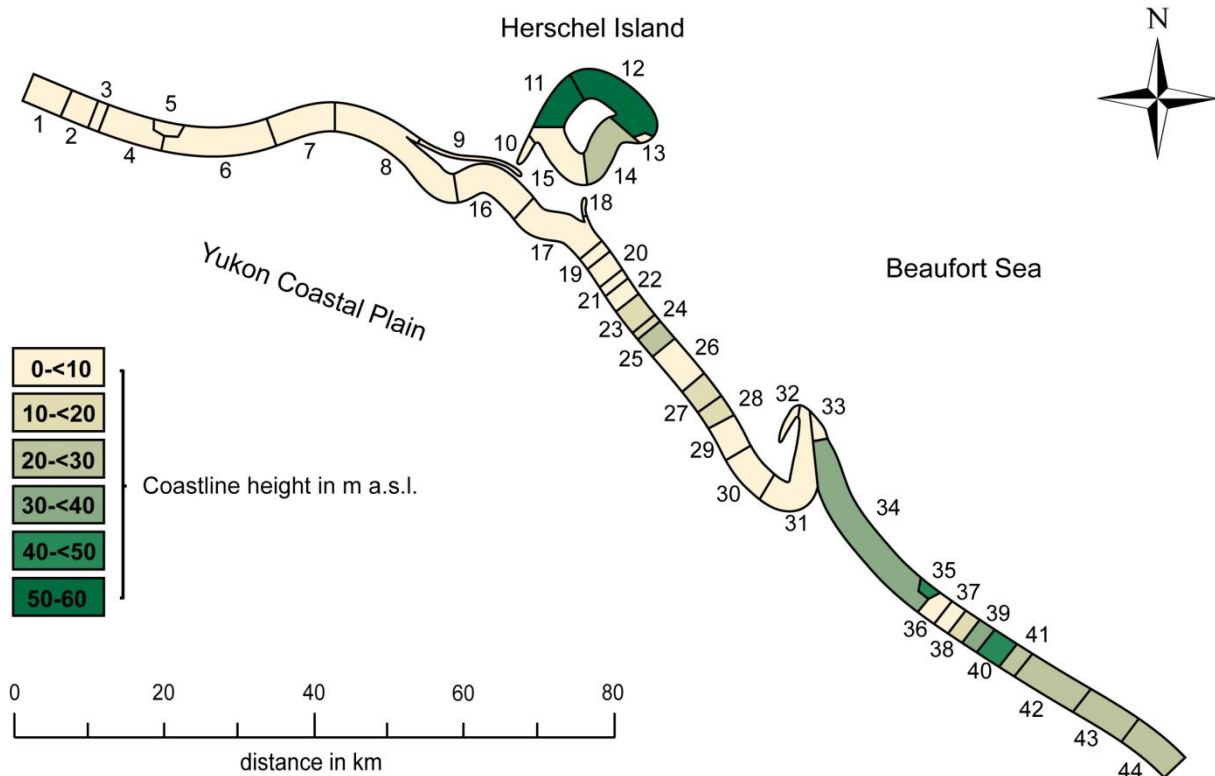


Figure 4.15: Average coastline height along the Yukon Coastal Plain.

4.6 DOC stocks

The estimated DOC stocks are presented in three scenarios (Figure 4.16). Scenario I is the DOC stock conducted by incorporating the 25%-quartile of the measured DOC concentrations in all samples into the DOC stock calculation (section 3.4). Scenario II and III are the 50%-quartile (median) and 75%-quartile of the measured DOC concentrations in all ice samples. All three scenarios are presented to give a range of possible DOC stocks in the terrain units along the Yukon Coastal Plain.

The western coastal part has in general low DOC stocks, ranging from 0.1 (scenario I and II) to 0.2 g/m³ (scenario III). No DOC stocks in all scenarios can be found at parts of Clarence Lagoon (TU 2 and 3), at Malcolm River fan (TU 7 and 8) and Nuneluk Spit (TU 9). Higher DOC stocks have been estimated for the western part of Clarence Lagoon (TU 1) and for parts of Komakuk Beach (TU 5). For Clarence Lagoon (TU 1), values range from 0.25 to 0.87 g/m³ (scenario I to III). For Komakuk Beach values range between 0.26 and 0.96 g/m³.

Herschel Island contains low amounts of DOC. For scenario I and II, the average DOC stock was 0.1 g/m^3 and for scenario III, 0.2 g/m^3 . The northern and western part of the island contains no or low amounts of DOC. Avadlek Spit (TU 10) and Simpson Point (TU 13) contain no DOC, whereas the west (TU 11) and east side (TU 12) of the island contain low DOC ranging at the west side from 0.02 to 0.08 g/m^3 (scenario I to III) and at the north side from 0.02 to 0.06 g/m^3 . More DOC is present at the east (TU 14) and south side (TU 15) of the island. For the east side, values range from 0.12 to 0.50 g/m^3 and for the south side from 0.17 to 0.34 g/m^3 .

The central part contains low DOC stocks with an average of 0.1 g/m^3 in scenario I, reaching 0.2 g/m^3 in scenario II and 0.3 g/m^3 in scenario III. No DOC stocks are estimated for Catton Point (TU 18), Whale Cove (TU 20), Stokes Point (TU 26), Phillips Bay W (TU 29) and Babbage River Delta (TU 31). Higher values can be found at Workboat Passage (TU 16 and 17). For Workboat Passage W (TU 16), values range from 0.46 to 0.96 g/m^3 (scenario I to III) and for Workboat Passage E (TU 17), from 0.29 to 0.60 g/m^3 . The highest DOC stock in this coastal part is estimated for Whale Cove E, with values ranging from 0.54 to 1.41 g/m^3 . DOC stocks for Roland Bay (TU 22 to 24), Stokes Point (TU 25 to 27) and Phillips Bay (TU 28 to 30) are in general low ($0 < 0.3 \text{ g/m}^3$), except at Phillips Bay NW (TU 28), where values are higher, ranging from 0.18 to 0.53 g/m^3 .

The eastern part is generally low in DOC stocks, with average values ranging from 0.1 to 0.2 g/m^3 (scenario I to III). No DOC stocks were calculated for Kay Point Spit (TU 32) and King Point Lagoon (TU 36). With exception of three terrain units, the DOC stocks comprised between 0.0 and 0.3 g/m^3 for all scenarios. Higher values are obtained for Kay Point (TU 33) with values ranging from 0.27 and 0.55 g/m^3 (from scenario I to III) and King Point (TU 37) with values ranging from 0.21 and 0.44 g/m^3 . The highest values are derived for King Point SE (TU 38), where values range between 0.38 to 1.27 g/m^3 .

In conclusion, the DOC stock on the Yukon Coastal Plain is low in all scenarios with values of 0.09 , 0.15 and 0.24 g/m^3 for scenarios I to III. The central part of the coast contains the highest DOC stocks of all parts with values ranging from 0.1 to 0.3 g/m^3 , depending on the scenario. The average DOC stocks for the western and eastern part as well as for Herschel Island are the same with values ranging from 0.1 to 0.2 g/m^3 (also depending on the scenario). At the mainland directly south of Herschel Island (Workboat Passage and Whale Cove), at parts of Komakuk Beach, Clarence Lagoon, and King Point, values are higher, reaching maximum values of 1.2 to 1.5 g/m^3 for scenario III.

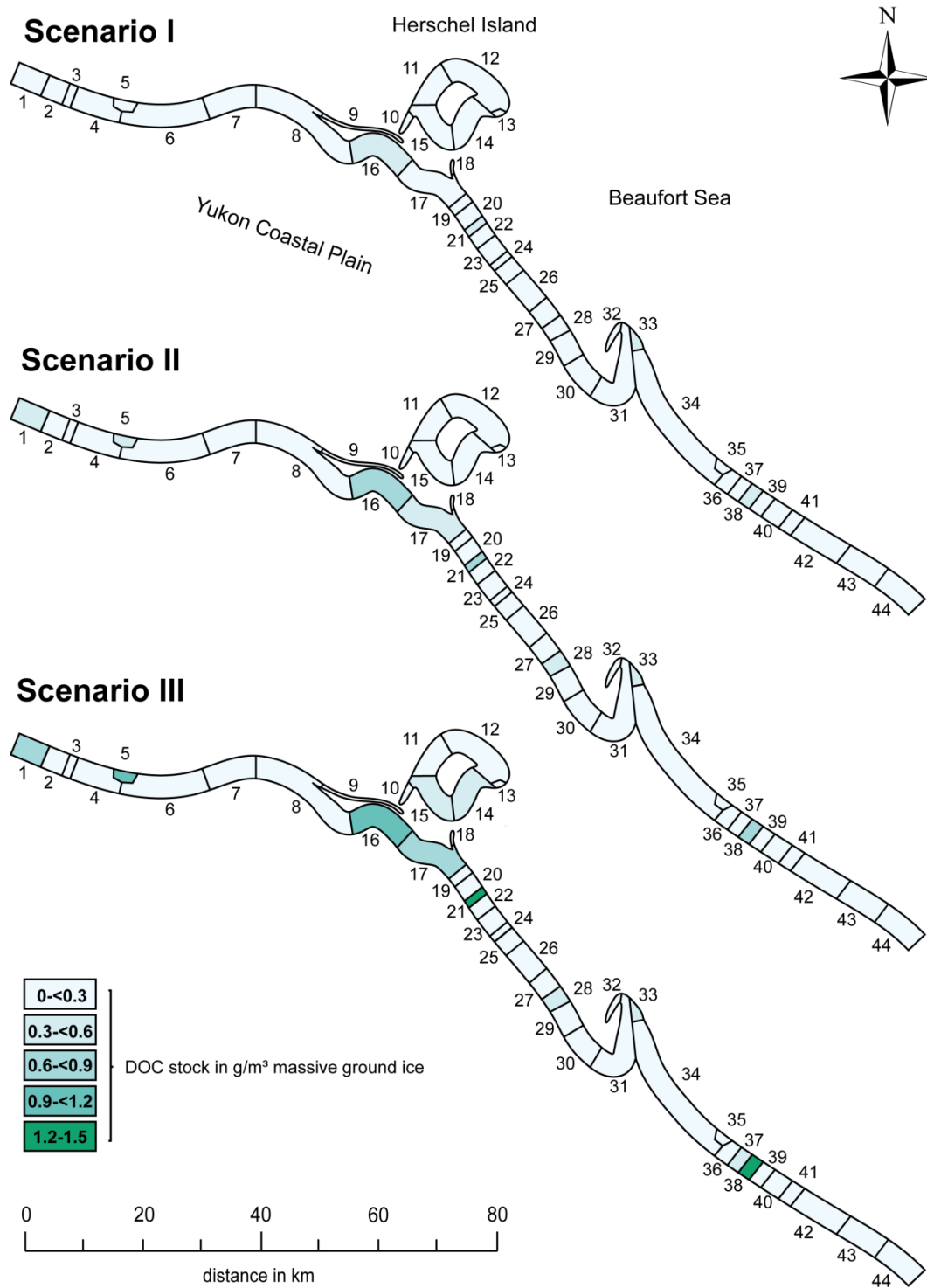


Figure 4.16: Three scenarios of possible DOC stocks in massive ground ice along the Yukon Coastal Plain.

4.7 DOC fluxes

The DOC fluxes are presented in three scenarios (Figure 4.17). Scenario A is the DOC flux estimated by incorporating the average DOC stocks of scenario I (section 4.6). Scenario B and C are the 50%-quartile (median) and 75%-quartile derived from DOC stock scenarios II and III (section 4.6). All three scenarios are presented to give a range of possible DOC fluxes from the terrain units.

The western part of the coastal plain is characterized by low estimated DOC fluxes of 1.4, 2.3 or 3.8 kg/yr (for scenarios A, B and C, respectively). No DOC fluxes are derived for parts of Clarence Lagoon (TU 2 and 3), Malcolm River fan (TU 7 and 8) and Nunaluk Spit (TU 9). DOC fluxes occur, however, from Komakuk Beach (TU 4 to 6) and parts of Clarence Lagoon (TU 1). The highest values for Komakuk Beach at TU 6 are 4.0, 5.4 or 8.3 kg/yr (scenario A to C) and for Clarence Lagoon 4.9, 9.8 or 17.1 kg/yr.

Herschel Island can be divided into a south-western part with low DOC fluxes and a north-eastern part with higher DOC fluxes. On average, the DOC flux from coasts of the island is 6.8, 15.2 or 27.1 kg/yr (scenario A to C). No DOC is released from Avadlek Spit (TU 10), Simpson Point (TU 13) and the south side of Herschel Island (TU 15) in any of the scenarios. The western part releases DOC fluxes of 6.1, 13.0 or 23.0 kg/yr (scenario A to C). The highest DOC fluxes are 11.7, 23.9 or 41.9 kg/yr, and at the east side (TU 14) 23.2, 54.1 or 97.5 kg/yr. DOC fluxes are particularly strong on the east side of the island.

The central part of the coast is characterized by low DOC flux rates. In all scenarios, values are between 0 and 20.0 kg/yr with an average DOC release of 0.6, 0.9 or 1.4 kg/yr (scenario A to C). No DOC is released from Catton Point (TU 18), parts of Whale Cove (TU 20 and 21), Stokes Point (TU 26), parts of Phillips Bay (TU 28 and 29) and the Babbage River Delta. The highest values are estimated for Workboat Passage (TU 16 and 17) and Phillipps Bay (TU 30). The highest DOC fluxes in the eastern part of Workboat Passage (TU 17) were 3.4, 4.6 or 7.0 kg/yr (scenario A to C) and in Phillips Bay (TU 30) 2.3, 3.1 or 4.7 kg/yr.

DOC fluxes from the central part are very low with values not exceeding 7.0 kg/yr. Higher amounts of DOC are released into the Beaufort Sea from the eastern part of the coast. On average, the DOC flux is 6.5, 11.4 or 19.1 kg/yr (scenario A to C). No DOC is released from Kay Point spit (TU 32), King Point NW (TU 35) or King Point Lagoon (TU 36). The highest DOC fluxes are estimated to come from Kay Point (TU 33 and 34), King Point SE (TU 38) and Shingle Point W (TU 42). The release of DOC from Kay Point (TU 33) is 13.1, 17.8 or 27.2 kg/yr (scenario A to C), for Kay Point SE (TU 34) 26.4, 43.3 or 71.2 kg/yr (scenario A to C) and from Shingle Point W (TU 42) 7.4, 13.7 or 23.4 kg/yr (scenario A to C). The terrain

unit with the highest flux is the south-eastern part of King Point (TU 38) with values of 27.5, 53.0 or 91.4 kg/yr (scenario A to C). The remaining terrain units have low DOC flux rates not exceeding 15.0 kg/yr.

Total fluxes for the whole Yukon Coastal Plain were calculated for each of the three scenarios (Figure 4.17). In scenario A, a total amount of 148 kg/yr of DOC is released in the southern Beaufort Sea. For scenario B and C the calculated DOC fluxes for the entire coast are 274 and 466 kg/yr.

In conclusion, the DOC fluxes along the coastal plain vary for the different coastal parts. The western and the central part have low DOC fluxes. In the western part, values of 1.4, 2.3 or 3.8 kg/yr (scenario A to C) are average, while values from the central part of the coast are low (0.6, 0.9 or 1.4 kg/yr for scenarios A, B and C). Herschel Island and the eastern part have higher average DOC flux rates ranging of 6.8, 15.2 or 27.1 kg/yr (scenario A to C for Herschel Island) and 6.5, 11.4 or 19.1 kg/yr (scenario A to C for the eastern part).

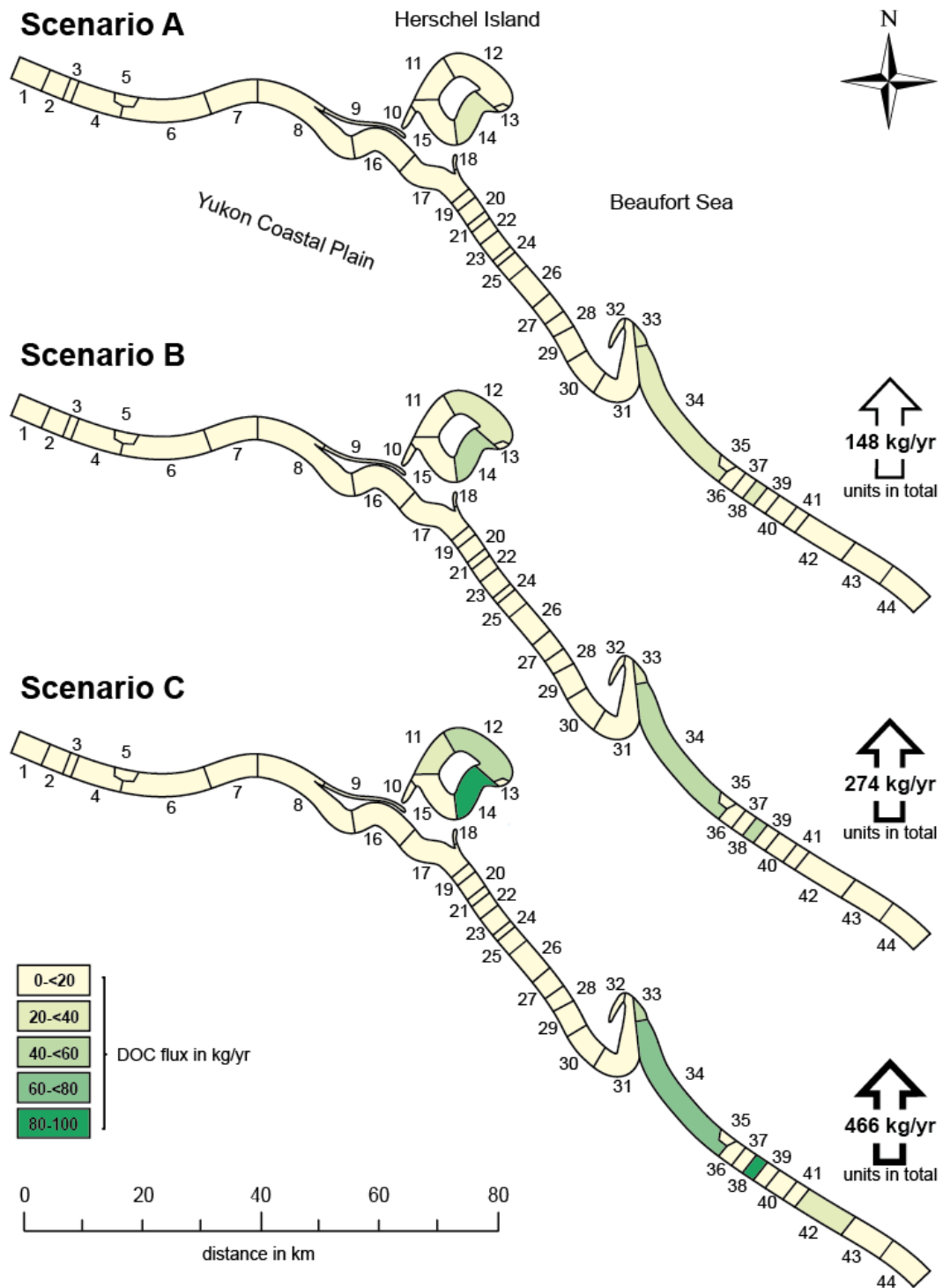


Figure 4.17: Three scenarios for possible DOC fluxes from massive ground ice along the Yukon Coastal Plain (Scenario A is the DOC flux estimated by using 25%-quartile DOC stocks. Scenarios B and C are the 50%-quartile (median) and 75%-quartile).

5 Discussion

The discussion is structured into four parts. The first part focuses on the amount of DOC stored in massive ground ice and suggests explanations for its origin and sources. It discusses in detail the genesis of the investigated massive ice bodies and ice wedges to support these hypotheses. The second part aims to describe how much of the DOC could be released by coastal erosion (DOC fluxes) into the Beaufort Sea, along with parameters that primarily control this process. This part also compares the calculated DOC fluxes from coastal erosion with known DOC fluxes from rivers and discusses the difference in magnitude. The third part is an attempt to put the DOC released by coastal erosion into the greater context of the carbon budget of the southern Beaufort Sea and the Arctic region as a whole. The last part of the discussion is devoted to the role and fate of DOC in the near-shore zone.

5.1 Origin of massive ground ice and sources of DOC

Ground ice classifications in North America differentiate ground ice types based on the source and the main transfer process of water at the time of freezing (MACKAY 1971, JOHNSTON 1981, COUTURE 2010). These ground ice types can in turn be related to DOC stocks to associate ground ice origin to DOC occurrence and quantity.

5.1.1 Massive ice bodies

In the western Canadian Arctic, massive ground ice bodies occur mainly near the limits of previous glaciations (FRENCH & HARRY 1990) and are interpreted either as having grown in situ (also called intra-sedimental) or having been buried (Figure 5.1). It can be segregated-intrusive ice (MACKAY 1971, MACKAY & DALLIMORE 1992), buried pleistocene glacier ice (FRENCH & HARRY 1990, LACELLE et al. 2004) or even originate from buried snowbanks and from frozen river, sea or lake water (POLLARD 1990, FRITZ et al. 2011b). In this region, for both main massive ground ice types (intra-sedimental and buried), the water supply generally comes from glaciers (RAMPTON 1982).

Segregated (intra-sedimental) ice bodies can be formed by three different processes. Firstly, they can be fed by groundwater (of glacial origin) that is migrating towards a freezing front during permafrost aggradation (LACELLE et al. 2004). Secondly, it can develop by pore water expulsion and thirdly by the freeze up of pressurized glacial meltwater on the base of permafrost immediately after deglaciation (LACELLE et al. 2007). Buried ice bodies, on the other hand are discrete ice bodies formed by the burial of snowbanks, lake ice, river ice or glacier ice by large amounts of sediment.

On the Yukon Coastal Plain, with the disintegration of the glacier front, the conditions required to generate both ice types were met, namely through the presence of remnant glacier ice and high-pore water pressures in meltwater saturated sediments (FRITZ et al. 2011b).

Buried glacier ice bodies are relicts of the Wisconsin Ice Sheet (RAMPTON 1982, LACELLE et al. 2007, FRITZ et al. 2011b) that covered large parts of the area in the Pleistocene (FRITZ et al. 2012). The Yukon Coastal Plain was characterized by stagnant glacier ice that facilitated burial during deglaciation (FRITZ et al. 2011b). Segregated ice is found in morainal and lacustrine deposits, fine grained alluvium, colluvium and organic deposits. In general, massive ice bodies are located at the interface of glacial till and the underlying sediments, favorable for its formation. Most segregated ice in glacial till is formed during and immediately after Late Wisconsin Glaciation (RAMPTON 1982). Along the shore of the Yukon Coastal Plain, massive ice bodies are commonly exposed at sea cliffs with steep slopes, or in retrogressive thaw slumps (RAMPTON 1982, LANTUIT & POLLARD 2008).

On Herschel Island, two episodes of ground ice genesis are represented in the permafrost sediments (POLLARD 1990). On the one hand recent (Holocene) ground ice that is younger than ~10 ka BP and on the other hand ground ice that dates back to the period of Mid to Late Wisconsin, older than ~10 ka BP (POLLARD 1990). The investigated massive ice body in thaw slump D (TSD12-MI) on Herschel Island was object to several studies (e.g. POLLARD 1990, FRITZ et al. 2011b) and was interpreted by FRITZ et al. (2011b) as basal regelation glacier ice using isotopic signatures. This can be supported by the glaciotectionic deformation structures of the ice-rich diamictic layer above the massive ice body and facies similar to those from basal ice layers of contemporary Arctic ice caps (FRITZ et al. 2011b). In contrast to that, RAMPTON (1982) and RAMPTON & MACKAY (1971) postulated that deformation structures can also occur by local differences in permafrost aggradation rates and ice formations due to different overburden pressures. Furthermore, sediment layers in three taken ice samples, TSD-12-MI-03, TSD12-MI-06 and TSD12-MI-09 (section 4.1.5), might indicate a segregated origin according a proposed genetic classification by POLLARD & DALLIMORE (1988) and GELL (1976), shown in table 5.1. Consequently, an origin as deformed segregated or segregated-intrusive ice cannot be excluded as both ice types, basal regelation ice and massive segregated and/or segregated-intrusive ice might have coexisted in a proglacial environment (FRITZ et al. 2011b).

For massive ice body KP12-MI in the eastern part of the Yukon Coastal Plain the origin is highly uncertain. Low to non-detectable DOC concentrations (median 1.76 mg/L) in the samples which are only slightly higher than DOC concentrations observed in basal glacier ice

(1.0 mg/L) from John Evans Glacier on Ellesmere Island (SKIDMORE et al. 2000) might indicate an origin as buried glacier ice. Samples taken in layers IIa and IIb (chapter 4, section 1.8), revealed no detectable DOC concentrations, similar to those of glacier ice (BARKER et al. 2006, SKIDMORE et al. 2000). The absence of glaciotectionic structures could however suggest a segregated origin for the ice body. This is supported by linear layers of air bubbles in clear ice found in layer IIb and dirty ice in layer IIc (chapter 4, section 1.8) that contained several sediment layers, which is typical for segregated ice supplied by subsurface water according to a genetic massive ground ice classification by GELL (1976) and POLLARD & DALLIMORE (1988) (Figure 5.1). Another possibility might be an origin from small proglacial meltwater ponds as the massive ice body is similar in texture to an ice body investigated by FRITZ et al. 2011b in the north of Herschel Island. This is indicated by a layer of blue ice found in ice body KP12-MI in unit IIb (section 4.1.8).

For HIWCS12-MI the origin is also uncertain. One of the samples (HIWCS12-MI-02) consists of clear and air-bubble rich ice with a sediment layer greater than 2 mm thick. These properties are representative for buried glacier ice according to the genetic classification by GELL (1976) and POLLARD & DALLIMORE (1988) (Figure 5.1). The other sample (HIWCS12-MI-03) was composed of dirty ice with sediment layers more related to segregated ice. As these results are contradictory, the origin remains uncertain.

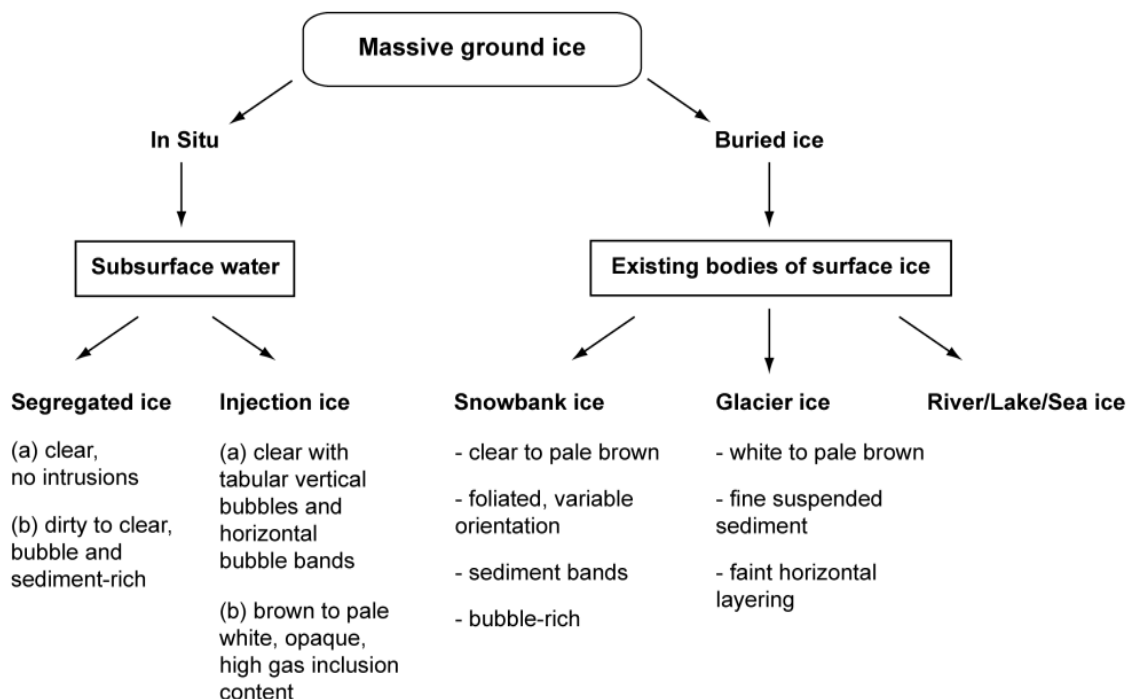


Figure 5.1: Genetic classification of massive ground ice, modified after POLLARD (1990) and based on studies of GELL (1976) and POLLARD & DALLIMORE (1988).

There are various processes that might explain the presence of DOC in the ice bodies. The results obtained in this study suggest a strong link between the DOC concentration and the

surrounding sediment. That is indicated by a strong relationship (coefficient of determination) between ice content (i.e. the inverse of sediment content) and the DOC concentration ($R^2=0.81$) that is presented in Figure 5.2. There are different pathways and sources for the organic carbon that can explain this strong relationship. It could be either introduced during water migration through the sediment, by interactions of basal regelation ice with subglacial sediment, and/or was contained in glacier ice before.

In the case of water migration, the explanation could be linked to the prolonged contact between intra-sedimental water with the enclosing, organic carbon-rich sediment (ZIMOV et al. 2006a, FRITZ et al. 2011b), before or during the freezing process. The organic carbon could be dissolved by the water during migration through the soil, or through the ice segregation process. This is supported by soil extraction experiments executed by DOU et al. (2008), which showed that different liquids (sea water, pure water) can lead to extraction of soil organic carbon to DOC. ARTINGER et al. (2000) reported that DOC in form of humic acids can originate from sedimentary organic carbon in the soil. Studies on CO_2 and $\delta^{13}\text{C}$ in debris-rich ice that grew in-situ from the freezing of subglacial meltwater revealed that water gained higher CO_2 and $\delta^{13}\text{C}$ values during movement through the sediments (LACELLE et al. 2004). As arctic soils have been storing large quantities of carbon in unglaciated regions prior to the last glacial maximum (ZIMOV et al. 2006a, 2006b) and in areas that have been deglaciated since the last glacial maximum (HARDEN et al. 1992), sediments contain high amounts of organic carbon (TARNOCAI et al. 2009, HUGELIUS et al. 2013) and form a reservoir for the dissolution of POC into DOC. An origin of DOC in massive ice supplied by carbon stored in contained sediments is also supported by measured pH and electrical conductivity which rise with sediment content in the samples, reflecting exchange processes between the sediment and the ice (FRITZ et al. 2011b). Higher pH and electrical conductivity are indicators for the carbonaceous marine sediments, which most of Herschel Island is composed of (FRITZ 2008). These marine sediments were upthrust by the Laurentide Ice Sheet (MACKAY 1959, BURN 2009). According to a study of COUTURE (2010), these nearshore sediments contain organic carbon (TOC) contents between 0.3 and 7.9 % (average 1.5 %) that might be the reservoir for DOC detected in massive ground ice samples.

KNIGHT (1997) showed that basal and englacial debris can affect the hydrochemistry of basal regelation ice through interactions between water, ice and solutes. Permafrost soils that were overridden by glaciers and affected by abrasion processes are probably the main source of organic carbon in subglacial sediments. This organic material is mainly composed of cyanobacterial mats, plant material and roots (SKIDMORE et al. 2000).

If massive ground ice originates from glacier ice, DOC could also have already been contained in glacier ice before. A survey of BARKER et al. (2006) at John Evans Glacier on the Canadian Archipelago revealed that DOC concentrations in glacial meltwater are on average 0.26 mg/L. Investigations on Victoria Glacier in Antarctica revealed that at the edge between glacier ice and basal ice high DOC concentrations (>40 mg/L) could occur.

The DOC contents observed in samples of this study do not necessarily represent the DOC contents at the time of dissolution or inclusion in the ice. Indeed, the DOC in these bodies could also have been degraded by biochemical processes. THURMAN (1985) identified different processes that can lead to such a decrease in DOC concentrations. It could be either used by microbes in the ground water as food supply or it was absorbed at the surface of the aquifer, where it was biochemically degraded and removed as CO₂. As a result, the DOC contents can be considered as minimum contents at the time of inclusion and/or dissolution.

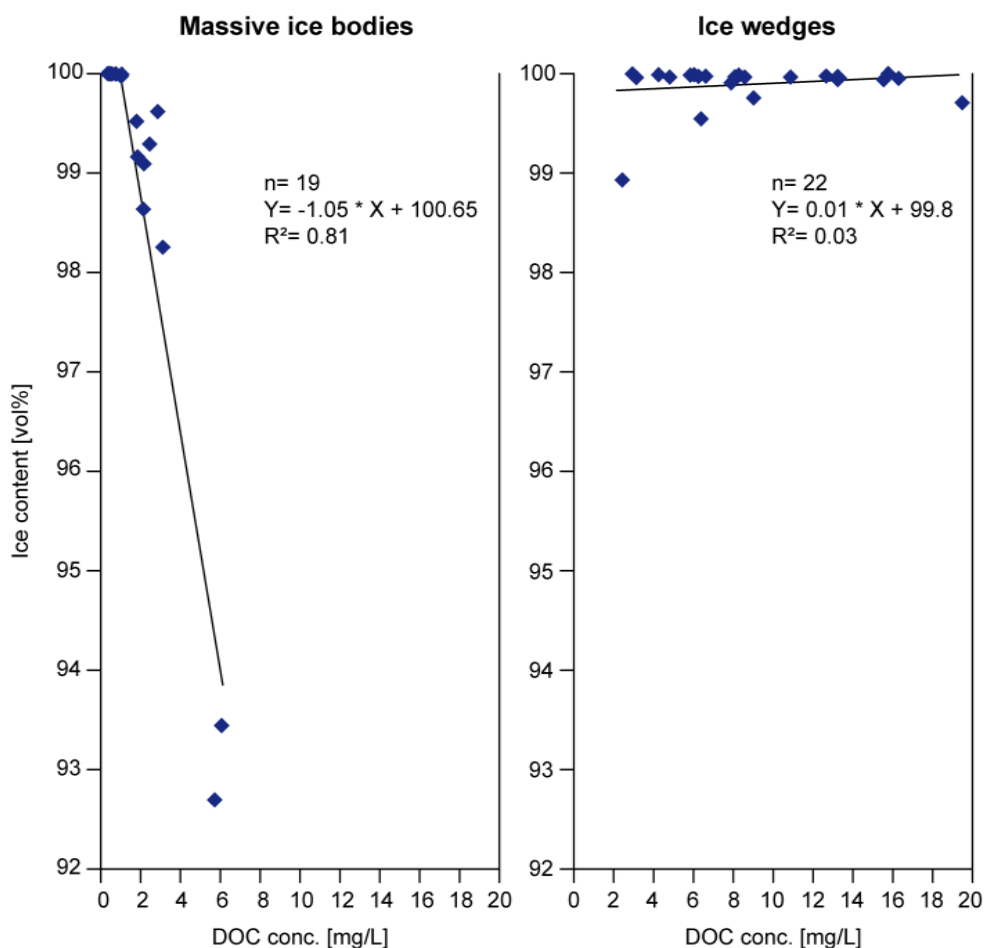


Figure 5.2: Relationship between volumetric ice contents and DOC concentrations in massive ground ice bodies and ice wedges.

5.1.2 Ice wedges

The ice wedges investigated in this study developed under warmer conditions at the Holocene Thermal Maximum, approximately 11.2 to 6.5 ka BP (RAMPTON 1982, FRITZ et al 2011b). They have formed at any time since the deposition of the sediments that contain them (RAMPTON 1982). Ice wedges are formed by thermal contraction and cracking of permafrost sediments during winter. In spring, these developed cracks were filled with meltwater from snow (MACKAY 1990, FRENCH 2007). Besides melting snow, ice wedge growth can be fed by dry snow accumulating in the crack and hoarfrost, as indicated by isotopic studies of ST-JEAN et al. (2011). As ice wedges are mainly supplied by meltwater in spring the DOC concentrations in ice wedge samples are likely linked to the transport of organic material by meltwater into small ponds that fill the throughs. During freezing in winter, parts of this material became part of the ice wedge.

The incorporated DOC could therefore be either derived from the dissolution of organic material that accumulated in the meltwater ponds during spring or from DOC already present in the peaty active layer that was transported into the through. In the study area, at approximately 10 ka BP, a warmer period of deep-thaw of permafrost associated with peat formation occurred (POLLARD 1990) with conditions favorable to induce transport of organic carbon into ice wedges. The correlation between sediment content and DOC concentration is very low for ice wedges ($R^2=0.03$), which indicates that sediments are not the main source of organic carbon in the ice wedges but cannot entirely be excluded as sediments were detected in ice wedge samples (section 4.1).

For the investigated ice wedges TSA12-IW, TSC12-IW, TSD12-IW1, TSD12-IW2, RB12-IW and KP12 (section 4.1), it is supposed that the DOC is mainly derived from the peaty active layer and organic material that was transported into the crack. This is indicated by the very low sediment contents in all ice wedges (<1 %) and visible organic material and plant detritus found in most of the samples. Some of the ice wedges (i.e. TSC12-IW) possibly developed during the Holocene Thermal Maximum (KAUFMAN et al. 2009). This is indicated by a thaw unconformity above the surface of the ice wedge (section 4.1.2), indicating a former active layer (FRENCH & SHUR 2010). Peaty lenses found in sediments directly above the ice wedge support that fact.

Higher DOC concentrations within ice wedges might be explained by warmer and moister conditions during the Holocene Thermal Maximum. These favorable climate conditions lead to stronger vegetation as warmer climate affects the plant productivity (DAVIDSON et al. 2000). This abundant vegetation might have supported the organic carbon yields to the ice wedge.

The capped ice wedges TSC12-IW and TSD12-IW1 (section 4.1.2 and 4.1.3) could be explained by slumping that occurred during warmer periods in the past. This happened possibly more than 5,000 years ago, during the Holocene Thermal Maximum (RAMPTON 1982, KAUFMAN et al. 2009) as indicated by an ice lens in ice wedge TSD12-IW1 (section 4.1.3) within the 1.5 to 3.0 m of the ground surface. This ice lens probably originates from permafrost degradation during the last 5,000 years (RAMPTON 1973).

5.1.3 Comparison between massive ice bodies and ice wedges

As the results in Figure 5.3 indicate, DOC concentrations are approximately eight times higher in ice wedges (median 8.0 mg/L) than in massive ice bodies (median 1.1 mg/L). A reason for this could be the different genesis of both ground ice features stated above. Larger input of organic material during the genesis of ice wedges during spring in form of organic compounds and material transported with meltwater into the cracks might be responsible for higher organic carbon concentrations than sediment organic carbon that was incorporated in or serve as source for massive ground ice bodies.

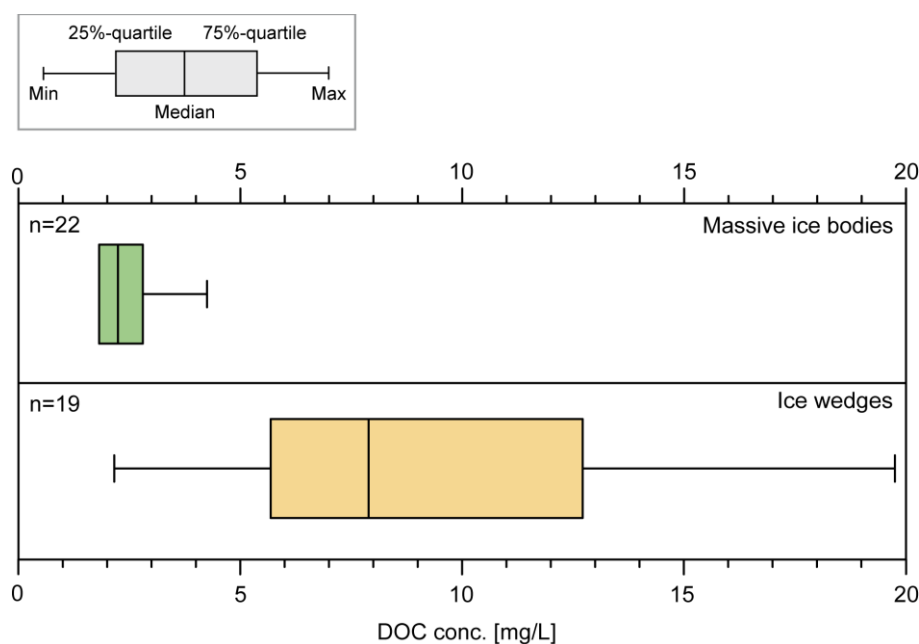


Figure 5.3: Box plots of DOC concentrations in massive ice bodies and ice wedges.

In conclusion, the origin of the DOC found in massive ground ice bodies cannot be fully determined, but it is likely that particulate organic carbon in the enclosing sediment served as the DOC source. The DOC in ice wedges originates mainly from meltwater that filled the cracks in spring that contained organic compounds from the vegetation. The restricted set of data and information about cryostructures, hydrochemistry and isotopic signatures available for this study does not allow to determine, which process was the primary driver of DOC release.

5.2 DOC fluxes from coastal erosion

5.2.1 DOC fluxes and its control factors

The estimated DOC fluxes from the Yukon Coastal Plain are controlled by five factors in each terrain unit: coast length, coastline height, annual coastal erosion rate, volumetric massive ground ice content, and DOC stock (section 3.5). For each DOC flux scenario (A, B and C) presented (Figure 4.17), the flux rates were related to these five factors to determine their influence on the release of DOC. As coastline length is different for each terrain unit, DOC fluxes were normalized from kg/yr to g/m/yr to extract which factor, coastline height, coastal erosion rate, massive ground ice content, or DOC stock, is influencing the DOC flux the most. This was achieved by correlating (coefficient of determination) these factors with the DOC flux for each of the coastal parts (West, Herschel Island, Central, East).

Western coastal part

In the western part of the coast, calculations yielded no DOC fluxes at parts of Clarence Lagoon (TU 2 and 3), Malcolm River fan (TU 7 and 8) and Nunaluk Spit. This can be explained by the absence of massive ground ice in these fluvial and marine units. The higher DOC fluxes estimated for Komakuk Beach (TU 4 to 6) and parts of Clarence Lagoon (TU 1) can be explained by potentially higher amounts of massive ground ice (16 vol%) in lacustrine deposits (COUTURE 2010). Higher DOC amounts, ranging from 0.26 to 0.96 g/m³ (average all terrain units 0.15 g/m³), can be found at Komakuk Beach W1 (TU 5), probably due to highly organic silty sand or clay in lacustrine sediments (RAMPTON 1982). Massive ground ice contents are high in this unit with 40 vol% (average all terrain units 10 vol%), but a low coastline height of 3.5 m (average all terrain units 12.2 m), a short coast length of 1.9 km (average coast length all terrain units 7 km) and lower erosion rates of 0.68 m/yr (average all terrain units 0.73 m/yr) limit the DOC flux to 4.2 kg/yr (average all terrain units 6.2 kg/yr). This is similar for Clarence Lagoon W (TU 1). The massive ground ice content is high (35 vol%) and DOC stocks can reach values between 0.25 and 0.87 g/m³. But the factors coastline length (6.3 km), coastline height (5.0 m) and erosion rate (0.62 m/yr) are limiting the DOC flux to maximum 17.1 kg/yr.

After transforming the DOC fluxes from kg/yr to g/m/yr, the fluxes from the western part showed a strong relationship to DOC stocks ($R^2=0.96$). DOC stocks range from 0.1 to 0.2 g/m³ (average whole coast 0.15 g/m³) and massive ground ice contents ($R^2=0.96$) of 10 vol% on average (average all terrain units 10 vol%). Also, the coastline height with an average value of 2.5 m (average all terrain units 12.2 m) shows a strong relationship to the DOC fluxes with $R^2=0.56$. As DOC stocks are mainly controlled by the content of massive ground

ice ($R^2=0.80$), and since only this ground ice feature was object of this study, higher DOC fluxes from Komakuk Beach and Clarence Lagoon can be explained by the clayey and silty lacustrine sediments with high contents of massive ground ice of up to 16 vol% (RAMPTON 1982).

Herschel Island

For Herschel Island the absence of massive ground ice at Avadlek Spit (TU 10) and Simpson Point (TU 13) is responsible for the absence of DOC fluxes from these units as ground ice contents in marine deposits are generally low (RAMPTON 1982) and for Herschel Island 0 vol% (COUTURE 2010). The non-existing DOC fluxes from the south side (TU 15) can be explained by the fact that no coastal erosion is reported. Higher DOC fluxes occur especially from the north and east side of the island. These fluxes are in the range of 11.7 to 41.9 kg/yr (average all terrain units 6.2 kg/yr) at the north side of the island (TU 12). As DOC stocks range from 0.02 to 0.06 g/m³ (average all terrain units 0.15 g/m³) and massive ground ice contents with 9 vol% (average all terrain units 10 vol%) are low, DOC fluxes can mainly explained by moderate erosion rates of 0.71 m/yr (average all terrain units 0.73 m/yr) and the coast length of this unit of 16.7 km (average coast length all terrain units 7 km). A main factor for higher DOC contributions is the very high coastline height of 60.0 m (average whole coast 12.2 m), that supplies a huge amount of sediment that possibly contain DOC. Nevertheless, coastline height at the west side (TU 11) is also very high with 56.0 m. The massive ground ice content of 10 vol%, erosion rate of 0.95 m/yr, and DOC stocks of 0.02 to 0.08 g/m³ are also similar to the north side of Herschel Island, but DOC fluxes are much lower with 6.1 to 23.0 kg/yr. This could be due to the shorter coastline length of 5.6 km. The highest DOC fluxes from Herschel Island from the east side (TU 14) can be explained by a higher massive ground ice content of 28 vol% and a higher DOC stock ranging from 0.12 to 0.34 that are amplified by coastline height (24.5 m) and a moderate erosion rate of 0.75 kg/yr.

After transforming the DOC fluxes from kg/yr to g/m/yr, the fluxes yielded from Herschel Island are strongly correlated with the massive ground ice content of 10 vol% in this unit (average all terrain units 10 vol%) with $R^2=0.72$. The remaining input factors like DOC stock ($R^2=0.33$), coastline height ($R^2=0.20$) and erosion rate ($R^2=0.31$) showed low to moderate relationships to DOC flux rates.

Central coastal part

The central part is characterized by low DOC flux rates. The non-occurring DOC fluxes from Catton Point (TU 18), Whale Cove (TU 20), Stokes Point (TU 26) and Phillips Bay W (TU 29) can be explained by the absence of massive ground ice in these units. The estimated non-occurring DOC fluxes from the eastern part of Whale Cove (TU 19) and Phillips Bay NW (TU

28) arise from the lack of coastal erosion. Highest DOC fluxes occur at Workboat Passage (TU 16 to 17) and Phillips Bay (TU 30). The higher DOC fluxes from Workboat Passage W (TU 16), in the range from 2.2 to 4.5 kg/yr (average all terrain units 6.2 kg/yr), are interpreted mainly by higher DOC stocks ranging from 0.46 to 0.96 g/m³ (average whole coast 0.15 g/m³), and high massive ground ice contents of 22 vol% (average whole coast: 10 vol%), as cliff height with 5.0 m (average all terrain units 12.2 m), coast length with 1.8 km (average units 7 km) and coastal erosion rate with 0.52 m/yr (average whole coast 0.73 m/yr) are low. In the eastern part of Workboat Passage (TU 17), DOC fluxes ranging from 3.4 to 7 kg/yr can be explained primarily by high massive ground ice content (15 vol%), a coastline length of 10.1 km and DOC stocks ranging from 0.29 to 0.60 g/m³ and secondarily by a low coastal erosion rate of 0.38 m/yr. At Phillips Bay (TU 30), the higher DOC fluxes ranging between 2.3 and 4.7 kg/yr can be explained mainly by a high coastal erosion rate of 1.3 m/yr, as well as by a low coastline height (6.5 m), low massive ground ice content (6 vol%), and low DOC stocks ranging between 0.04 to 0.08 g/m³.

After transforming the DOC fluxes from kg/yr to g/m/yr, the fluxes from the central part showed no strong relationship to any of the input factors for the determination of DOC fluxes. The strongest relationship can be found for DOC stocks and DOC flux ($R^2=0.18$) and massive ground ice content ($R^2=0.10$).

Eastern coastal part

The eastern part of the coast is partly characterized by higher DOC fluxes, especially at Kay Point SE (TU 34) and King Point SE (TU 38). The remaining parts are dominated by low values of annual DOC releases. No DOC fluxes occur from Kay Point Spit (TU 32), King Point NW (TU 35) and King Point Lagoon (TU 36). This can be explained by the absence of massive ground ice at Kay Point Spit (TU 32) and King Point Lagoon (TU 36), and no occurring coastal erosion at King Point NW (TU 35). Highest DOC fluxes are calculated for Kay Point (TU 33 and 34), King Point SE (TU 38), and Shingle Point W (TU 42). The high annual release rates of DOC from Kay Point (TU 33) between 13.1 to 27.2 kg/yr (average all terrain units 6.2 kg/yr) is mainly explained by large DOC stocks ranging from 0.27 to 0.55 g/m³ (average all terrain units 0.15 g/m³), a very high coastal erosion rate of 2.65 m/yr (average all terrain units 0.73 m/yr) and high massive ground ice contents of 14 vol% (average all terrain units 10 vol%) as coastline height of 7.0 m (average all terrain units: 12.2 m) and coastline length of 2.7 km (average all terrain units 7 km) are low. The high DOC fluxes from Kay Point SE (TU 34), ranging from 26.4 to 71.2 kg/yr, are mainly accounted by a long coastline (22.5 km), a high coastline of 30.0 m, and high coastal erosion rates (0.96 m/yr) as massive ground ice content (9 vol%), and DOC stocks, ranging from 0.04 to 0.11 g/m³, are low. Higher DOC fluxes from Shingle Point W (TU 42) of 7.4 to 23.4 kg/yr can be

mainly explained by a long coastline (11.3 km), a high coastline height (26.0 m) and moderate massive ground ice contents (14 vol%), as coastal erosion (0.38 m/yr) and DOC stocks (0.07 to 0.21 g/m³) are low. Another terrain unit with higher DOC fluxes is King Point (TU 38), with values ranging from 27.5 to 91.4 kg/yr. This can be interpreted primarily by high massive ground ice contents (47 vol%), large DOC stocks (0.38 to 1.27 g/m³) and a high coastal erosion rate of 1.6 m/yr. Secondly, a short coastline of 3.8 km and a moderate coastline height of 12.0 m is influencing the DOC fluxes.

After transforming the DOC fluxes from kg/yr to g/m/yr, the fluxes from the eastern part correlated strongly with massive ground ice contents ($R^2=0.81$) and DOC stocks ($R^2=0.97$). Weaker relationships were observed for coastal erosion rates ($R^2=0.17$) and coastline height ($R^2=0.08$), which is remarkable as coastal erosion rates are the highest in this coastal part with 1.1 m/yr.

Total Yukon Coastal Plain

For the total Yukon Coastal Plain relationships between DOC flux and its control factors are expressed in Figure 5.4. Along the coastal plain the DOC fluxes mainly show a moderate relationship ($R^2=0.35$) to massive ground ice contents that is in average 10 vol% and DOC stocks ($R^2=0.26$) that is in average 0.15 g/m³. Higher massive ground ice contents occur in terrain units composed of morainal and lacustrine material. According to RAMPTON (1982), these geological units have high ice contents, as they are composed of clayey and silty material favorable for ice segregation (FRENCH 2007). This silty-clayey frozen sediment could be found in most of the investigated profiles (section 4.1), close to the sampled massive ice features, as samples had been taken only from lacustrine and ice-thrust moraine units. In contrast, in marine, fluvial and glaciofluvial units, lower volumes or no massive ground ice was found. This could be due to lack of fine-grained sediments favorable for ground ice formation (RAMPTON 1982, FRENCH & SHUR 2010).

For the control factor coastline height no relationship to DOC fluxes can be found ($R^2=0.03$). The relationship between coastal erosion and DOC fluxes is weak ($R^2=0.19$). In contrary, POC fluxes estimated by COUTURE (2010) and PING et al. (2011) showed a stronger relationship between coastline heights and organic carbon fluxes with $R^2=0.68$ and $R^2=0.50$ compared to organic carbon fluxes in this study ($R^2=0.03$). This can possibly explained by the different methods used for calculations. COUTURE (2010) used area instead of coastline length to estimate the carbon fluxes. Another reason could be that COUTURE (2010) assumed low POC values for high cliffs, and high POC values for low cliffs, due to the thick organic cover at low cliffs. Another point is that the volume of sediment containing POC is probably higher than the volume of massive ground ice containing DOC that is scattered

throughout the sediment. This is supported by the weak relationship of DOC stocks and coastline height in this study ($R^2=0.01$).

The relationship between POC fluxes and erosion rates are with $R^2=0.42$ (COUTURE 2010) weaker in this study for DOC ($R^2=0.18$). This is possibly due to the fact that same erosion rates were used for carbon flux calculations, but contents of POC in permafrost are exponentially higher than DOC. LANTUIT et al. (2012) reported that the largest factor for coastal erosion along the arctic coasts are waves and storm surges. Increased erosion rates along the coast of the Alaskan Beaufort Sea (MARS & HOUSEKNECHT 2007, JONES et al. 2008, 2009a, 2009b) showed a relationship to high ground ice contents and very low backshore elevations. In this study, this phenomenon was observed in the western part of the Yukon Coastal Plain, where relationships of low coastline height and DOC flux are moderate with $R^2=0.56$. Ground ice and low backshore elevation support coastal erosion as they limit the quantity of eroded material supplied by a storm. This material is quickly removed from the beach by waves and the exposed coastline is vulnerable for the next storm event (LANTUIT et al. 2012). According to this, the high coastline of the Yukon Coast is a limiting factor with regard to increased storm frequencies that probably lead to coastal erosion as more material has to be removed by wave action from the beach.

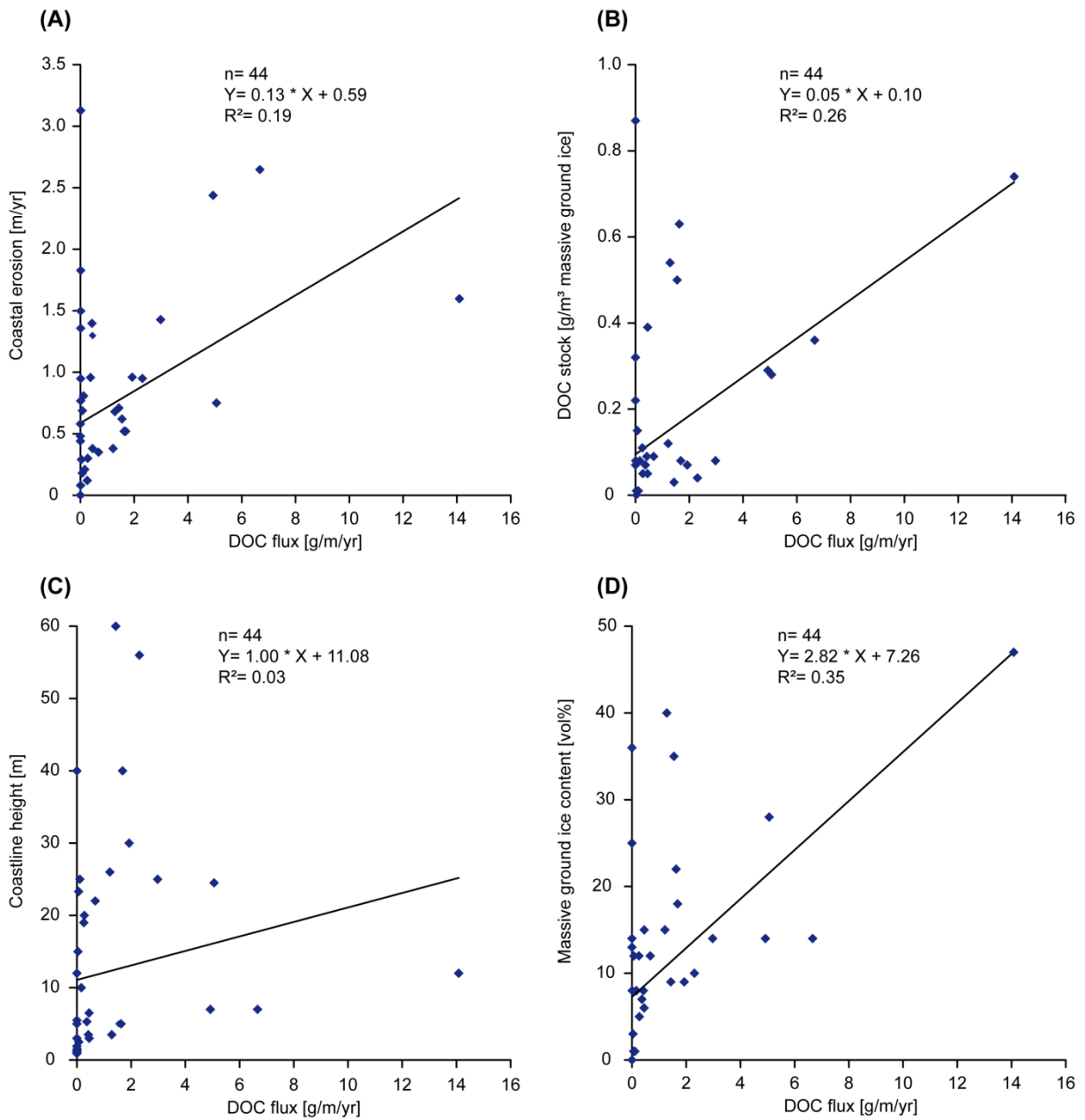


Figure 5.4: Relationship between estimated DOC fluxes and control factors coastal erosion (A), DOC stocks (B), coastline height (C) and volumetric massive ground ice content (D).

5.2.2 Possible sources of error

Quantities of DOC stocks and estimates of DOC fluxes provided by this study are related to various possible sources of error, including:

- a) unknown precise volumes of ground ice in permafrost
- b) absence of pore ice in DOC stock and flux estimations
- c) possible contaminations of samples during processing
- d) inaccuracies of coastline lengths.

a)

An accurate determination of ground ice volumes in permafrost is difficult (COUTURE 2010). Previous studies (e.g. POLLARD & FRENCH 1980) focused only on the top ten metres of permafrost soil and disregarded deeper layers (COUTURE 2010). The thickness of massive ice bodies reveals the largest uncertainties. COUTURE (2010) incorporated a maximal thickness of 9.0 m for massive ice bodies in the calculation of ground ice contents, used in this study for the estimation of DOC fluxes. Nevertheless, field observation showed that the thickness of massive ice bodies can be far greater, for example in thaw slump D on Herschel Island with a visible thickness of 14.0 m (section 4.1.5). This is supported by investigations of MACKAY (1971), where massive ice bodies in the ground revealed a mean thickness of 13.0 m. According to COUTURE (2010), massive ice contents could potentially be three times higher in some terrain units.

b)

The calculated DOC fluxes are only a part of the total annual DOC fluxes, as pore ice that makes up the largest volume of the ground ice content along the Yukon Coastal Plain, is not considered. On average, total ground ice volume including pore ice is 46 vol% along the Yukon Coastal Plain (COUTURE 2010). As massive ground ice (massive ice bodies and ice wedges) compose only 10 vol% of permafrost sediments, the pore ice volume is assumed to be 36 vol%. Since pore ice makes up the largest part of the volumetric ice content and DOC concentrations are expected to be higher in sediment-rich pore ice (DOU et al. (2008), DOC fluxes are expected to increase exponentially if pore ice is incorporated.

c)

Measurements of DOC concentrations in the laboratory and sampling had been carried out very carefully as contamination can occur quickly. Contamination could possibly lead to three to four times higher DOC values, as shown in the range of values detected in the processing of blanks (Table 5.1). For that reason, overestimation might occur. However, the

contamination in all processed blanks was still below the detection limit (1.0 mg/L), indicating that contamination was kept to a minimum.

Table 5.1: DOC concentration in laboratory process blanks.

Blank ID	DOC conc.
Blank 1-1	0.797
Blank 1-2	0.163
Blank 2-1	0.265
Blank 2-2	0.229

d)

The length of the coastline was used for DOC flux calculations. The problematic point is that the length of a coastline depends strongly on the scale used in a study. The same coastline, if at different map scales, will show different lengths. This concept of fractal coastlines was first conceptualized by RICHARDSON (1961) and MANDELBROT (1967). As coastal erosion rates are computed using the length of the coastline, the obtained results can vary greatly depending on the scale of the coastline used for the estimation of these rates. Scale related errors of 30 % can occur (LANTUIT et al. 2009). This error in the calculation of coastal erosion was also identified in projects with the goal to quantify nutrient fluxes to the nearshore zone (e.g. BARTLEY et al. 2001, SMITH 2005). To mitigate this issue, COUTURE (2010) established a buffer from the shoreline with GIS to estimate the inland eroded area and compute planimetric erosion, as recommended by LANTUIT et al. (2012).

5.3 DOC fluxes and the arctic carbon budget

5.3.1 DOC fluxes from coastal erosion

Various studies, e.g. BROWN et al. (2003), JORGENSEN et al. (2003), GRIGORIEV & RACHOLD (2003) and RACHOLD et al. (2003), published under the Arctic Coastal Dynamics Framework (RACHOLD et al. 2005a), indicate that coastal erosion is a major source of sediment and total organic carbon input to the Arctic Ocean (RACHOLD et al. 2005a). In the following section, the fluxes of DOC from coastal erosion are discussed in the light of existing studies, and are compared to fluxes from rivers. Table 5.2 presents DOC, POC and TOC concentrations and fluxes from coastal erosion and arctic rivers. After that, DOC fluxes from massive ground ice are extrapolated on a circum-arctic scale to compare them to the release of POC by river discharge and by coastal retreat. For a better comparison, all values for carbon concentration are given in mg/L, and all values for fluxes had been transformed into Mt/yr.

The values for DOC concentrations in massive ground ice (massive ice bodies and ice wedges) obtained in this study are moderate with 6.6 mg/L, on average. In comparison, measurements by FRITZ et al. (2010) on ice wedges revealed an average DOC concentration of 7.5 mg/L. DOUGLAS et al. (2011) reported much higher values (8.7 to 21.2 mg/L) for cave ice in the subarctic but the genesis of the ice is different and the values not directly comparable.

The DOC fluxes from massive ground ice are very low with 0.3×10^{-6} Mt/yr. This can be explained by the fact that massive ground ice in this study makes up on average approximately only 10.0 vol% of the whole sediment along the Yukon Coastal Plain. Additionally, DOC concentrations in massive ground ice are low (average 6.6 mg/L), and the sediment content is also very low with 0.6 vol%. DOC stocks were shown earlier to be positively correlated with sediment content. This DOC flux is much lower than the DOC flux of 0.001 Mt/yr and POC flux of 0.04 Mt/yr derived by COUTURE (2010) for the exact same coastal section of the Canadian Beaufort Sea. In LANTUIT's (2010, unpublished) study for the calculation of DOC fluxes, pore ice that probably contain more DOC (WEEGE, personal communication), was taken into account, leading to these higher DOC fluxes.

Higher values for DOC and TOC fluxes are supplied by JORGENSON & BROWN (2005) from the Alaskan Beaufort Sea with DOC fluxes of 0.002 Mt/yr and TOC fluxes of 0.18 Mt/yr. Similar values of TOC fluxes for the Alaskan Beaufort Sea have been derived by PING et al. (2011) with 0.15 Mt/yr. These values would fit with the POC fluxes of 0.04 Mt/yr derived by COUTURE (2010) for the shorter Yukon coastline. Higher organic carbon inputs from the Alaskan Beaufort Sea can be explained primarily by the longer coastline, but also by the higher coastal erosion rates between 1.6 m/yr (JORGENSON & BROWN 2005) and 1.2 m/yr (PING et al. 2011) in comparison to 0.7 m/yr for the Yukon Coastal Plain (HARPER et al. 1985). Another reason is that some studies did not include ground ice in their calculations of material fluxes (e.g. HARPER 1982) but were later used for POC flux calculations on the Yukon coast (HILL et al. 1991), which, in turn, can lead to underestimations of material fluxes (COUTURE 2010).

In conclusion, DOC fluxes from massive ground ice are very low and not directly comparable to fluxes of POC. Organic carbon fluxes from massive ground ice seem to play only a marginal role in the carbon budget as long as pore ice is not incorporated in these calculations.

Table 5.2: Comparison of annual organic carbon fluxes by coastal erosion and rivers into the Beaufort Sea.

Coastal erosion	Conc.			Flux			Reference
	DOC [mg/L]	POC [mg/L]	TOC [mg/L]	DOC [Mt/yr]	POC [Mt/yr]	TOC [Mt/yr]	
Canadian Beaufort Sea							
Yukon Coastal Plain	4.3	-	-	0.3×10^{-6}	36.4×10^{-6}	-	This study
	-	-	-	0.001 ^a	0.04 ^b	-	^a LANTUIT (2010, unpublished) ^b COUTURE (2010)
Alaskan Beaufort Sea							
	-	-	-	0.0018	-	0.18	JORGENSEN & BROWN (2005)
	-	-	-	-	-	0.15	PING et al. (2011)
Total Beaufort Sea							
	-	-	-	-	-	0.09	RACHOLD et al. (2004)
Rivers	DOC [mg/L]	POC [mg/L]	TOC [mg/L]	DOC [Mt/yr]	POC [Mt/yr]	TOC [Mt/yr]	Reference
Canadian Beaufort Sea							
Mackenzie	5.2 ^c	7.2 ^d	12.5 ^d	1.3 ^e	2.1 ^e	4.1 ^{g,h}	^c SPITZY & LEENHEER (1991)
				1.4 ^f	2.3 ^g		^d DEGENS et al. (1991)
				1.7 ^g			^e MACDONALD et al. (1998)
							^f RAYMOND et al. (2007)
							^g MCGUIRE et al. (2009) and r. w.
							^h RACHOLD et al. (2004)
Alaskan Beaufort Sea							
Sag	4.0	2.3	6.3	0.026	0.015	0.041	MCGUIRE et al. (2009) and r. w.
Kuparuk	11.6	1.5	13.1	0.014	0.0018	0.016	MCGUIRE et al. (2009) and r. w.
Colville	7.3	6.26	13.6	0.11	0.094	0.205	MCGUIRE et al. (2009) and r. w.
Total Canadian Arctic							
	5.1	5.8	11.6	1.9	2.15	4.3	RACHOLD et al. (2004) and r. w.

5.3.2 Coastal erosion vs. River discharge

Concentrations of DOC in massive ground ice and rivers are similar (Table 5.2). On average, values for massive ice bodies and ice wedges in this study are 4.3 mg/L and comparable to DOC concentrations of the Mackenzie River with 5.2 mg/L (SPITZY & LEENHERR 1991). Similar values were measured for the Colville River in Alaska with 7.3 mg/L (MCGUIRE et al. 2009). Slightly lower and higher values were obtained for the Sag River with 4.0 mg/L and the Kuparuk River with 11.6 mg/L, respectively (MCGUIRE et al. 2009 and r. w.).

Most recent estimations indicate that DOC fluxes from coastal erosion are much lower than DOC fluxes from rivers (Table 5.2). However, determinations of DOC fluxes by coastal erosion are rare and available for small coastal sections only. For the Yukon Coastal Plain, an approximately 300 km long part of the Canadian Beaufort Sea coast, DOC fluxes of 0.001 Mt/yr were calculated by LANTUIT (2010, unpublished). JORGENSEN & BROWN (2005) estimated 0.0018 Mt/yr for the Alaskan Beaufort Sea with a length of 1957 km, but focusing on selected locations along that coastline. Much lower values have been revealed by this study with 0.3×10^{-6} Mt/yr for DOC fluxes from massive ground ice. These DOC fluxes are minimal in comparison to DOC fluxes from the Mackenzie River, which has the largest organic carbon input of any arctic river (RACHOLD et al. 2004). Recent estimations vary between 1.3 Mt/yr (MACDONALD et al. 1998), 1.4 Mt/yr (RAYMOND et al. 2007) and 1.7 Mt/yr (MCGUIRE et al. 2009). DOC inputs from the Sag River (0.026 Mt/yr), the Kuparuk River (0.014 Mt/yr) and the Colville River (0.11 Mt/yr) (MCGUIRE et al. 2009 and r. w.) are much lower than from the Mackenzie River, but much higher than DOC input from coastal erosion, even if catchments are small.

RACHOLD et al. (2005a) compared coastal erosion and river input for TOC values at a circum-arctic level, based on a database of RACHOLD et al. (2004). This study revealed four times higher values for TOC release by rivers (4.4 Mt/yr) than by coastal erosion (0.9 Mt/yr) illustrated in Figure 5.5. This pattern also applies in the Siberian parts of the Arctic Ocean. Only in the East Siberian Sea, TOC fluxes by coastal erosion are higher than by rivers, probably due to low river discharge from the two major rivers Kolyma and Indigirka. In this study, however, DOC contribution from coastal erosion was not included and TOC for coastal erosion equated POC contribution.

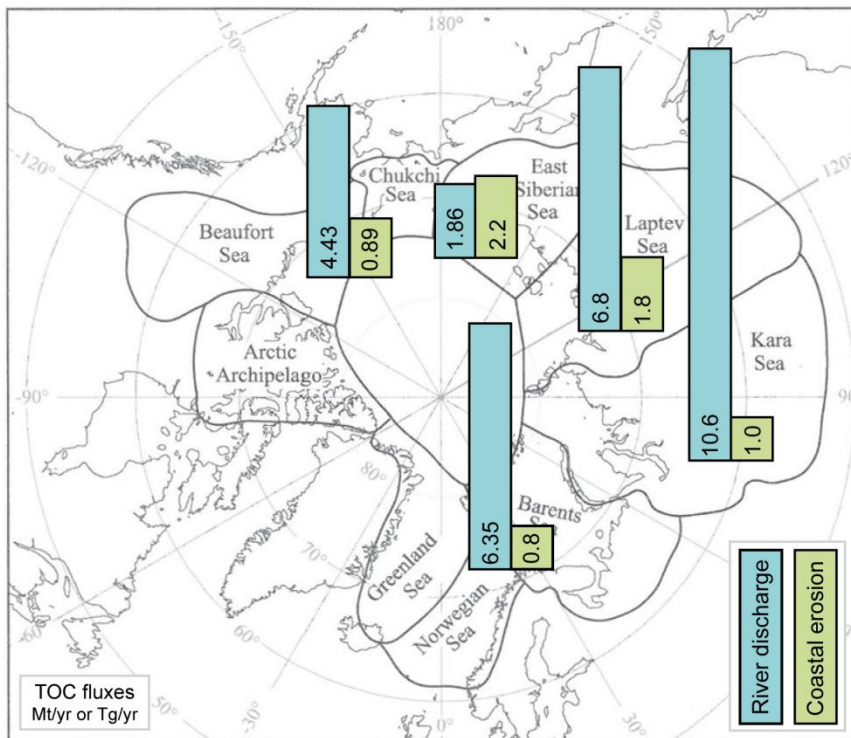


Figure 5.5: Comparison of total organic carbon fluxes from rivers and coastal erosion, modified after RACHOLD et al. (2005b), based on a database from RACHOLD et al. 2004.

Besides the quantitatively higher release of DOC from rivers in comparison to coastal erosion, there are some major qualitative differences in discharge patterns and age of the yielded DOC.

Arctic rivers have a high seasonal variability in discharge (DRENZEK et al. 2007). During the freshet from May to July, after arctic rivers become free of ice, they deliver more than 90 % of the annual discharge (CAUWET & SIDOROV 1996, HOLMES et al. 2000). In these months of peak discharge, most of the DOC is exported (BENNER et al. 2004, DRENZEK et al. 2007). In contrast to river discharge, the release of organic carbon by coastal erosion occurs mainly by wave action (LANTUIT et al. 2012) in sea ice free months of the year during strong storm events. These storms become increasingly frequent in late August and September (JONES et al. 2009a). The storms mostly coming from western, north-western and eastern direction in the study area (SOLOMON 1995) and can generate waves up to more than 4 m that foster coastal erosion (PINCHIN et al. 1985).

The DOC yielded by rivers is dominated by contemporary sources (BENNER et al. 2004, GUO & MACDONALD 2006, NEFF et al. 2006), mainly derived by terrestrial biomass production in form of C3 terrestrial vegetation (YUNKER et al. 1991), supported by stable isotope compositions by GUO et al. (2007). Terrestrial sources account for ~64 % of DOC in the Mackenzie River (GUO et al. 2007). In contrast, POC mainly originates from old soil

organic carbon (SOC) sequestered in permafrost or deep soil horizons (GUO et al. 2007). This is confirmed by radiocarbon ages of DOC and POC which are distinctly different.

DOC radiocarbon ages for the Mackenzie River correspond to ages between 390 to 1440 a BP (GUO et al. 2007). A simple model by RAYMOND et al. (2007) predicts that ~50 % of DOC exported during the Arctic spring thaw is 1 to 5 years old, 25 % is 6 to 10 years in age, and 15 % is 11 to 20 years old. This young DOC is presumably semi-labile in character (RAYMOND et al. 2007). The age of DOC can be linked to hydrology, as older DOC becomes more apparent under base flow conditions (SCHIFF et al. 1997, 1998). Older POC enters the river either due to river bank erosion or thawing of permafrost rather than from surface soils which contain relatively young SOC (GUO et al. 2007).

There is a lack of studies regarding the origin and the age of organic carbon derived by coastal erosion. Most studies do not differentiate between organic carbon yields by river discharge or coastal erosion in the near shore zone, thus a comparison is difficult (e.g. DUNTON et al. 2006). A study by COUTURE (2010) of $\delta^{13}\text{C}$ concentrations in near-shore sediments of the Beaufort Sea indicated that 92 % of this particulate organic carbon is terrigenous. Nevertheless, sediments can also be derived from the Mackenzie to some extent, as its water discharge dominates the organic carbon input to the Beaufort Sea shelf (DUNTON et al. 2006). With the assumption that eroding material derived from cliffs and thawed permafrost is probably older (GUO et al. 2007), it is assumed that organic carbon released by coastal erosion is old as the coast of the Beaufort Sea is dominated by cliffs with an average height of 6.74 m (LANTUIT et al. 2012). Most of this older material is released into the Beaufort Sea through erosion, as surface runoff is low due to the low annual precipitation rates of 161.3 mm (METEOROLOGICAL SERVICE OF CANADA 2006).

A major difference between both systems is the relation of POC and DOC. Whereas DOC is dominant in the discharge of rivers (MCGUIRE et al. 2009), POC is by far dominant for the input of organic material by coastal erosion. First estimations gave a DOC/POC ratio of ~1% in mass (LANTUIT 2010, unpublished). With regard to POC values derived by COUTURE (2010) for the Yukon Coastal Plain, this study provides a DOC/POC ratio of ~0.01%. This ratio is important because of the labile character of DOC (THURMAN 1985) that enters the Arctic Ocean and the possible relevance for further biogeochemical processes in the Arctic Ocean as it is more reactive than POC (COUTURE 2010). Riverine organic matter, in contrast, is refractory and mainly composed of soil-derived humic substances (DITTMAR & KATTNER 2003). However, large amounts of DOC are also exported in arctic rivers (LOBBES et al. 2000). This carbon pool is predominantly young and potentially bio-reactive (BENNER et al. 2004). In comparison to DOC derived from coastal erosion, river derived

dissolved organic matter (DOM) has undergone extensive degradation before entering the ocean (AMON et al. 2001, AMON et al. 2003).

5.3.3 Incorporation of DOC fluxes into the Arctic carbon budget

This study provides the first circum-arctic DOC flux values from massive ground ice into the Arctic Ocean. The extrapolation is based on a comprehensive Arctic coast database (LANTUIT et al. 2012) that includes coast lengths (SOLURI & WOODSON 1990), backshore elevations, annual coastal erosion rates, and ground ice contents of fourteen main arctic coastal regions, visible in Table 5.3. With known average DOC stocks in massive ground ice computed in this study, and the known approximate volume of massive ground ice in permafrost soils (COUTURE 2010), it was possible to extrapolate circum-arctic DOC fluxes. This first approximation yielded a value of 1.87×10^6 Mt/yr (1.87 tons per year) DOC released by coastal erosion from massive ground ice along the arctic coastal rim (Table 5.3).

Table 5.3: Extrapolated DOC fluxes from massive ground ice on a circum-arctic scale, modified and adapted after LANTUIT et al. (2012).

	Coast length [km]	Coastline height [m]	Coastal erosion rate [m/yr]	MGI content [vol%]	DOC flux rate [$\times 10^{-6}$ Mt/yr]
Canadian Beaufort Sea	5672	6.74	1.12	2.94	0.18
American Beaufort Sea	3376	1.54	1.15	2.69	0.02
American Chukchi Sea	4662	4.98	0.49	2.40	0.04
Canadian Archipelago	4656	no data	0.01	1.42	no data
Svalbard	8782	13.96	0.00	0.00	0.00
Russian Chukchi Sea	2736	14.54	0.27	1.39	0.02
Barent Sea	17965	10.52	0.42	1.62	0.19
Kara Sea	25959	14.04	0.68	2.37	0.85
Laptev Sea	16927	11.91	0.73	1.71	0.37
East Siberian Sea	8942	8.79	0.87	1.96	0.20
Arctic Ocean	99677	9.67	0.57	1.85	1.87

In the following, circum-arctic DOC fluxes from the erosion of massive ground ice are incorporated into the Arctic carbon budget (Figure 5.6) and compared with published numbers of organic carbon stocks and fluxes to evaluate their possible significance. It compares organic carbon fluxes from rivers and coastal erosion and gives an overview of terrestrial and marine DOC stocks.

The main source of both riverine and coastal erosion fluxes is organic carbon stored in vegetation (60-70 Pg) and soils (1400-1500 Pg)(MCGUIRE et al. 2009 and r. w.).

Circum-arctic DOC fluxes of 2×10^6 Tg/yr from massive ground ice were estimated in this study. As no studies had been recently carried out to investigate DOC in permafrost soils and ground ice, this is the only value available that can be incorporated in a circum-arctic carbon budget. As expected, this value is by far lower than ~ 8 Pg/yr of POC (MCGUIRE et al. 2009) that is released by coastal erosion.

In contrast to coastal erosion, DOC fluxes by rivers are by far greater. The discharge of DOC ranges between 18-26 Tg/yr (DITTMAR & KATTNER 2003) and 33 Tg/yr (MCGUIRE et al. 2009). POC fluxes range between 4-6 Pg/yr (DITTMAR & KATTNER 2003, MCGUIRE et al. 2009) and are much smaller than DOC fluxes but comparable with POC fluxes from coastal erosion (STEIN & MACDONALD 2004). After entering the Arctic Ocean, DOC becomes part of the Arctic Ocean stocks and is exposed to various biogeochemical processes and transportation cycles. This Arctic carbon budget is substantially influenced by riverine and coastal sources of organic carbon (ANDERSON et al. 1998, STEIN & MACDONALD 2004) and is composed of approximately 9 Pg organic carbon.

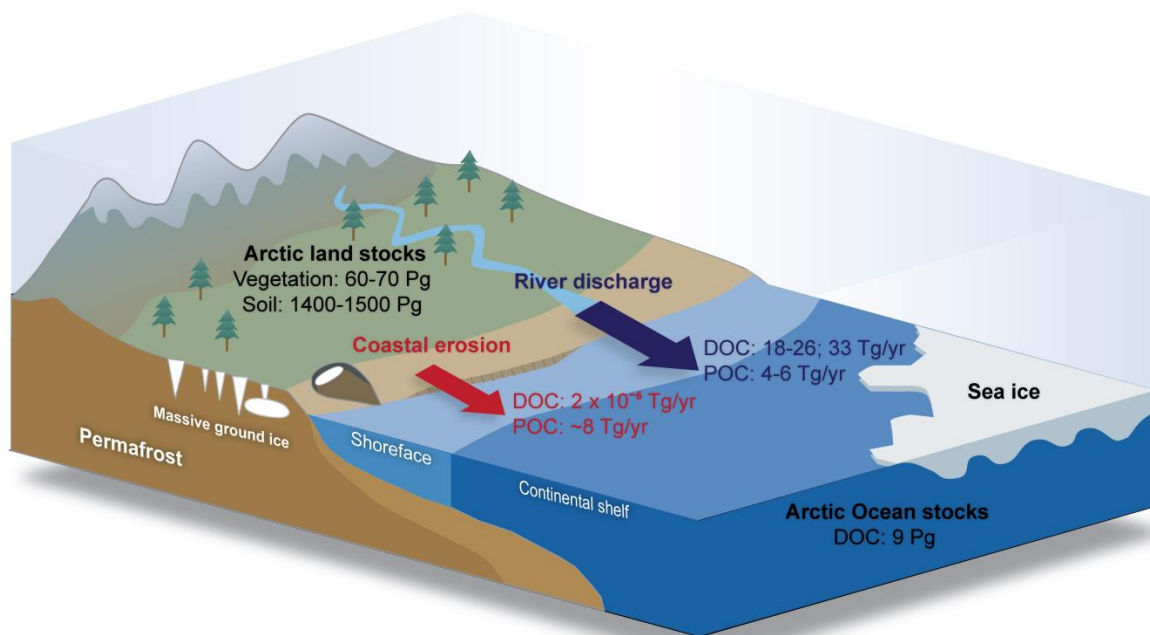


Figure 5.6: Arctic carbon budget incorporating DOC fluxes from massive ground ice eroded at the coast.

Estimated DOC fluxes released into the Canadian Beaufort Sea would therefore be among the highest on a circum-arctic scale if estimated per meter of coastline. In total, DOC fluxes in the Canadian Beaufort Sea are the highest in North America, but much lower than the

ones from the Russian Arctic coast. As estimated DOC fluxes for the Canadian Beaufort Sea are the highest on the American Continent it is assumed that the shores of the Canadian Arctic could play a key role in the transfer of DOC from terrestrial to the marine system.

In conclusion DOC fluxes from massive ground ice released by coastal erosion are only a marginal part of the terrestrial organic carbon flux to the Arctic Ocean. Nevertheless, coastal erosion plays an exceptional role in the Arctic as it is a component especially vulnerable to climate change (STEIN & MACDONALD 2004). Besides the partly known small DOC fluxes revealed by this study, coastal erosion in the Arctic is an important source of POC to the Arctic Ocean, and this flux is likely to increase with warming due to the loss of the protective sea ice buffer, increasing storm activity, and thawing of coastal permafrost (JORGENSEN & BROWN 2005, RACHOLD et al. 2004, RACHOLD et al. 2005a).

5.4 Fate of DOC in the near shore zone

Three scenarios of DOC fluxes were created in this thesis, yielding values in the range of 144 kg/yr (Scenario A), 274 kg/yr (Scenario B) and 466 kg/yr (Scenario C). The fate of this terrigenous organic material is one of the big unsolved questions in marine geochemical studies (AMON 2004). There are three main pathways for the eroded DOC upon its entrance into the nearshore zone: biogeochemical transformation, incorporation into the food web or offshore transfer (Figure 5.7).

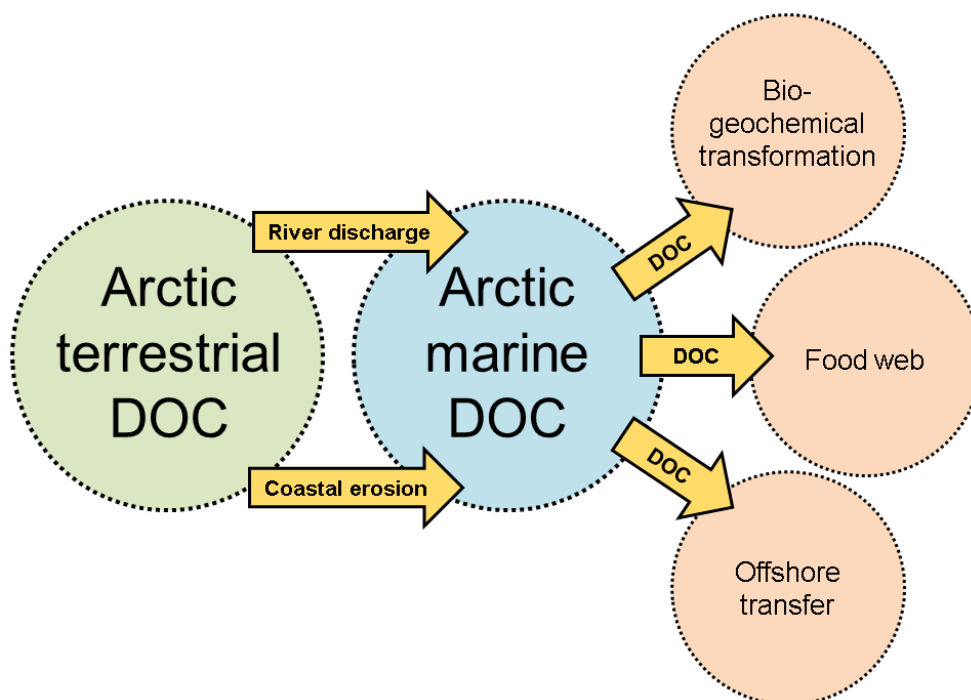


Figure 5.7: Fate of DOC in the nearshore zone.

Biogeochemical transformation processes play an important role for the reactivity of DOC in the water column but are still poorly understood. Various forms of bacteria are the most important consumers and essential for the degradation of DOC in estuarine, coastal and oceanic waters (COTTRELL & KIRCHMAN 2003, BAUER & BIANCHI 2011). Aromatic compounds, typical for terrigenous organic carbon, like tannin and lignin, presumably make the DOC pool refractory to microbes (AITKENHEAD-PETERSON et al. 2003). However, high levels of aromaticity and light absorbance potentially make this same DOC more susceptible to photochemical alteration (BAUER & BIANCHI 2011). CORY et al. (2013) showed that newly exposed DOC from thermokarst sites is more than 40 % more susceptible to microbial conversion to CO₂ when exposed to ultraviolet (UV) light. This indicates that sunlight may act as a catalyst in the conversion of frozen terrestrial carbon to carbon gases in the atmosphere (CORY et al. 2013). Nevertheless, sea ice cover reduces UV-penetration and may limit terrigenous DOC photo-mineralization for extended periods of the year (BÉLANGER et al. 2006). As the natural settings are variable at the coast, it is difficult to assess which biogeochemical process prevails at a certain location.

The most labile DOC parts are re-mineralized within weeks (AMON 2004). HANSELL et al. (2004) estimated a half-life of ~7 years for terrestrial DOC in the Arctic Ocean, with photic microbial activity and reactions being the most probable causes of degradation. According to experiments conducted by HOOD et al. (2009) to determine the lability of DOC, 23 to 66 % (average 45 %) of terrigenous DOC is bioavailable. According to this conservative estimate, and the estimated DOC flux scenarios of this study, bioavailable and labile DOC is in the range of 65 kg/yr (Scenario A), 123 kg/yr (Scenario B) and 210 kg/yr (Scenario C).

Coastal waters are highly important for arctic nearshore ecosystems (CARMACK & MACDONALD 2002, CLARKE & HARRIS 2003, FORBES et al. 2011), but the fate of the terrigenous carbon in arctic coastal food webs is largely unknown (DUNTON et al. 2006). The coast of the Beaufort Sea is characterized by massive freshwater discharge from the Mackenzie River along with numerous smaller rivers (DUNTON et al. 2006) and high coastal retreat rates (DUNTON et al. 2006, LANTUIT et al. 2012) transporting high amounts of organic carbon from upland regions into the near shore zone (DUNTON et al. 2006, COUTURE 2010). This release provides consumers along the coast of the Beaufort Sea with large amounts of terrigenous derived carbon (CARMACK & WASSMANN 2006). Isotopic tracer studies in barrier island lagoon systems along the western Beaufort Sea showed that terrestrial carbon supplies between 30 to 50 % of the total dietary requirements of amphidromous fishes. Calculations from isotopic mixing equations indicate cod from lagoons may derive 70 % of their carbon from terrestrial sources. Besides, terrestrial derived organic

carbon can be embedded into crustacean communities, which are the base of the arctic coastal food web (FORBES et al. 2011).

The majority of terrestrial derived DOC is transported over the shelf to the continental shelf edge. This is indicated by the conservative distribution pattern of DOC along the salinity gradient (CAUWET & SIDOROV 1996). Hence, most of the DOC is not subject to flocculation processes in the nearshore and enters the outer shelf of the Arctic Ocean (AMON 2004). Transport pathways of organic carbon off the shelf are influenced by complex circulation patterns including jets, filaments, various currents, and tides. In general, the export happens more readily along narrow rather than wide continental shelves and is known to be highly episodic (DUCKLOW & MCCALLISTER 2004) as it can occur via episodic events such as storms (HILL et al. 1991, HÉQUETTE et al. 2001). With regard to these processes, the narrow continental shelf area of the Yukon Coast has a strong impact on the fate of the organic carbon in the southern Beaufort Sea (COUTURE 2010) as material is probably transported rapidly to the shelf edge. Depending on the salinity (CAUWET & SIDOROV 1996), DOC is then transported to surface waters, to intermediate waters of the open ocean, or to the Canadian Basin (AAGARD et al. 1985).

6 Conclusions and Outlook

The aim of this study was to determine the amounts and the origin of dissolved organic carbon (DOC) contained in massive ground ice and to estimate DOC fluxes from the Yukon Coastal Plain into the southern Canadian Beaufort Sea (Arctic Ocean). Based on measured DOC concentrations in different ground ice bodies and with the help of average parameters for coastal geomorphic and geological properties, three scenarios of possible DOC fluxes were established and brought into the context of arctic organic carbon fluxes by coastal erosion and rivers. The following specific conclusions can be drawn from this thesis:

- The concentration of DOC in massive ice bodies and ice wedges along the Yukon Coastal Plain ranges between 1.03 and 19.48 mg/L with an average of 4.30 mg/L. This is consistent with DOC concentrations found in ground water, interstitial water, and glacier meltwater. On the basis of DOC concentrations, equated DOC stocks in massive ground ice ranging between 0.09 to 0.24 g/m³ for the cliffs of the whole Yukon coast. The concentration of DOC strongly depends on the genetic ice type. Ice wedges have approximately eight times higher DOC concentrations than massive ground ice bodies of glacial or segregated origin. Linear regression analysis between ice content, sediment content and DOC concentration revealed that higher DOC values in massive ground ice bodies are strongly coupled with sediment contents. In ice wedges, no statistically significant correlation was found. Massive ground ice bodies and ice wedges have a different genesis. Massive ground ice bodies are fed by meltwater migrating through the soil during segregation or during contact between the glacier and basal sediments. Ice wedges are fed by inflow of meltwater from the top of the tundra in spring. This leads to the assumption that organic carbon stored in the upper permafrost is the main source of DOC in massive ice bodies. For ice wedges, organic carbon transported from surface vegetation is supposed to be the main source of DOC.
- DOC fluxes from the Yukon Coastal Plain are in the range of 148 to 466 kg/yr, depending on the scenario used in the study. The highest DOC fluxes were estimated for morainal parts on Herschel Island and Kay Point in the eastern part of the mainland coast. The influence of cliff height on DOC fluxes from massive ground ice is low, whereas the impact of coastal erosion, massive ground ice content and DOC stock is stronger. Comparisons between the estimated DOC fluxes in this study with arctic rivers revealed that DOC fluxes from massive ground ice are much lower than riverine contributions to the arctic organic carbon budget. Extrapolations of DOC

fluxes from massive ground ice on a circum-arctic scale show that DOC fluxes from the Canadian Beaufort Sea are the highest in the North American Arctic and are among the highest on a circum-arctic scale. For that reason, it is suggested that the ice-rich permafrost coasts of the Canadian Beaufort Sea might play a major role in the transfer of DOC from terrestrial to marine ecosystems systems, especially when DOC concentrations in pore ice will be incorporated. Coastal erosion-induced DOC fluxes into the nearshore zone of the southern Canadian Beaufort Sea remain, however, low in the context of the whole arctic carbon budget.

Analysis of DOC in permafrost is challenging, because the interaction of ground ice and the surrounding sediments is hardly understood and transfer processes occurring during or immediately after sampling could be sources of contamination. To mitigate this issue, controlled sampling conditions and a multiplication of the number of samples available are necessary.

In the coming years, additional samples of massive ground ice will be taken to extend the database. Measurements will not only focus on DOC but also on ions and isotopes to characterize the origin and genesis of massive ground ice. Additionally, dating of DOC could help to determine its origin. As the origin and the exact vertical extent of the massive ice bodies are also still debated, more information on the genesis of the ice will also contribute to refine hypotheses on the origin of the DOC.

During the expedition “Yukon Coast 2013”, samples from pore ice, which are typically much more challenging to collect, will be taken and analyzed to incorporate them in existing DOC flux estimations established in this study. By including pore ice samples, it will be possible to describe the total DOC stock in permafrost as pore ice is the main ice type along the Yukon Coastal Plain. It will also help us to better understand the interaction between ice and sediment and its role in the dissolution of organic carbon.

As no direct DOC measurements have been carried out in the nearshore zone yet, the fate of DOC in the marine realm remains rather uncertain and will form a central topic of coming investigations. In the upcoming expeditions, transects from the coast to the shelf edge are planned to monitor the pathways of DOC. Furthermore, investigations on the biogeochemical characteristics of DOC will be carried out to gain insights about the provenance and lability of DOC that is delivered by coastal erosion into the ocean. With that knowledge, information about degradation and photochemical transformation processes could be reconstructed. These investigations will contribute to update the existing arctic organic carbon budget and create a better understanding of carbon transfer processes between land, ocean and atmosphere.

References

AAGARD, K. (1984): The Beaufort Undercurrent. In: BARNES, P. W., SCHELL, D. M. & REIMNITZ, E. (eds.): The Alaskan Beaufort Sea: Ecosystems and Environments. Academic Press, New York. p. 44-71.

ACIA - Arctic Climate Impact Assessment (2004): Impacts of a warming Arctic. Cambridge University Press, New York. 141 p.

ACIA - Arctic Climate Impact Assessment (2005): Arctic Climate Impact Assessment. Cambridge University Press, New York. 1042 p.

AGRICULTURE CANADA EXPERT COMMITTEE ON SOIL SURVEY (1987): The Canadian System of Soil Classification. 2nd ed. Agriculture Canada Publication 1646. 164p.

AITKENHEAD-PETERSON, J., MCDOWELL, W. & NEFF, J. (2003): Sources, production, and regulation of allochthonous dissolved organic matter inputs to surface waters. In: FINDLAY, E. G. & SINSABAUGH, R. L. (eds.): Aquatic Ecosystems – Interactivity of Dissolved Organic Matter. Academic Press San Diego. 512 p.

ALLEY, R.B., MAROTZKE, J., NORDHAUS, W.D., OVERPECK, J.T., PETEET, D.M., PIELKE, R.A., PIERREHUMBERT, R.T., RHINES, P.B., STOCKER, T.F., TALLEY, L.D. & WALLACE, J.M. (2003): Abrupt climate change. *Science* 299. p. 2005-2010.

AMAP - Arctic Monitoring and Assessment Programme (2011): SWIPA - Snow, Water, Ice and Permafrost in the Arctic. 16 p.

AMON, R.M., FITZNAR, H.-P. & BENNER, R. (2001): Linkages among the bioreactivity, chemical composition, and diagenetic state of marine dissolved organic matter. *Limnology and Oceanography* 46. p. 287-297.

AMON, R.M., BUDÉUS, G. & MEON, B. (2003): Dissolved organic carbon distribution and origin in the Nordic Seas: Exchanges with the Arctic Ocean and the North Atlantic. *Journal of Geophysical Research: Oceans* (1978–2012) 108.

AMON, R.M.W. (2004): The Role of Dissolved Organic Matter for the Organic Carbon Cycle in the Arctic Ocean. In: STEIN, R. & MACDONALD, R.W. (eds.): The Organic Carbon Cycle in the Arctic Ocean. Springer Verlag, Berlin. 367 p.

- ANDERSON, L.G., OLSSON, K. & CHERICI, M. (1998): A carbon budget for the Arctic Ocean. *Global Biogeochemical Cycles* 12. p. 455-465.
- ANISIMOV, O. & RENEVA, S. (2006): Permafrost and changing climate: the Russian perspective. *AMBIO: A Journal of the Human Environment* 35. p. 169-175.
- ARTINGER, R., BUCKAU, G., GEYER, S., FRITZ, P., WOLF, M. & KIM, J. (2000): Characterization of groundwater humic substances: influence of sedimentary organic carbon. *Appl Geochem* 15. p. 97-116.
- ATKINSON, D.E. (2005): Observed storminess patterns and trends in the circum-arctic coastal regime. *Geo-Mar Lett* 25, p. 98-109.
- ARÉ, F.E. (1988): Thermal abrasion of sea coasts. *Polar Geography and Geology* 12. 159 p.
- BALLANTYNE, C.K. & HARRIS, C. (1994): *The Periglaciation of Great Britain*. CUP Archive. 335 p.
- BARCELONA, M.J. (1984): TOC determinations in ground water. *Ground water* 22. p. 18-24.
- BARINGER, M.O., ARNDT, D.S. & JOHNSON, M.R. (2010): State of the Climate in 2009. *B Am Meteorol Soc*. 91.
- BARKER, J., SHARP, M., FITZSIMONS, S. & TURNER, R. (2006): Abundance and dynamics of dissolved organic carbon in glacier systems. *Arctic, Antarctic, and Alpine Research* 38. p. 163-172.
- BARTLEY, J., BUDDEMEIER, R. & BENNETT, D. (2001): Coastline complexity: a parameter for functional classification of coastal environments. *Journal of Sea Research* 46. p. 87-97.
- BAUER, J. & BIANCHI, T. (2011): Dissolved organic carbon cycling and transformations. *Treatise on Estuarine and Coastal Science*. In: WOLANSKI, E. & MCLUSKY, D. S. (eds.): *Treatise on Estuarine and Coastal Science* 5. Waltham Academic Press. 767 p.
- BELANGER, S., XIE, H., KROTKOV, N., LAROUCHE, P., VINCENT, W. F. & BABIN, M. (2006): Photomineralization of terrigenous dissolved organic matter in Arctic coastal waters from 1979 to 2003: Interannual variability and implications of climate change. *Global Biogeochemical Cycles* 20.
- BENNER, R., BENITEZ-NELSON, B., KAISER, K. & AMON, R.M. (2004): Export of young terrigenous dissolved organic carbon from rivers to the Arctic Ocean. *Geophys Res Lett* 31.

- BLUME, H.-P., BRÜMMER, G.W., HORN, R., KANDELER, E., KÖGEL-KNABNER, I., KRETZSCHMAR, R., STAHR, K. & WILKE, B.-M. (2010): Scheffer/Schachtschabel: Lehrbuch der Bodenkunde. Spektrum Akademischer Verlag, Heidelberg. 569 p.
- BOCKHEIM, J., HINKEL, K. (2007): The importance of "Deep" organic carbon in permafrost-affected soils of arctic Alaska. *Soil Science Society of America Journal* 71. p. 1889-1892.
- BOSTOCK, H.S. (1970): Physiographic subdivisions of Canada. In: DOUGLAS, R.J.W. (ed.): *Geology and Economic Minerals of Canada*. Geological Survey of Canada Economic Report. p. 10-30.
- BOUCHARD, M. (1974): *Géologie de depots de L'Ile Herschel, Territoire du Yukon*. Thesis. Université de Montréal.
- BROWN, R.J.E. & KUPSCH, W.O. (1974): Permafrost terminology. National Research Council of Canada. 62 p.
- BURN, C. (2009): After Whom is Herschel Island Named? *Arctic* 62. p. 317-323.
- BROWN, J., FERRIANS, O.J., HEGINBOTTOM, J. & MELNIKOV, E. (1997): Circum-Arctic map of permafrost and ground-ice conditions. US Geological Survey Reston.
- BROWN, J., JORGENSON, M.T., SMITH, O.P. & LEE, W. (2003): Long-term rates of coastal erosion and carbon input, Elson Lagoon, Barrow, Alaska, Eighth International Conference on Permafrost. p. 21-25.
- CALLAGHAN, T.V., JOHANSSON, M., PROWSE, T.D., OLSEN, M.S. & REIERSEN, L.O. (2011): Arctic Cryosphere: Changes and Impacts. *Ambio* 40. p. 3-5.
- CARMACK, E.C. & MACDONALD, R.W. (2002): Oceanography of the Canadian Shelf of the Beaufort Sea: A setting for marine life. *Arctic* 55. p. 29-45.
- CARMACK, E. & WASSMANN, P. (2006): Food webs and physical–biological coupling on pan-Arctic shelves: unifying concepts and comprehensive perspectives. *Progress in Oceanography* 71. p. 446-477.
- CAUWET, G. & SIDOROV, I. (1996): The biogeochemistry of Lena River: organic carbon and nutrients distribution. *Mar Chem* 53. p. 211-227.
- CHAPIN, F.S., BERMAN, S., CALLAGHAN, M., CONVEY, T. V., CRÉPIN, P., DANELL, A.-S., DUCKLOW, K., FORBES, H., KOFINAS, B., MCGUIRE, G., NUTTALL, A. D., VIRGINIA, M., YOUNG, R., ZIMOV, O, CHRISTENSEN, S. A., GODDUHN, T., MURPHY, A., WALL, E. J.,

- & ZOCKLER, D. (2005): Polar Systems. In: HASSAN, R., SCHOLE, R. & ASH, N. (eds.): Ecosystems and human well-being: current state and trends 1. Island Press, Washington D. C. p. 717-743.
- CLARKE, A. & HARRIS, C.M. (2003): Polar marine ecosystems: major threats and future change. *Environmental Conservation* 30. p. 1-25.
- COOPER, L.W., BENNER, R., MCCLELLAND, J.W., PETERSON, B.J., HOLMES, R.M., RAYMOND, P.A., HANSELL, D.A., GREBMEIER, J.M. & CODISPOTI, L.A. (2005): Linkages among runoff, dissolved organic carbon, and the stable oxygen isotope composition of seawater and other water mass indicators in the Arctic Ocean. *Journal of Geophysical Research: Biogeosciences* (2005–2012) 110.
- CORY, R.M., CRUMP, B.C., DOBKOWSKI, J.A. & KLING, G.W. (2013): Surface exposure to sunlight stimulates CO₂ release from permafrost soil carbon in the Arctic. *Proceedings of the National Academy of Sciences* 110, p. 3429-3434.
- COTTRELL, M.T. & KIRCHMAN, D.L. (2003): Contribution of major bacterial groups to bacterial biomass production (thymidine and leucine incorporation) in the Delaware estuary. *Limnology and Oceanography* 48. p. 168-178.
- COUTURE, N., HOQUE, M.A. & POLLARD, W.H. (1998): Modelling the erosion of ice-rich deposits along the Yukon Coastal Plain. *Proceedings Ninth International Conference on Permafrost*. Fairbanks, Alaska.
- COUTURE, N., ROBINSON, S.D. & BURGESS, M.M. (2000): Climate change, permafrost degradation, and infrastructure adaptation: preliminary results from a pilot community case study in the Mackenzie Valley. *Current Research 2000-B2*, p. 1-9.
- COUTURE, N. (2010): Fluxes of Soil Organic Carbon from Eroding Permafrost Coasts, Canadian Beaufort Sea. Department of Geography. McGill University, Montréal.
- CURRY, J.A., ROSSOW, W.B., RANDALL, D. & SCHRAMM, J.L. (1996): Overview of Arctic cloud and radiation characteristics. *J Climate* 9, p. 1731-1764.
- DALLIMORE, S.R., WOLFE, S.A. & SOLOMON, S.M. (1996): Influence of ground ice and permafrost on coastal evolution, Richards Island, Beaufort Sea coast, NWT. *Canadian Journal of Earth Sciences* 33, p. 664-675.
- DAVIDSON, E. A., TRUMBORE, S. E. & AMUNDSON, R. (2000): Biogeochemistry: soil warming and organic carbon content. *Nature* 408. p. 789-790.

- DeCONTO, R.M., GALEOTTI, S., PAGANI, M., TRACY, D., SCHAEFER, K., ZHANG, T., POLLARD, D. & BEERLING, D.J. (2012): Past extreme warming events linked to massive carbon release from thawing permafrost. *Nature* 484, p. 87-91.
- DE KROM, V. (1990): Retrogressive thaw slumps and active layer slides on Herschel Island, Yukon. Thesis. McGill University Montréal, Québec.
- DITTMAR, T. & KATTNER, G. (2003): The biogeochemistry of the river and shelf ecosystem of the Arctic Ocean: A review. *Mar Chem* 83. p. 103-120.
- DOU, F., PING, C.-L., GUO, L. & JORGENSEN, T. (2008): Estimating the impact of seawater on the production of soil water-extractable organic carbon during coastal erosion. *Journal of environmental quality* 37. p. 2368-2374.
- DOUGLAS, T., JORGENSEN, M., KANEVSKIY, M., ROMANOVSKY, V., SHUR, Y. & YOSHIKAWA, K. (2008): Permafrost dynamics at the Fairbanks Permafrost Experimental Station near Fairbanks, Alaska. *Proceedings, NICOP (Vol. I)*. p. 373-378.
- DOUGLAS, T.A., FORTIER, D., SHUR, Y.L., KANEVSKIY, M.Z., GUO, L., CAI, Y. & BRAY, M.T. (2011): Biogeochemical and geocryological characteristics of wedge and thermokarst-cave ice in the CRREL permafrost tunnel, Alaska. *Permafrost and Periglacial Processes* 22. p. 120-128.
- DUCKLOW, H.W. & MCCALLISTER, S.L. (2004): The biogeochemistry of carbon dioxide in the coastal oceans. *The sea* 13. p. 269-315.
- DUNTON, K.H., WEINGARTNER, T. & CARMACK, E.C. (2006): The nearshore western Beaufort Sea ecosystem: circulation and importance of terrestrial carbon in arctic coastal food webs. *Progress in Oceanography* 71. p. 362-378.
- ERMOLAEV, M. (1932): Geological and geomorphological description of Bolshoi Lyakhovskii Island: *Trudy SOPS AN SSSR. Yakut ser. No. 7 (In Russian)*.
- DRENZEK, N.J., MONTLUÇON, D.B., YUNKER, M.B., MACDONALD, R.W. & EGLINTON, T.I. (2007): Constraints on the origin of sedimentary organic carbon in the Beaufort Sea from coupled molecular ^{13}C and ^{14}C measurements. *Mar Chem* 103. p. 146-162.
- FORBES, D.L. & FROBEL, D. (1985): Coastal erosion and sedimentation in the Canadian Beaufort Sea. Geological Survey of Canada.

- FORBES, D.L. (1989): Coastal erosion and nearshore profile variability in the southern Beaufort Sea, Ivvavik National Park, Yukon Territory. Geological Survey of Canada Open File 3531. p. 28.
- FORBES, D. & TAYLOR, R. (1994): Ice in the shore zone and the geomorphology of cold coasts. *Progress in Physical Geography* 18. p. 59-89.
- FORBES, D.L., SOLOMON, S.M. & FROBEL, D. (1995): Report of the 1992 coastal surveys in the Beaufort Sea. Open File 3053, Geological Survey of Canada. p. 39.
- FORBES, D.L. (1997): Coastal erosion and nearshore profile variability in the southern Beaufort Sea, Ivvavik National Park, Yukon Territory. Geological Survey of Canada Open File 3531. p. 28.
- FORBES, D.L., KREMER, H., LANTUIT, H., RACHOLD, V. & REIERSEN, L.O. (2011): State of the Arctic coast 2010: scientific review and outlook. *Land-Ocean Interactions in the Coastal Zone*. Institute of Coastal Research.
- FORTIER, D., ALLARD, M. & SHUR, Y. (2007): Observation of rapid drainage system development by thermal erosion of ice wedges on Bylot Island, Canadian Arctic Archipelago. *Permafrost and Periglacial Processes* 18. p. 229-243.
- FRENCH, H. & HARRY, D. (1990): Observations on buried glacier ice and massive segregated ice, western Arctic coast, Canada. *Permafrost and Periglacial Processes* 1. p. 31-43.
- FRENCH, H. (2007): *The periglacial environment*. Wiley. 458 p.
- FRENCH, H. & SHUR, Y. (2010): The principles of cryostratigraphy. *Earth-Science Reviews* 101. p. 190-206.
- FREY, K.E. & SMITH, L.C. (2005): Amplified carbon release from vast West Siberian peatlands by 2100. *Geophys Res Lett* 32.
- FRITZ, M. (2008): Late Quaternary paleoenvironmental records from a glacially and permafrost affected island in the Canadian Arctic (Herschel Island, Yukon Coastal Plain). Institute for Geographical Sciences. University of Greifswald, Greifswald. p. 147.
- FRITZ, M., LANTUIT, H., MEYER, H. & OPEL, T. (2011a): Dissolved Organic Carbon (DOC) in Ground Ice: Is It Significant? Unpublished.
- FRITZ, M., WETTERICH, S., MEYER, H., SCHIRRMEISTER, L., LANTUIT, H. & POLLARD, W.H. (2011b): Origin and characteristics of massive ground ice on Herschel Island (western Canadian

Arctic) as revealed by stable water isotope and Hydrochemical signatures. *Permafrost and Periglacial Processes* 22. p. 26-38.

FRITZ, M., WETTERICH, S., SCHIRRMEISTER, L., MEYER, H., LANTUIT, H., PREUSSER, F. & POLLARD, W.H. (2012): Eastern Beringia and beyond: Late Wisconsinan and Holocene landscape dynamics along the Yukon Coastal Plain, Canada. *Palaeogeogr Palaeocl* 319. p. 28-45.

GELL, A.W. (1976): Underground ice in permafrost, Mackenzie Delta - Tyktoyaktuk Peninsula, NWT. Unpublished Thesis. University of British Columbia.

GILLIE, R.D. (1987): Shore profile surveys, Canadian Beaufort Sea coast. Open File 1826, Geological Survey of Canada. p. 21.

GRIGORIEV, M. & RACHOLD, V. (2003): The degradation of coastal permafrost and the organic carbon balance of the Laptev and East Siberian Seas. *Proceedings of the 8th International Conference on Permafrost*. p. 21-25.

GROSSE, G., HARDEN, J., TURETSKY, M., MCGUIRE, D., CAMILL, P., TARNOCAI, C., FROLKING, S., SCHUUR, E.A.G., JORGENSON, T., MARCHENKO, S., ROMANOVSKY, V., WICKLAND, K.P., FRENCH, N., WALDROP, M., BOURGEOU-CHAVEZ, L. & STRIEGL, R.G. (2011): Vulnerability of high-latitude soil organic carbon in North America to disturbance. *Journal of Geophysical Research* 116.

GUO, L., TANAKA, T., WANG, D., TANAKA, N. & MURATA, A. (2004): Distributions, speciation and stable isotope composition of organic matter in the southeastern Bering Sea. *Mar Chem* 91. p. 211-226.

GUO, L. & MACDONALD, R. (2006): Source and transport of terrigenous organic matter in the upper Yukon River: Evidence from isotope ($\delta^{13}\text{C}$, $\delta^{14}\text{C}$, and $\delta^{15}\text{N}$) composition of dissolved, colloidal, and particulate phases. *Global Biogeochem. Cycles* 20.

GUO, L., PING, C.-L. & MACDONALD, R.W. (2007): Mobilization pathways of organic carbon from permafrost to arctic rivers in a changing climate. *Geophys Res Lett* 34.

HANDBOOK WTW (1989): pH-Fibel: Einführung in die pH- und Redox-Meßtechnik. Wiss.-techn. Werkstätten GmbH, Weilheim.

HANDBOOK WTW (1989): pH-Fibel: Einführung in die pH- und Redox-Meßtechnik. Wiss.-techn. Werkstätten GmbH, Weilheim.

- HANSELL, D.A. & CARLSON, C.A. (2001): Marine dissolved organic matter and the carbon cycle. *Oceanography* 14. p. 41-49.
- HANSELL, D.A., KADKO, D. & BATES, N.R. (2004): Degradation of terrigenous dissolved organic carbon in the western Arctic Ocean. *Science* 304. p. 858-861.
- HARDEN, J.W., MARK, R.K., SUNDQUIST, E.T. & STALLARD, R.F. (1992): Dynamics of soil carbon during deglaciation of the Laurentide ice sheet. *Science* 258. p. 1921-1924.
- HARPER, J.R., REIMER, P.D. & COLLINS, A.D. (1985): Canadian Beaufort Sea physical shore zone analysis. Geological Survey of Canada.
- HARPER, J.R. (1990): Morphology of the Canadian Beaufort Sea coast. *Marine Geology* 91. p. 75-91.
- HARRIS, S.A., FRENCH, H.M., HEGINBOTTOM, J.A., JOHNSTON, G.H., LADAYI, B., SEGO, D.C. & EVERDINGEN, R.O. (1988): Glossary of permafrost and related ground ice terms. Ottawa.
- HARRY, D., FRENCH, H. & POLLARD, W. (1988): Massive ground ice and ice-cored terrain near Sabine Point, Yukon Coastal Plain. *Canadian Journal of Earth Sciences* 25. p. 1846-1856.
- HEDGES, J.I. (1992): Global Biogeochemical Cycles - Progress and Problems. *Mar Chem* 39. p. 67-93.
- HEDGES, J.I. (2002): Why dissolved organics matter; A marine retrospective. In: HANSELL, D.A. & CARLSON, C.A. (eds.): *Biogeochemistry of marine dissolved organic matter*. Academic Press. p. 1-33.
- HEGINBOTTOM, J.A., BROWN, J., HUMLUM, O. & SVENSSON, H. (2012): Permafrost and Periglacial Environments. In: WILLIAMS, R.S.J. & FERRIGNO, J.G. (eds.): *State of the Earth's Cryosphere at the Beginning of the 21st Century: Glaciers, Global Snow Cover, Floating Ice, and Permafrost and Periglacial Environments*. 78 p.
- HEQUETTE, A. & BARNES, P.W. (1990): Coastal retreat and shoreface profile variations in the Canadian Beaufort Sea. *Marine Geology* 91. p. 113-132.
- HÉQUETTE, A., DESROSIERS, M., HILL, P.R. & FORBES, D.L. (2001): The influence of coastal morphology on shoreface sediment transport under storm-combined flows. *Canadian Beaufort Sea. Journal of Coastal Research* 17. p. 507-516.
- HILL, P.R. (1990): Coastal geology of the King Point area, Yukon Territory, Canada. *Marine geology* 91. p. 93-111.

- HILL, P.R., BLASCO, S.M., HARPER, J.R. & FISSEL, D.B. (1991): Sedimentation on the Canadian Beaufort Shelf. *Continental Shelf Research* 11. p. 821-842.
- HINTERMAIER-ERHARD, G. & ZECH, W. (1997): Wörterbuch der Bodenkunde: Systematik, Genese, Eigenschaften, Ökologie und Verbreitung von Böden. Enke Verlag, Stuttgart. 338 p.
- HINZMAN, L.D., FUKUDA, M., SANDBERG, D.V., CHAPIN, F.S. & DASH, D. (2003): FROSTFIRE: An experimental approach to predicting the climate feedbacks from the changing boreal fire regime. *J. Geophys. Res* 108. p. FFR 9-1–FFR 9-6.
- HOLMES, R., PETERSON, B., GORDEEV, V., ZHULIDOV, A., MEYBECK, M., LAMMERS, R. & VÖRÖSMARTY, C. (2000): Flux of nutrients from Russian rivers to the Arctic Ocean: Can we establish a baseline against which to judge future changes? *Water Resources Research* 36. p. 2309-2320.
- HOLMES, R.M., MCCLELLAND, J.W., RAYMOND, P.A., FRAZER, B.B., PETERSON, B.J. & STIEGLITZ, M. (2008): Lability of DOC transported by Alaskan rivers to the Arctic Ocean. *Geophysical Research Letters* 35.
- HOOD, E., FELLMAN, J., SPENCER, R.G., HERNES, P.J., EDWARDS, R., D'AMORE, D. & SCOTT, D. (2009): Glaciers as a source of ancient and labile organic matter to the marine environment. *Nature* 462. p. 1044-1047.
- HÖLTING, B. (1996): Einführung in die allgemeine und angewandte Hydrogeologie. Enke Verlag, Stuttgart. 383 p.
- HUGELIUS, G., TARNOCAI, C., BROLL, G., CANADELL, J., KUHR, P. & SWANSON, D. (2013): The Northern Circumpolar Soil Carbon Database: spatially distributed datasets of soil coverage and soil carbon storage in the northern permafrost regions. *Earth System Science Data* 5. p. 3-13.
- IPCC (2007): Climate change 2007: the physical science basis. Intergovernmental Panel on Climate Change. 996 p.
- JOHNSON, K., SOLOMON, S., BERRY, D. & GRAHAM, P. (2003): Erosion progression and adaptation strategy in a northern coastal community. 8th International Conference on Permafrost, p. 21-25.
- JOHNSTON, G. (1981): Permafrost-Engineering Design and Construction. Associate Committee on Geotechnical Research, National Research Council of Canada. John Wiley & Sons.

- JONES, P.D. & MOBERG, A. (2003): Hemispheric and large-scale surface air temperature variations: an extensive revision and an update to 2001. *J Climate* 16. p. 206-223.
- JONES, B.M., HINKEL, K.M., ARP, C.D. & EISNER, W.R. (2008): Modern erosion rates and loss of coastal features and sites, Beaufort Sea coastline, Alaska. *Arctic* 61. p. 361-372.
- JONES, B., ARP, C., JORGENSEN, M., HINKEL, K., SCHMUTZ, J. & FLINT, P. (2009a): Increase in the rate and uniformity of coastline erosion in Arctic Alaska. *Geophys Res Lett* 36.
- JONES, B.M., ARP, C.D., BECK, R.A., GROSSE, G., WEBSTER, J.M. & URBAN, F.E. (2009b): Erosional history of Cape Halkett and contemporary monitoring of bluff retreat, Beaufort Sea coast, Alaska. *Polar Geography* 32. p. 129-142.
- JORGENSEN, M., MACANDER, M., JORGENSEN, J., PING, C. & HARDEN, J. (2003): Ground ice and carbon characteristics of eroding coastal permafrost at Beaufort Lagoon, northern Alaska. *ICOP* 2003.
- JORGENSEN, M. & BROWN, J. (2005): Classification of the Alaskan Beaufort Sea Coast and estimation of carbon and sediment inputs from coastal erosion. *Geo-Mar Lett* 25. p. 69-80.
- KANEVSKIY, M., SHUR, Y., FORTIER, D., JORGENSEN, M. & STEPHANI, E. (2011): Cryostratigraphy of late Pleistocene syngenetic permafrost (yedoma) in northern Alaska, Itkillik River exposure. *Quaternary Research* 75. p. 584-596.
- KATTSOV, V. & KÄLLÉN, E. (2005): Future changes of climate: modelling and scenarios for the Arctic region. In: SYMON, C., ARRIS, L. & HEAL, B. (Eds.): *Arctic Climate Impact Assessment (ACIA)*. Cambridge University Press, New York, Cambridge. p. 99-150.
- KAUFMAN, D.S., SCHNEIDER, D.P., MCKAY, N.P., AMMANN, C.M., BRADLEY, R.S., BRIFFA, K.R., MILLER, G.H., OTTO-BLIESNER, B.L., OVERPECK, J.T. & VINTHER, B.M. (2009): Recent warming reverses long-term Arctic cooling. *Science* 325. p. 1236-1239.
- KNIGHT, P.G. (1997): The basal ice layer of glaciers and ice sheets. *Quaternary Science Reviews* 16. p. 975-993.
- KOBAYASHI, N., VIDRINE, J., NAIRN, R. & SOLOMON, S. (1999): Erosion of frozen cliffs due to storm surge on Beaufort Sea Coast. *Journal of coastal research* 15. p. 332-344.
- KÖHLER, H., MEON, B., GORDEEV, V.V., SPITZY, A. & AMON, R.M.W. (2003): Dissolved organic matter (DOM) in the estuaries of Ob and Yenisei and the adjacent Kara-Sea, Russia. In: STEIN, R.,

FAHL, K., FÜTTERER, D.K., GALIMOV, E.M. & STEPANETS, O.V. (eds.): Siberian river run-off in the Kara Sea. Proc. Mar. Sci.

LACELLE, D., BJORNSON, J., LAURIOL, B., CLARK, I. & TROUTET, Y. (2004): Segregated-intrusive ice of subglacial meltwater origin in retrogressive thaw flow headwalls, Richardson Mountains, NWT, Canada. Quaternary Science Reviews 23. p. 681-696.

LACELLE, D., LAURIOL, B., CLARK, I.D., CARDYN, R. & ZDANOWICZ, C. (2007): Nature and origin of a Pleistocene-age massive ground-ice body exposed in the Chapman Lake moraine complex, central Yukon Territory, Canada. Quaternary Research 68. p. 249-260.

LACHENBRUCH, A.H. (1962): Mechanics of thermal contraction cracks and ice-wedge polygons in permafrost. Geological Society of America Special Papers 70. p. 1-66.

LACHNIET, M.S., LAWSON, D.E. & SLOAT, A.R. (2012): Revised ¹⁴C dating of ice wedge growth in interior Alaska (USA) to MIS 2 reveals cold paleoclimate and carbon recycling in ancient permafrost terrain. Quaternary Research 78. p. 217-225.

LAMBERT, S.J. (1995): The Effect of Enhanced Greenhouse Warming on Winter Cyclone Frequencies and Strengths. J Climate 8. p. 1447-1452.

LAMMERS, R.B., SHIKLOMANOV, A.I., VÖRÖSMARTY, C.J., FEKETE, B.M. & PETERSON, B.J. (2001): Assessment of contemporary Arctic river runoff based on observational discharge records. Journal of Geophysical Research: Atmospheres (1984–2012) 106. p. 3321-3334.

LANTUIT, H. & POLLARD, W. (2005): Temporal stereophotogrammetric analysis of retrogressive thaw slumps on Herschel Island, Yukon Territory. Natural Hazards and Earth System Sciences 5. p. 413-423.

LANTUIT, H. & POLLARD, W.H. (2008): Fifty years of coastal erosion and retrogressive thaw slump activity on Herschel Island, southern Beaufort Sea, Yukon Territory, Canada. Geomorphology 95. p. 84-102.

LANTUIT, H., RACHOLD, V., POLLARD, W., STEENHUISEN, F., ØDEGÅRD, R. & HUBBERTEN, H.-W. (2009): Towards a calculation of organic carbon release from erosion of Arctic coasts using non-fractal coastline datasets. Marine Geology 257. p. 1-10.

LANTUIT, H. (2010): DOC fluxes from the Yukon Coastal Plain. Unpublished.

LANTUIT, H. & SCHIRRMEISTER, L. (2011): Permafrost und Mensch. Polarforschung 81. p. 69-75.

- LANTUIT, H., OVERDUIN, P.P., COUTURE, N., WETTERICH, S., ARE, F., ATKINSON, D., BROWN, J., CHERKASHOV, G., DROZDOV, D., FORBES, D.L., GRAVES-GAYLORD, A., GRIGORIEV, M., HUBBERTEN, H.W., JORDAN, J., JORGENSON, T., ODEGARD, R.S., OGORODOV, S., POLLARD, W.H., RACHOLD, V., SEDENKO, S., SOLOMON, S., STEENHUISEN, F., STRELETSKAYA, I. & VASILIEV, A. (2012): The Arctic Coastal Dynamics Database: A New Classification Scheme and Statistics on Arctic Permafrost Coastlines. *Estuaries and Coasts* 35. p. 383-400.
- LEENHEER, J., MALCOLM, R., MCKINLEY, P. & ECCLES, L. (1974): Occurrence of dissolved organic carbon in selected ground-water samples in the United States. *U.S. Geological Survey Journal of Research* 2. p. 361-369
- LETSCHER, R.T., HANSELL, D.A., KADKO, D. & BATES, N.R. (2012): Dissolved organic nitrogen dynamics in the Arctic Ocean. *Mar Chem.* 148. p. 1-9
- LEWIS, C. & FORBES, D. (1975): Sediments and sedimentary processes, Yukon Beaufort Sea coast. Environmental-Social Committee, Northern Pipelines, Task Force on Northern Oil Development.
- LEWKOWICZ, A.G. (1987): Headwall retreat of ground-ice failures, Banks Island, North-west Territories. *Canadian Journal of Earth Sciences* 24. p. 1077-1085.
- LIDE, D.R., BAYSINGER, G., KEHIAIAN, H.V., BERGER, L.I., KUCHITSU, K., GOLDBERG, R.N., ROTH, D.L., HAYNES, W.M. & ZWILLINGER, D. (2008): Properties of ice and supercooled water. In: LIDE, D.R. (ed.): *CRC Handbook of Chemistry and Physics*. CRC Press, Boca Raton, Florida.
- MACDONALD, R.W., SOLOMON, S.M., CRANSTON, R.E., WELCH, H.E., YUNKER, M.B. & GOBEIL, C. (1998): A sediment and organic carbon budget for the Canadian Beaufort shelf. *Marine Geology* 144. p. 255-273.
- LOBBES, J.M., FITZNAR, H.P. & KATTNER, G. (2000): Biogeochemical characteristics of dissolved and particulate organic matter in Russian rivers entering the Arctic Ocean. *Geochimica et Cosmochimica Acta* 64. p. 2973-2983.
- MACDOUGALL, A.H., AVIS, C.A. & WEAVER, A.J. (2012): Significant contribution to climate warming from permafrost carbon feedback. *Nature* 3. p. 719-721
- MACKAY, J.R. (1959): Glacier ice-thrust features of the Yukon coast. *Geographical Bulletin* 13. p. 5-21.
- MACKAY, J.R. (1966): Segregated epigenetic ice and slumps in permafrost. Mackenzie Delta area. *NWT Geographical Bulletin* 8. p. 59-80.

- MACKAY, J.R. (1971): The origin of massive icy beds in permafrost, western Arctic coast, Canada. *Canadian Journal of Earth Sciences* 8. p. 397-422.
- MACKAY, J.R. (1972a): Offshore permafrost and ground ice, southern Beaufort Sea, Canada. *Canadian Journal of Earth Sciences* 9. p. 1550-1561.
- MACKAY, J.R. (1972b): The world of underground ice. *Annals of the Association of American Geographers* 62. p. 1-22.
- MACKAY, J. (1986): Fifty years (1935 to 1985) of coastal retreat west of Tuktoyaktuk, District of Mackenzie. *Current Research, Part A, Geological Survey of Canada, Paper 86*.
- MACKAY, J.R. (1989): Massive ice: some field criteria for the identification of ice types. *Current Research Part G (Paper 89-1G)*. p. 5-11.
- MACKAY, J.R. (1990): Some observations on the growth and deformation of epigenetic, syngenetic and anti-syngenetic ice wedges. *Permafrost and periglacial processes* 1. p. 15-29.
- MACKAY, J.R. & DALLIMORE, S.R. (1992): Massive ice of the Tuktoyaktuk area, western Arctic coast, Canada. *Canadian Journal of Earth Sciences* 29. p. 1235-1249.
- MANDELROT, B.B. (1967): How long is the coast of Britain. *Science* 156. p. 636-638.
- MANSON, G.K. & SOLOMON, S.M. (2007): Past and future forcing of Beaufort Sea coastal change. *Atmosphere-Ocean* 45. p. 107-122.
- MANUAL SHIMADZU/TOC-V (2008): Shimadzu TOC-V Series Total Organic Carbon Analyser. TOC-V CPH/CPN, TOC-Control V, Version 2.00. Kyoto, Japan.
- MARS, J. & HOUSEKNECHT, D. (2007): Quantitative remote sensing study indicates doubling of coastal erosion rate in past 50 yr along a segment of the Arctic coast of Alaska. *Geology* 35. p. 583-586.
- MATTHEWS JR, J. (1975): Incongruence of macrofossil and pollen evidence. A case from the Late Pleistocene of the northern Yukon coast. *Geological Survey of Canada Paper 75-1B*. p. 139-146.
- MCDONALD, B.C. & LEWIS, C.P. (1973): Geomorphologic and sedimentologic processes of rivers and coasts, Yukon Coastal Plain. *Environmental-Social Program, Northern Pipelines*. 245 p.

- MCGILLVRAY, D.G., AGNEW, T.A., MCKAY, G.A., PILKINGTON, G.R. & HILL, M.C. (1993): Report summary of impacts of climate change on Beaufort sea-ice regime: Implications for the Arctic petroleum industry. Prepared for Climate Change Digest, Atmospheric Environment Service.
- MCGUIRE, A.D. & CHAPIN, F.S. (2006): Climate feedbacks in the Alaskan boreal forest. In: CHAPIN, F. S., OSWOOD, M. W., VAN CLEVE, K., VIREECK, L. A. & VERBYLA, D. L. (eds.): *Alaska's changing boreal forest*. Oxford. 354 p.
- MCGUIRE, A.D., ANDERSON, L.G., CHRISTENSEN, T.R., DALLIMORE, S., GUO, L.D., HAYES, D.J., HEIMANN, M., LORENSON, T.D., MACDONALD, R.W., ROULET, N. (2009): Sensitivity of the carbon cycle in the Arctic to climate change. *Ecological Monographs* 79. p. 523-555.
- METEOROLOGICAL SERVICE OF CANADA (2006): Temperature and precipitation 1971-2000 Komakuk Beach. <http://climate.weatheroffice.ec.gc.ca/>. (Access: 28th of April 2013)
- MEYBECK, M. (1982): Carbon, nitrogen, and phosphorus transport by world rivers. *Am. J. Sci* 282. p. 401-450.
- NEFF, J.C. & HOOPER, D.U. (2002): Vegetation and climate controls on potential CO₂, DOC and DON production in northern latitude soils. *Global Change Biology* 8. p. 872-884.
- NEFF, J., FINLAY, J., ZIMOV, S., DAVYDOV, S., CARRASCO, J., SCHUUR, E. & DAVYDOVA, A. (2006): Seasonal changes in the age and structure of dissolved organic carbon in Siberian rivers and streams. *Geophys Res Lett* 33.
- OECHEL, W.C., HASTINGS, S.J., VOURLITIS, G., JENKINS, M., RIECHERS, G. & GRULKE, N. (1993): Recent change of Arctic tundra ecosystems from a net carbon dioxide sink to a source. *Nature* 361. p. 520-523.
- OPSAHL, S., BENNER, R. & AMON, R.M.W. (1999): Major flux of terrigenous dissolved organic matter through the Arctic Ocean. *Limnological Oceanography* 44. p. 2017-2023.
- OVERDUIN, P.P. & COUTURE, N. (2006): The 6th Annual Arctic Coastal Dynamics (ACD) Workshop, Oct. 22-26, 2006. Groningen, Netherlands.
- OVEREEM, I., ANDERSON, R., WOBUS, C., MATELL, N., URBAN, F., CLOW, G. & STANTON, T. (2010): The Impact of Sea Ice Loss on Wave Dynamics and Coastal Erosion Along the Arctic Coast, AGU Fall Meeting Abstracts. p. 5.

PETRONE, K.C., JONES, J.B., HINZMAN, L.D. & BOONE, R.D. (2006): Seasonal export of carbon, nitrogen, and major solutes from Alaskan catchments with discontinuous permafrost. *Journal of Geophysical Research* 111.

PINCHIN, B., NAIRN, R. & PHILPOTT, K. (1985): Beaufort Sea Coastal Sediment Study: Numerical estimation of sediment transport and nearshore profile adjustment at coastal sites in the Canadian Beaufort Sea. *Geol Surv Can Open File* 1259.

PING, C.L., MICHAELSON, G.J., GUO, L., JORGENSEN, M.T., KANEVSKIY, M., SHUR, Y., DOU, F. & LIANG, J. (2011): Soil carbon and material fluxes across the eroding Alaska Beaufort Sea coastline. *Journal of Geophysical Research: Biogeosciences* (2005–2012) 116.

POLLARD, W. & FRENCH, H. (1980): A first approximation of the volume of ground ice, Richards Island, Pleistocene Mackenzie Delta, Northwest Territories, Canada. *Canadian Geotechnical Journal* 17. p. 509-516.

POLLARD, W. & DALLIMORE, S. (1988): Petrographic characteristics of massive ground ice, Yukon Coastal Plain, Canada, Permafrost, Proceedings of the 5th International Conference, Trondheim, Norway. p. 224-229.

POLLARD, W. (1990): The nature and origin of ground ice in the Herschel Island area, Yukon Territory, Proceedings. Fifth Canadian Permafrost Conference, Québec. p. 23-30.

POLLARD, W.H. (1998): Arctic Permafrost and Ground Ice. In: WEATHERHEAD, E. & MORSETH, C.M. (eds.): Chapter 11: Climate Change, Ozone and ultraviolet Radiation. *Arctic Monitoring and Assessment Program Report*.

POST, W.M., EMANUEL, W.R., ZINKE, P.J. & STANGENBERGER, A.G. (1982): Soil carbon pools and world life zones. *Nature* 298. p. 156-159.

POTTER, B.B. & WIMSATT, J.C. (2012): USEPA method 415.3: Quantifying TOC, DOC, and SUVA. *Journal AWWA* 104.

RACHOLD, V., GRIGORIEV, M.N., ARÉ, F.E., SOLOMON, S., REIMNITZ, E., KASSENS, H. & ANTONOW, M. (2000): Coastal erosion vs riverine sediment discharge in the Arctic Shelf seas. *Int J Earth Sci* 89. p. 450-460.

RACHOLD, V., LACK, M. & GRIGORIEV, M. (2003): A Geo Information System (GIS) for circum-Arctic coastal dynamics, Proceedings of the 8th International Conference on Permafrost. Zurich (Switzerland), 21-25 July 2003. p. 923-927.

- RACHOLD, V., EICKEN, H., GORDEEV, V.V., GRIGORIEV, M.N., HUBBERTEN, H.-W., LISITZIN, A.P., SHEVCHENKO, V.P. & SCHIRRMESTER, L. (2004): Modern terrigenous organic carbon input to the Arctic Ocean. In: STEIN, R. & MACDONALD, R.W. (eds.): *The Organic Carbon Cycle in the Arctic Ocean*. Springer Verlag, Berlin. p. 33-55.
- RACHOLD, V., ARÉ, F.E., ATKINSON, D.E., CHERKASHOV, G. & SOLOMON, S.M. (2005a): Arctic coastal dynamics (ACD): An introduction. *Geo-Mar Lett* 25. p. 63-68.
- RACHOLD, V., LANTUIT, H., COUTURE, N. & POLLARD, W.H. (2005b): Arctic Coastal Dynamics. Report of the 5th International Workshop. *Berichte zur Polar- und Meeresforschung* 429. p. 1-127.
- RAMPTON, V. & MACKAY, J.R. (1971): Massive Ice and Icy Sediments Throughout the Tuktoyaktuk Peninsula, Richards Island: And Nearby Areas, District of Mackenzie. Department of Energy, Mines and Resources.
- RAMPTON, V.N. (1973): The influence of ground ice and thermokarst upon the geomorphology of the Mackenzie Beaufort region. *Research in Polar and Alpine Geomorphology*.
- RAMPTON, V.N. (1976): Map Quaternary Geology Yukon Coastal Plain Yukon Territory-Northwest Territories.
- RAMPTON, V.N. (1982): Quaternary Geology of the Yukon Coastal Plain. *Geological Survey of Canada Bulletin* 317. 49 p.
- RAYMOND, P.A., MCCLELLAND, J., HOLMES, R., ZHULIDOV, A., MULL, K., PETERSON, B., STRIEGL, R., AIKEN, G. & GURTOVAYA, T. (2007): Flux and age of dissolved organic carbon exported to the Arctic Ocean: A carbon isotopic study of the five largest arctic rivers. *Global Biogeochemical Cycles* 21.
- REIMNITZ, E. & WOLF, S.C. (1998): Are north slope surface alluvial fans pre-Holocene relicts? US Government Printing Office.
- RICHARDSON, L.F. (1961): The problem of contiguity: an appendix of statistics of deadly quarrels. *General systems yearbook* 6. p. 139-187.
- ROMANOVSKY, V.E., GRUBER, S., INSTANES, A., JIN, H., MARCHENKO, S.S., SMITH, S.L., TROMBOTTO, D. & WALTER, K.M. (2007): Frozen ground. In: UNEP (ed.): *Global Outlook for Ice and Snow*. p. 183-200.
- ROWELL, D.L. (1994): *Bodenkunde: Untersuchungsmethoden und ihre Anwendungsgebiete*. Springer Verlag, Berlin, Heidelberg, New York. 617 p.

SCHAEFER, K., LANTUIT, H., ROMANOVSKY, V.E., SCHUUR, E.A.G. & GÄRTNER-ROER, I. (2012): Policy Implications of Warming Permafrost. UNEP.

SCHROEDER, D. (1992): *Bodenkunde in Stichworten*. Berlin, Stuttgart. 175 p.

SHAVER, G.R., CANADELL, J., CHAPIN III, F., GUREVITCH, J., HARTE, J., HENRY, G., INESON, P., JONASSON, S., MELILLO, J. & PITELKA, L. (2000): Global Warming and Terrestrial Ecosystems: A Conceptual Framework for Analysis: Ecosystem responses to global warming will be complex and varied. Ecosystem warming experiments hold great potential for providing insights on ways terrestrial ecosystems will respond to upcoming decades of climate change. Documentation of initial conditions provides the context for understanding and predicting ecosystem responses. *BioScience* 50. p. 871-882.

SHAW, J., TAYLOR, R.B., FORBES, R.B., RUZ, M.-H. & SOLOMON, S. (1998): Sensitivity of the coasts of Canada to sea-level rise. *GSC Bulletin* 505.

SHUR, Y.L. & JORGENSEN, M.T. (2007): Patterns of permafrost formation and degradation in relation to climate and ecosystem. *Permafrost and Periglacial Processes* 18. p. 7-19.

SKIDMORE, M.L., FOGHT, J.M. & SHARP, M.J. (2000): Microbial life beneath a high Arctic glacier. *Applied and Environmental Microbiology* 66. p. 3214-3220.

SMITH, C.S. (1989): *Soil and vegetation of Herschel Island*. Research Branch, Agriculture Canada.

SMITH, C.A.S., KENNEDY, C.E., HARGRAVE, A.E. & MCKENNA, K.M. (1989): *Soil and vegetation survey of Herschel Island, Yukon Territory*. Yukon Soil Survey Report. 101 p.

SMITH, S.L., BURGEES, M.M. & HEGINBOTTOM, J.A. (2001): Permafrost in Canada, a challenge to northern development. In: BROOKS, G.R. (ed.): *A Synthesis of Geological Hazards in Canada*. Geological Survey of Canada. p. 241-264.

SMITH, S.V. (2005): Length of the global coastal zone. In: CROSSLAND, C.J., KREMER, H.H., LINDEBOOM, H.J., MARSHALL CROSSLAND, J.I. & LE TISSIER, M.D.A. (eds.): *Coastal fluxes in the Anthropocene*. Springer Verlag, Berlin, Heidelberg, New York.

SOLOMON, S. & COVILL, R. (1995): Impacts of the September 1993 storm on the Beaufort Sea. *Proceedings of the 1995 Canadian Coastal Conference*. p. 779-795.

SOLOMON, S.M. (2005): Spatial and temporal variability of shoreline change in the Beaufort-Mackenzie region, northwest territories, Canada. *Geo-Mar Lett* 25. p. 127-137.

SOLURI, E.A. & WOODSON, V.A. (1990): World vector shoreline. *International Hydrographic Review* LXVII (1). p. 27-35.

SPITZY, A. & LEHNHERR, J. (1991): DOC in rivers. In: DEGENS, E.T., KEMPE, S. & RICHEY, J.E. (eds.): *Biogeochemistry of Major World Rivers*.

STEIN, R. & MACDONALD, R.W. (2004): *The Organic Carbon Cycle In The Arctic Ocean*. Springer Verlag, Berlin, Heidelberg. 367 p.

ST-JEAN, M., LAURIOL, B., CLARK, I.D., LACELLE, D. & ZDANOWICZ, C. (2011): Investigation of ice-wedge infilling processes using stable oxygen and hydrogen isotopes, crystallography and occluded gases (O₂, N₂, Ar). *Permafrost and Periglacial Processes* 22. p. 49-64.

STRAUSS, J., SCHIRRMEISTER, L., WETTERICH, S., BORCHERS, A., DAVYDOV, S.P. (2012): Grain-size properties and organic-carbon stock of Yedoma Ice Complex permafrost from the Kolyma lowland, northeastern Siberia. *Global Biogeochemical Cycles* 26.

STRIEGL, R.G., AIKEN, G.R., DORNBLASER, M.M., RAYMOND, P.A. & WICKLAND, K.P. (2005): A decrease in discharge-normalized DOC export by the Yukon River during summer through autumn. *Geophys Res Lett* 32.

TARNOCAI, C., CANADELL, J.G., SCHUUR, E.A.G., KUHR, P., MAZHITOVA, G. & ZIMOV, S. (2009): Soil organic carbon pools in the northern circumpolar permafrost region. *Global Biogeochemical Cycles* 23.

TELANG, S.A., POCKLINGTON, R., NAIDU, A.S., ROMANKEVICH, E.A., GITELSON, I.I. & GLADYSHEV, M.I. (1991): Carbon and mineral transport in major North American, Russian Arctic, and Siberian rivers: the St. Lawrence, the Mackenzie, the Yukon, the Arctic Alaskan Rivers, the Arctic Basin Rivers in the Soviet Union, and the Yenisei. In: DEGENS, E.T., KEMPE, S. & RICHEY, J.E. (eds.): *Biogeochemistry of Major World Rivers*. Wiley, Chichester, UK. p. 75-104.

THURMAN, E.M. (1985): *Organic geochemistry of natural waters*. Kluwer Academic Pub, Dordrecht. 507 p.

ULRICH, M., MORGENSTERN, A., GÜNTHER, F., REISS, D., BAUCH, K.E., RÖSSLER, S. & SCHIRRMEISTER, L. (2010): Thermokarst in Siberian ice-rich permafrost: Comparison to asymmetric scalloped depressions on Mars. *Journal of Geophysical Research Planets* 115.

UNEP (2012): *Policy Implications of Warming Permafrost*. 38 p.

U.S. ARCTIC RESEARCH COMMISSION (2003): Climate Change, Permafrost, and Impacts on Civil Infrastructure. Special Report 01-03. Arlington, Virginia.

VAN EVERDINGEN, R.O. (1998): Multi-language glossary of permafrost and related ground-ice terms in Chinese, English, French, German, Icelandic, Italian, Norwegian, Polish, Romanian, Russian, Spanish, and Swedish. International Permafrost Association, Terminology Working Group.

VAN EVERDINGEN, R.O., 2005. Mult-language glossary of Permafrost and related ground-ice terms. International Permafrost Association.

VASILIEV, A. (2003): Permafrost controls of coastal dynamics at the Marre-Sale key site, Western Yamal, Proceedings of the 8th International Conference on Permafrost. p. 1173-1178.

VONK, J., SÁNCHEZ-GARCÍA, L., VAN DONGEN, B., ALLING, V., KOSMACH, D., CHARKIN, A., SEMILETOV, I., DUDAREV, O., SHAKHOVA, N. & ROOS, P. (2012): Activation of old carbon by erosion of coastal and subsea permafrost in Arctic Siberia. *Nature* 489. p. 137-140.

VON LOZINSKI, W. (1909): Über die mechanische Verwitterung der Sandsteine im gemäßigten Klima. *Bulletin international de l'Académie des Sciences de Cracovie. Classe des Sciences mathématiques et Naturelles* 1. p. 1-25.

WASHBURN, A.L. (1979): *Geocryology: a survey of periglacial processes and environments*. Wiley. 406 p.

WEEGE, S. (pHD candidate, Alfred Wegener Institute for Polar and Marine Research), personal communication (Date: 20th March2013).

WEISE, O.R. (1983): *Das Periglazial: Geomorphologie und Klima in gletscherfreien, kalten Regionen*. Gebr. Borntraeger.

WELSH, S.L. & RIGBY, J.K. (1971): Botanical and physiographic reconnaissance of northern Yukon. *Brigham Young Univ. Sci. Bull. Biol* 14.

WOLFE, S., DALLIMORE, S. & SOLOMON, S. (1998): Coastal permafrost investigations along a rapidly eroding shoreline, Tuktoyaktuk, NWT. *Permafrost: Proceedings of the Seventh International Conference*. Yellowknife, NWT. June 23-27. p. 1125-1131.

WOODS, G.C., SIMPSON, M.J., PAUTLER, B.G., LAMOUREUX, S.F., LAFRENIÈRE, M.J. & SIMPSON, A.J. (2011): Evidence for the enhanced lability of dissolved organic matter following permafrost slope disturbance in the Canadian High Arctic. *Geochimica et Cosmochimica Acta* 75. p. 7226-7241.

WOLFE, S., KOTLER, E. & DALLIMORE, S. (2001): Surficial characteristics and the distribution of thaw landforms (1970 to 1999), Shingle Point to Kay Point, Yukon Territory. Geological Survey of Canada, Open File 4115. p. 18.

WURL, O. & HOLMES, M. (2008): The gelatinous nature of the sea-surface microlayer. *Mar Chem* 110. p. 89-97.

YUNKER, M.B., MACDONALD, R.W., FOWLER, B.R., CRETNEY, W.J., DALLIMORE, S.R. & MCLAUGHLIN, F.A. (1991): Geochemistry and fluxes of hydrocarbons to the Beaufort Sea shelf: A multivariate comparison of fluvial inputs and coastal erosion of peat using principal components analysis. *Geochimica et Cosmochimica Acta* 55. p. 255-273.

ZIMOV, S., DAVYDOV, S., ZIMOVA, G., DAVYDOVA, A., SCHUUR, E., DUTTA, K. & CHAPIN, F. (2006a): Permafrost carbon: Stock and decomposability of a globally significant carbon pool. *Geophys Res Lett* 33.

ZIMOV, S.A., SCHUUR, E.A.G. & CHAPIN, F.S. (2006b): Permafrost and the global carbon budget. *Science* 312. p. 1612-1613.

ZHANG, T., BARRY, R.G., KNOWLES, K., HEGINBOTTOM, J. & BROWN, J. (1999): Statistics and characteristics of permafrost and ground-ice distribution in the Northern Hemisphere 1. *Polar Geography* 23. p. 132-15

Appendix

This chapter serves as data base for all extrapolated DOC concentrations and the estimated DOC stocks. Furthermore it includes all input variables for the calculation of DOC fluxes and the estimated DOC fluxes for all terrain units along the Yukon Coastal Plain. Besides the measured DOC concentrations in blanks are documented in this section.

Appendix 1

- Overview of input variables for the calculation of DOC stocks

Appendix 2

- Overview of input variables for the calculation of DOC fluxes

Appendix 3

- Overview of calculated DOC stocks and fluxes

Appendix 1

Location name	Coast section	Density of pure ice at -10°C	Vol. massive ground ice content	DOC conc. ice wedges (25%-quartile)	DOC conc. ice wedges (Median)	DOC conc. ice wedges (75%-quartile)	DOC conc. massive i. b. (25%-quartile)	DOC conc. massive i. b. (Median)	DOC conc. massive i. b. (75%-quartile)
		[g/cm ³]	[d. n.]	[mg/L]	[mg/L]	[mg/L]	[mg/L]	[mg/L]	[mg/L]
Clarence Lagoon W	West	0.91027	0.35	5.8915	7.9835	12.2125	0	1.061	2.3145
Clarence Lagoon	West	0.91027	0.00	5.8915	7.9835	12.2125	0	1.061	2.3145
Clarence Lagoon E	West	0.91027	0.00	5.8915	7.9835	12.2125	0	1.061	2.3145
Komakuk Beach W2	West	0.91027	0.07	5.8915	7.9835	12.2125	0	1.061	2.3145
Komakuk Beach W1	West	0.91027	0.40	5.8915	7.9835	12.2125	0	1.061	2.3145
Komakuk Beach	West	0.91027	0.08	5.8915	7.9835	12.2125	0	1.061	2.3145
Malcolm River fan	West	0.91027	0.00	5.8915	7.9835	12.2125	0	1.061	2.3145
Malcolm River fan w. b. i.	West	0.91027	0.00	5.8915	7.9835	12.2125	0	1.061	2.3145
Nunaluk Spit	West	0.91027	0.00	5.8915	7.9835	12.2125	0	1.061	2.3145
Avadlek Spit	HI	0.91027	0.00	5.8915	7.9835	12.2125	0	1.061	2.3145
Herschel Island W	HI	0.91027	0.10	5.8915	7.9835	12.2125	0	1.061	2.3145
Herschel Island N	HI	0.91027	0.09	5.8915	7.9835	12.2125	0	1.061	2.3145
Simpson Point	HI	0.91027	0.00	5.8915	7.9835	12.2125	0	1.061	2.3145
Herschel Island E	HI	0.91027	0.28	5.8915	7.9835	12.2125	0	1.061	2.3145
Herschel Island S	HI	0.91027	0.14	5.8915	7.9835	12.2125	0	1.061	2.3145
Workboat Passage W	Central	0.91027	0.22	5.8915	7.9835	12.2125	0	1.061	2.3145
Workboat Passage E	Central	0.91027	0.15	5.8915	7.9835	12.2125	0	1.061	2.3145
Catton Point	Central	0.91027	0.00	5.8915	7.9835	12.2125	0	1.061	2.3145
Whale Cove W	Central	0.91027	0.08	5.8915	7.9835	12.2125	0	1.061	2.3145
Whale Cove	Central	0.91027	0.00	5.8915	7.9835	12.2125	0	1.061	2.3145
Whale Cove E	Central	0.91027	0.36	5.8915	7.9835	12.2125	0	1.061	2.3145
Roland Bay NW	Central	0.91027	0.12	5.8915	7.9835	12.2125	0	1.061	2.3145
Roland Bay W	Central	0.91027	0.12	5.8915	7.9835	12.2125	0	1.061	2.3145
Roland Bay E	Central	0.91027	0.03	5.8915	7.9835	12.2125	0	1.061	2.3145

Location name	Coast section	Density of pure ice at -10°C	Vol. massive ground ice content	DOC conc. ice wedges (25%-quartile)	DOC conc. ice wedges (Median)	DOC conc. ice wedges (75%-quartile)	DOC conc. massive i. b. (25%-quartile)	DOC conc. massive i. b. (Median)	DOC conc. massive i. b. (75%-quartile)
		[g/cm ³]	[d. n.]	[mg/L]	[mg/L]	[mg/L]	[mg/L]	[mg/L]	[mg/L]
Stokes Point W	Central	0.91027	0.12	5.8915	7.9835	12.2125	0	1.061	2.3145
Stokes Point	Central	0.91027	0.00	5.8915	7.9835	12.2125	0	1.061	2.3145
Stokes Point SE	Central	0.91027	0.08	5.8915	7.9835	12.2125	0	1.061	2.3145
Phillips Bay NW	Central	0.91027	0.25	5.8915	7.9835	12.2125	0	1.061	2.3145
Phillips Bay W	Central	0.91027	0.00	5.8915	7.9835	12.2125	0	1.061	2.3145
Phillips Bay	Central	0.91027	0.06	5.8915	7.9835	12.2125	0	1.061	2.3145
Babbage River Delta	Central	0.91027	0.00	5.8915	7.9835	12.2125	0	1.061	2.3145
Kay Point spit	East	0.91027	0.00	5.8915	7.9835	12.2125	0	1.061	2.3145
Kay Point	East	0.91027	0.14	5.8915	7.9835	12.2125	0	1.061	2.3145
Kay Point SE	East	0.91027	0.09	5.8915	7.9835	12.2125	0	1.061	2.3145
King Point NW	East	0.91027	0.13	5.8915	7.9835	12.2125	0	1.061	2.3145
King Point lagoon	East	0.91027	0.00	5.8915	7.9835	12.2125	0	1.061	2.3145
King Point	East	0.91027	0.14	5.8915	7.9835	12.2125	0	1.061	2.3145
King Point SE	East	0.91027	0.47	5.8915	7.9835	12.2125	0	1.061	2.3145
Sabine Point W	East	0.91027	0.01	5.8915	7.9835	12.2125	0	1.061	2.3145
Sabine Point	East	0.91027	0.18	5.8915	7.9835	12.2125	0	1.061	2.3145
Sabine Point E	East	0.91027	0.14	5.8915	7.9835	12.2125	0	1.061	2.3145
Shingle Point W	East	0.91027	0.15	5.8915	7.9835	12.2125	0	1.061	2.3145
Shingle Point E	East	0.91027	0.05	5.8915	7.9835	12.2125	0	1.061	2.3145
Running River	East	0.91027	0.01	5.8915	7.9835	12.2125	0	1.061	2.3145

Appendix 2

Location name	Coast section	Coast length	Coastline height	Coastal erosion rate	Vol. massive ground ice content	DOC stock Scenario I (25%-quartile)	DOC stock Scenario II (Median)	DOC stock Scenario III (75%-quartile)
		[m]	[m]	[m/yr]	[vol%]	[g/m ³]	[g/m ³]	[g/m ³]
Clarence Lagoon W	West	6326	5.0	0.62	35.3	0.25	0.50	0.87
Clarence Lagoon	West	3139	1.0	0.44	0	0.00	0.00	0.00
Clarence Lagoon E	West	956	1.0	0.48	0	0.00	0.00	0.00
Komakuk Beach W2	West	7909	5.3	0.96	7.2	0.05	0.07	0.11
Komakuk Beach W1	West	1851	3.5	0.68	40.4	0.26	0.54	0.96
Komakuk Beach	West	12905	3.5	1.40	8.3	0.06	0.09	0.13
Malcolm River fan	West	8858	1.0	1.83	0	0.00	0.00	0.00
Malcolm River fan w. b. i.	West	33264	1.0	0.00	0	0.00	0.00	0.00
Nunaluk Spit	West	26458	1.2	0.95	0	0.00	0.00	0.00
Avadlek Spit	HI	5600	1.0	0.77	0	0.00	0.00	0.00
Herschel Island W	HI	5635	56.0	0.95	10.2	0.02	0.04	0.08
Herschel Island N	HI	16708	60.0	0.71	8.6	0.02	0.03	0.06
Simpson Point	HI	3165	1.0	0.00	0	0.00	0.00	0.00
Herschel Island E	HI	10691	24.5	0.75	28	0.12	0.28	0.50
Herschel Island S	HI	12140	5.5	0.00	13.9	0.17	0.22	0.34
Workboat Passage W	Central	1813	5.0	0.52	21.7	0.46	0.63	0.96
Workboat Passage E	Central	10120	3.0	0.38	14.6	0.29	0.39	0.60
Catton Point	Central	4745	1.4	0.00	0	0.00	0.00	0.00
Whale Cove W	Central	3765	1.5	0.08	7.9	0.06	0.08	0.12
Whale Cove	Central	2653	1.0	1.50	0	0.00	0.00	0.00
Whale Cove E	Central	812	5.0	0.00	35.7	0.54	0.87	1.41
Roland Bay NW	Central	2790	2.5	0.18	11.8	0.11	0.15	0.24
Roland Bay W	Central	2704	19.0	0.12	12.4	0.07	0.11	0.18
Roland Bay E	Central	2704	15.0	0.29	2.5	0.01	0.01	0.01
Stokes Point W	Central	2850	22.0	0.35	11.6	0.05	0.09	0.14
Stokes Point	Central	4869	1.9	1.36	0	0.00	0.00	0.00

Location name	Coast section	Coast length	Coastline height	Coastal erosion rate	Vol. massive ground ice content	DOC stock Scenario I (25%-quartile)	DOC stock Scenario II (Median)	DOC stock Scenario III (75%-quartile)
		[m]	[m]	[m/yr]	[vol%]	[g/m ³]	[g/m ³]	[g/m ³]
Stokes Point SE	Central	3940	10.0	0.21	7.6	0.06	0.08	0.12
Phillips Bay NW	Central	2575	12.0	0.00	25.3	0.18	0.32	0.53
Phillips Bay W	Central	4624	1.0	0.58	0	0.00	0.00	0.00
Phillips Bay	Central	6839	6.5	1.30	5.9	0.04	0.05	0.08
Babbage River Delta	Central	10704	3.0	0.00	0	0.00	0.00	0.00
Kay Point spit	East	4935	0.9	0.00	0	0.00	0.00	0.00
Kay Point	East	2668	7.0	2.65	14.4	0.27	0.36	0.55
Kay Point SE	East	22479	30.0	0.96	8.7	0.04	0.07	0.11
King Point NW	East	2895	40.0	0.00	12.5	0.04	0.07	0.13
King Point lagoon	East	1633	1.0	3.13	0	0.00	0.00	0.00
King Point	East	911	7.0	2.44	14.4	0.21	0.29	0.44
King Point SE	East	3765	12.0	1.60	46.8	0.38	0.74	1.27
Sabine Point W	East	2671	25.0	0.81	1.5	0.00	0.01	0.01
Sabine Point	East	2454	40.0	0.52	18.3	0.02	0.08	0.16
Sabine Point E	East	2384	25.0	1.43	13.9	0.03	0.08	0.16
Shingle Point W	East	11276	26.0	0.38	14.8	0.07	0.12	0.21
Shingle Point E	East	12016	20.0	0.30	5	0.03	0.05	0.07
Running River	East	12016	23.3	0.69	1.5	0.00	0.00	0.01
Sum		306215						
Min		812	0.9	0	0	0	0	0
Max		33264	60	3.13	46.8	0.54	0.87	1.41
Average		6959	12.2	0.73	10.5	0.09	0.15	0.24

Appendix 3

Location name	Coast section	DOC flux	DOC flux	DOC flux	DOC flux	DOC flux	DOC flux
		Scenario A (25%-quartile)	Scenario B (Median)	Scenario C (75%-quartile)	Scenario A (25%-quartile)	Scenario B (Median)	Scenario C (75%-quartile)
		[kg/yr]	[kg/yr]	[kg/yr]	[kg/m/yr]	[kg/m/yr]	[kg/m/yr]
Clarence Lagoon W	West	4.9	9.8	17.1	0.001	0.002	0.003
Clarence Lagoon	West	0.0	0.0	0.0	0	0	0
Clarence Lagoon E	West	0.0	0.0	0.0	0	0	0
Komakuk Beach W2	West	2.1	2.9	4.4	0	0	0.001
Komakuk Beach W1	West	1.1	2.4	4.2	0.001	0.001	0.002
Komakuk Beach	West	4.0	5.4	8.3	0	0	0.001
Malcolm River fan	West	0.0	0.0	0.0	0	0	0
Malcolm River fan w. b. i.	West	0.0	0.0	0.0	0	0	0
Nunaluk Spit	West	0.0	0.0	0.0	0	0	0
Avadlek Spit	HI	0.0	0.0	0.0	0	0	0
Herschel Island W	HI	6.1	13.0	23.0	0.001	0.002	0.004
Herschel Island N	HI	11.7	23.9	41.9	0.001	0.001	0.003
Simpson Point	HI	0.0	0.0	0.0	0	0	0
Herschel Island E	HI	23.2	54.1	97.5	0.002	0.005	0.009
Herschel Island S	HI	0.0	0.0	0.0	0	0	0
Workboat Passage W	Central	2.2	3.0	4.5	0.001	0.002	0.002
Workboat Passage E	Central	3.4	4.6	7.0	0	0	0.001
Catton Point	Central	0.0	0.0	0.0	0	0	0
Whale Cove W	Central	0.0	0.0	0.1	0	0	0
Whale Cove	Central	0.0	0.0	0.0	0	0	0
Whale Cove E	Central	0.0	0.0	0.0	0	0	0
Roland Bay NW	Central	0.1	0.2	0.3	0	0	0
Roland Bay W	Central	0.4	0.7	1.1	0	0	0
Roland Bay E	Central	0.1	0.1	0.2	0	0	0
Stokes Point W	Central	1.2	1.9	3.2	0	0.001	0.001
Stokes Point	Central	0.0	0.0	0.0	0	0	0

Location name	Coast section	DOC flux	DOC flux	DOC flux	DOC flux	DOC flux	DOC flux
		Scenario A (25%-quartile)	Scenario B (Median)	Scenario C (75%-quartile)	Scenario A (25%-quartile)	Scenario B (Median)	Scenario C (75%-quartile)
		[kg/yr]	[kg/yr]	[kg/yr]	[kg/m/yr]	[kg/m/yr]	[kg/m/yr]
Stokes Point SE	Central	0.5	0.6	1.0	0	0	0
Phillips Bay NW	Central	0.0	0.0	0.0	0	0	0
Phillips Bay W	Central	0.0	0.0	0.0	0	0	0
Phillips Bay	Central	2.3	3.1	4.7	0	0	0.001
Babbage River Delta	Central	0.0	0.0	0.0	0	0	0
Kay Point spit	East	0.0	0.0	0.0	0	0	0
Kay Point	East	13.1	17.8	27.2	0.005	0.007	0.01
Kay Point SE	East	26.4	43.3	71.2	0.001	0.002	0.003
King Point NW	East	0.0	0.0	0.0	0	0	0
King Point lagoon	East	0.0	0.0	0.0	0	0	0
King Point	East	3.3	4.5	6.9	0.004	0.005	0.008
King Point SE	East	27.5	53.0	91.4	0.007	0.014	0.024
Sabine Point W	East	0.2	0.3	0.4	0	0	0
Sabine Point	East	1.2	4.1	8.0	0	0.002	0.003
Sabine Point E	East	2.5	7.1	13.3	0.001	0.003	0.006
Shingle Point W	East	7.4	13.7	23.4	0.001	0.001	0.002
Shingle Point E	East	2.4	3.3	5.0	0	0	0
Running River	East	0.6	0.8	1.2	0	0	0
Sum		147.8	273.6	466.2	147.8	273.6	466.2
Min		0.0	0.0	0.0	0	0	0
Max		27.5	54.1	97.5	27.5	54.1	97.5
Average		3.4	6.2	10.6	3.4	6.2	10.6

Danksagung

Zunächst möchte ich mich bei Hugues Lantuit, Michael Fritz und Jens Strauß bedanken, die mir die Arbeit am Alfred-Wegener-Institut sowie die Anfertigung dieser Arbeit erst ermöglichten und mich mit fachlichen und persönlichen Ratschlägen zu jeder Zeit freundschaftlich unterstützt haben.

Des Weiteren möchte ich mich herzlich bei Prof. Dr. Karl-Tilman Rost seitens der Freien Universität Berlin und Prof. Dr. Hans-Wolfgang Hubberten seitens des Alfred-Wegener-Instituts für Polar- und Meeresforschung für die Betreuung und Begutachtung dieser Arbeit bedanken.

Ganz besonderer Dank gebührt Boris Radosavljevic und Samuel Stettner für die fachliche und vor allem persönliche Unterstützung und das Korrekturlesen sowie für die lustigen Stunden am AWI.

Herzlich bedanken möchte ich mich auch bei Nicole Couture für das Bereitstellen einer Vielzahl an verwendeten Daten.

Weiterer Dank gilt der ganzen COPER Gruppe am AWI, Steffi, Jule, Boris und Jaros sowie Ute, die mich immer freundlich unterstützen und in deren familiären Atmosphäre die Anfertigung der Arbeit sehr leicht fiel.

Herzlich bedanken möchte ich mich auch bei Antje und Micha, die mich während der Laborarbeit hervorragend betreut und unterstützt haben.

Herzlichster Dank geht an meinen Bruder Philipp, meine Eltern und meine Großeltern, die mich zu jeder Zeit und Lebenssituation unterstützt und immer den nötigen Rückhalt gegeben haben.

Allerherzlichster Dank auch an meine Freunde Stefan und Christin, die immer für mich da sind.

Schließlich möchte ich mich auch bei allen hier nicht genannten Freunden und Bekannten bedanken, die mich unterstützt und zum Erfolg dieser Arbeit beigetragen haben.

Selbständigkeitserklärung

Hiermit versichere ich, dass ich die vorliegende Arbeit selbstständig verfasst und keine anderen als die angegebenen Quellen und Hilfsmittel verwendet habe. Diese Arbeit wurde nach besten Wissen und Gewissen angefertigt.

Ort, Datum

Unterschrift George Tanski